SHEAR STRENGTH OF CONTINUOUS LIGHTLY REINFORCED T-BEAMS

BY

GREGORY P. PASLEY

SAMAR GOGOI

DAVID DARWIN

STEVEN L. McCABE

A Report on Research Sponsored by
THE NATIONAL SCIENCE FOUNDATION
Research Grant
MSM-8816158

UNIVERSITY OF KANSAS
LAWRENCE, KANSAS
DECEMBER 1990

ABSTRACT

The shear strength of continuous lightly reinforced concrete T-beams is studied. Six two-span T-beams with and without web reinforcement are tested. The primary variables are longitudinal reinforcement ratio (0.75% and 1.0%) and nominal stirrup strength (0 to 82 psi). The test results are analyzed and compared with the shear design provisions of "Building Code Requirements for Reinforced Concrete (ACI 318-89)" and predictions of other investigators, including predictions obtained using the modified compression field theory.

The tests indicate that ACI 318-89 overpredicts the concrete shear capacity of lightly reinforced beams without shear reinforcement. Little difference exists between shear cracking stresses in the negative and positive moment regions for beams in the current study. For both the negative and positive moment regions, the stirrup contribution to shear strength exceeds the value predicted by ACI 318-89. Stirrup contribution to shear strength increases with increasing flexural reinforcement ratio. Overall, the ACI 318-89 shear provisions are conservative for the beams tested in the current study. Two procedures based on the modified compression field theory are also conservative. ACI 318-89 better predicts the nominal shear strength of the beams in the current study than either of the modified compression field theory procedures.

ACKNOWLEDGEMENTS

This report is based on research performed by Samar Gogoi and Gregory P. Pasley in partial fulfillment of the requirements for the degree of M.S.C.E. The research was supported by the National Science Foundation under NSF Grant MSM-8816158 . The reinforcing steel was donated by the Sheffield Steel Corporation.

TABLE OF CONTENTS

TABLE OF CONTENTS (continued)

LIST OF TABLES

LIST OF FIGURES

LIST OF FIGURES (continued)

LIST OF FIGURES (continued)

LIST OF FIGURES (continued)

Chapter 1

INTRODUCTION

1.1 General

In spite of a large volume of experimental research devoted to the prediction of the shear capacity of reinforced concrete beams, much remains to be learned about the shear behavior of these members. The nature of shear failure of flexural members is such that it occurs suddenly, with little indication of distress, and is accompanied by a rapid reduction in the load carrying capacity of the member. This is of particular concern because the present ACI Building Code (3) shear design provisions appear to be unconservative for lightly reinforced flexural members, especially in negative moment regions. Lightly reinforced flexural members are widely used in practice, and provide the most economical section in most cases. Thus, a more reliable way of predicting the shear strength of such beams is necessary to insure adequate safety when these members are used.

The ACI Building Code design equations for reinforced concrete beams subjected to shear and flexure are primarily based on tests of simply supported beams having flexural reinforcement ratios above 1% (12,13,19,24,32,33,41). However, previous research (11,14,27,28,34,35,36,37,41) has shown that the shear cracking load predicted by these equations is unconservative for beams having longitudinal reinforcement ratios, ρ_w, less than 1%. Recent research (38,39,40) on lightly reinforced T-beams, with flexural reinforcement ratios less than 1%, provides evidence that concrete shear capacity is lower and shear reinforcement is less effective in negative moment regions than in positive moment regions. However, the ACI equations make no adjustments for the design of continuous beams in negative moment regions, based on the assumption that moment region has no effect on shear strength.

These deficiencies are accounted for, to some extent, by the ACI equations because they underestimate the contribution of shear reinforcement and require its use in beams where the shear load exceeds one-half of the design shear capacity of the concrete. The use of these equations, however, also results in non-uniform margins of safety in shear for structures designed with different percentages of flexural reinforcement.

The purpose of this research is to study the shear strength of continuous, lightly reinforced T-beams and the effects of flexural reinforcement ratio and degree of shear reinforcement on shear capacity. The cracking and ultimate shears are compared with the shear provisions of ACI Building Code (3) and the predictive equations of other investigators. The predicted shear response of beams obtained using the modified compression field theory (18,21,22,23,31,43) is compared with experimental results. The safety of current design procedures is investigated.

1.2 Background

In a reinforced concrete beam, flexural and shear stresses give rise to principal tensile stresses oriented at some angle with the longitudinal axis of the beam. The effects of shear are greatest near supports and in regions of concentrated load. As the load increases, cracks begin to appear in a direction perpendicular to the local principal tensile stresses. In regions where shear stress is low, the cracks form perpendicular to the axis of the beam. In regions of high shear stress, the cracks form and propagate at a lower angle and are often referred to as diagonal tension or shear cracks. Before the formation of shear cracks, most of the shear is carried by the concrete. Once diagonal tension cracks form, a redistribution of internal force takes place and the load is carried by five different mechanisms, as noted by ACI-ASCE Committee 426 (5):

1. Shear Stress: Shear transfer by concrete shear stress occurs in uncracked members or uncracked portions of members. Shear stress interacts with compressive and tensile stresses producing principal stresses that may cause additional diagonal cracking or concrete crushing.

2. Interface Shear Transfer: Interface shear transfer across a plane involves slippage along a preexisting crack. In monolithic concrete, a number of diagonal cracks may form, resulting in arch action and interface shear transfer across the crack planes. Other terms used for this mechanism include aggregate interlock, surface roughness shear transfer and shear friction.

3. Dowel Shear: This is the shearing displacement resisted by the longitudinal steel when it is intersected by a shear crack. This causes tension in the concrete surrounding the longitudinal steel, producing cracks along the steel.

4. Arch Action: Arch action is mainly effective in deep beams where it transfers a vertical concentrated force to a reaction, reducing the contribution of other types of shear transfer.

5. Shear Reinforcement: Shear reinforcing steel aids in carrying additional shear force after shear cracking; it contains the diagonal crack, thus delaying deep penetration of the diagonal crack into the compression zone; and slows down the decrease in interface shear transfer. It also helps to confine the longitudinal steel, thus increasing the shear contribution of the longitudinal steel by dowel action.

A systematic study by ACI-ASCE Committee 326 (4) of more than 440 tests on beams without web reinforcement indicated that the concrete shear capacity of beams primarily depends on the percentage of flexural reinforcement, ρ_w, the shear span-to-depth ratio, a/d, and the concrete compressive strength, f'_c, with other variables, like aggregate interlock and shear friction, playing a minor role in concrete shear strength. The present ACI Building Code

(3) equations for concrete shear capacity, which were first proposed by ACI-ASCE Committee 326 (4), were based on research done on simply supported beams having flexural reinforcement, ρ_w, above 1%. However, studies (11,14,27,28,34,35,36,37,41) have shown that the ACI shear equations overestimate the concrete shear capacity of beams having flexural reinforcement below 1%. However, since these studies (11,14,27,28,34,35,36,37,41) have been carried out on simply supported beams, it is not clear whether they apply to continuous beams. Recent research (38,39,40) on the negative moment region shear strength of lightly reinforced T-beams has shown a lower concrete shear capacity and stirrup reinforcement effectiveness in negative moment regions than in positive moment regions. This lower negative moment region shear strength is felt to be caused by a smaller effective concrete section resulting from cracking of the flanges and a lower bond strength for negative flexural reinforcement due to the top-bar effect. The T-beams in this research (38,39,40), however, were not truly continuous for negative bending, since they were loaded on a simple span with a 5 ft cantilever at one end to simulate continuity. In the case of truly continuous beams, with beam-girder connections and formation of hinges in the negative moment regions due to yielding of flexural reinforcement, it is unclear as to how the beams would behave in shear.

As reported by ACI-ASCE Committee 426 (5), the addition of web reinforcement helps in carrying additional shear force in three main ways: stirrups share a part of the shear force; stirrups restrict the growth of diagonal shear cracks, helping to increase interface shear transfer; and stirrups hold the flexural reinforcement in place, increasing the contribution of dowel action to shear strength. The ACI shear design provisions, however, consider only the direct stirrup contribution to shear strength and neglect the contributions of factors, like aggregate interlock, interface shear transfer, the stirrup confining effect on longitudinal steel. The ACI provisions for the stirrup contribution to shear strength assume that the critical diagonal tension crack has a horizontal projection equal to the effective depth of the beam. In

beams where the critical diagonal tension crack has a greater horizontal projection, it intersects more stirrups then predicted by the ACI provisions and thus the shear strength is higher. As a result, the ACI shear equations often underestimate the contribution of web reinforcement to the shear strength of beams (11,20,25,34,35).

To investigate these problems, an experimental study was conducted of the shear behavior of two-span continuous T-beams, with varying amounts of flexural and shear reinforcement.

1.3 Current Shear Design Provisions

The current design procedure employed by the ACI Building Code, ACI 318-89 (3), is to calculate the factored shear force of a member and to provide sufficient concrete and steel capacity to counter this load. This can be expressed as:

$$V_u \leq \phi(V_c + V_s) \qquad (1.1)$$

in which V_u is the factored shear force at the section considered; V_c is the nominal shear strength provided by the concrete; V_s is the nominal shear strength provided by the shear reinforcement; and ϕ is the strength reduction factor, taken equal to 0.85.

The provisions in ACI 318 require the use of stirrups where the factored shear force, V_u, exceeds one-half the design shear strength of concrete, ϕV_c. The equations for concrete shear capacity given by ACI 318 were established through experimental and analytical studies of typical flexural members (4) and represent the concrete shear strength in terms of concrete compressive strength, beam size, flexural reinforcement ratio, and the applied loads. The two equations presented in ACI 318 are:

$$V_c = 2\sqrt{f'_c}\, b_w d \qquad (1.2)$$

and

$$V_c = \left(1.9\sqrt{f'_c} + 2500\rho_w \frac{V_u d}{M_u}\right) b_w d \le 3.5\sqrt{f'_c}\, b_w d \qquad (1.3)$$

in which f'_c is the concrete compressive strength in psi; ρ_w is the flexural reinforcement ratio based on the web area, $A_s/(b_w d)$; M_u is the factored moment; d is the effective depth; and b_w is the width of the beam web. The values of $\sqrt{f'_c}$ are limited to 100 psi unless minimum values of shear reinforcement are used. $M_u/(V_u d)$ provides a measure of the ratio of flexural tension to shearing stresses. $M_u/(V_u d)$ is synonymous with the shear span-to-depth ratio, a/d, of a simply supported beam with point loads; for a general loading or beam configuration the $M_u/(V_u d)$ ratio gives an equivalent a/d ratio. Eq. 1.2 is a simplified form of Eq. 1.3. But due to the wide scatter of the data from which Eq. 1.3 was derived, it cannot be expected to give a true representation of concrete shear capacity.

The ACI Building Code requires that shear reinforcement be added when the factored shear, V_u, exceeds $\phi V_c/2$ for beams. The shear force contribution by stirrups, as predicted by the ACI code, is:

$$V_s = \frac{A_v f_{vy} d}{s} \qquad (1.4)$$

in which s is the shear reinforcement spacing; A_v is the shear reinforcement area within a length, s, of the beam; and f_{vy} is the steel yield stress. Eq. 1.4 is based on the assumption that the critical diagonal shear crack is inclined at an angle of about 45 degrees and intersects

stirrups over a length equal to the effective depth of the beam. This makes Eq. 1.4 underestimate the stirrup shear contribution in cases where the critical diagonal shear crack is flatter than 45 degrees. The ACI Building Code also specifies that the stirrup spacing, s, must not exceed one-half the effective depth, or 24 inches, and that the shear reinforcement, A_v, must be at least:

$$A_v = 50\frac{b_w s}{f_{vy}} \qquad (1.5)$$

which corresponds to a nominal shear reinforcement stress, $\rho_v f_{vy} = A_v f_{vy}/b_w s = V_s/b_w d$, of 50 psi. A_v in Eq. 1.5 must be multiplied by $f'_c/5000 \leq 3$ for $f'_c \geq 10000$ psi to allow $\sqrt{f'_c}$ to exceed 100 psi in Eq. 1.2 and 1.3. Otherwise, $\sqrt{f'_c}$ in Eq. 1.2 and 1.3 is limited to a maximum of 100 psi. The requirement for the higher value of A_v was added in 1989 (3).

1.4 Previous Research

Eqs. 1.2 and 1.3, which were developed based on research (12,13,19,24,32,33,41) done on beams with flexural reinforcement ratios greater than 1%, are unconservative for beams without shear reinforcement, $\rho_v f_{vy}=0$, and values of ρ_w less than 1% (11,14,27,28,34,35,36,37,41).

Kani (27) tested a series of simply supported rectangular beams with values of flexural reinforcement ratio, ρ_w, ranging from 0.5% to 2.8% and concrete compressive strength, f'_c, ranging from 2500 psi to 5000 psi. Shear span-to-effective depth ratios, a/d, ranged from 1 to 5. He observed that the shear strength equation in the ACI Building Code (3) overestimates the actual strength of members with values of ρ_w below 1% and shear span-to-effective depth

ratios above 2.5. He also noted that a change in f'_c produces a negligible variation in shear strength.

Mathey and Watstein (30) tested rectangular beams with a/d ratios ranging from 1.51 to 3.78 and values of ρ_w ranging from 0.47% to 3.05%. They found that for a/d ratios greater than 1.5 and values of ρ_w lower than 1%, the ACI (3) expressions for concrete shear strength are unconservative in some cases by as much as 47%. They suggested an expression for the nominal concrete shear stress, v_c:

$$v_c = \frac{3.1\sqrt{f'_c}\,Vd}{M} + 4000\,\rho_w \qquad (1.6)$$

in which V/M is the ratio of shear to maximum bending moment in the shear span in which the diagonal tension crack form.

Rajagopalan and Ferguson (37) combined their test data from 13 rectangular beams (10 without stirrups and 3 with stirrups), with a/d approximately equal to 4 and values of ρ_w ranging from 0.25% to 1.73% and 27 other beams with values of ρ_w less than 1.2%. They verified that Eqs. 1.2 and 1.3 overestimate the shear strength of concrete members. They also observed that in two beams with stirrups, the ACI maximum stirrup spacing requirement of d/2 was more restrictive than necessary. They proposed an expression for the nominal concrete shear stress, v_c:

$$v_c = V_c/(b_w d) = (0.8 + 100\rho_w)\sqrt{f'_c} \le 2\sqrt{f'_c} \qquad (1.7)$$

Zsutty (44) used dimensional and regression analyses of data from a large number of tests performed by others and recommended a new shear equation to better predict the shear

strength of beams without stirrups:

$$v_c = 59 (f'_c \rho_w \frac{d}{a})^{\frac{1}{3}} \quad (1.8)$$

Eq. 1.8 accurately accounts for concrete strength, flexural reinforcement ratio and shear span-to-effective depth ratio for beams with a/d ratio greater than 2.5. However, Eq. 1.8 overpredicts v_c for beams deeper than 12 in. Among others, Bazant and Kim (16) have observed that the average shear stress at failure decreases with increasing beam depth. This structural size effect is not modeled by Eq. 1.8.

Most of the studies cited above were concerned with rectangular cross sections; however, other cross sections have been tested. Placas and Regan (36) measured the shear capacity of sixty-three T, I and rectangular beams with a/d ratios ranging from 3.4 to 7.2 and ρ_w ranging from 0.98% to 4.2%. To predict the shear capacity of these sections, they proposed a semiempirical equation of the form:

$$v_{cr} = 8 (f'_c \, 100 \, \rho_w)^{\frac{1}{3}} \quad (1.9)$$

They imposed an upper bound of $12(f'_c)^{\frac{1}{3}}$ to limit the effect of large values of ρ_w in T-beams in which the main steel has only a limited effect on stress conditions in the web. Their equation provides results similar to those of Eq. 1.8 for a/d approximately equal to 4.

Due to the extensive research (11,14,27,28,34,35,36,37,41) done on shear strength of lightly reinforced concrete beams and the strong evidence for the lack of conservatism of Eqs. 1.2 and 1.3 for low values of ρ_w, ACI-ASCE Committee 426 (6) proposed an expression for v_c:

$$\sqrt{f'_c} \leq v_c = (0.8 + 120\rho_w)\sqrt{f'_c} \leq 2.3\sqrt{f'_c} \qquad (1.10)$$

which is a modified version of the expression, Eq. 1.7, presented by Rajagopalan and Ferguson (37).

To investigate the feasibility of the use of Eq. 1.10, Batchelor and Kwun (14) tested 10 continuous and 4 simply supported beams. They also considered the test data for 262 additional members. All beams had a shear span-to-depth ratio, a/d, greater than 2 and had no web reinforcement. Based on their analysis, they proposed another, still more conservative, variation on Eq. 1.7.

$$v_c = 1.10\sqrt{f'_c} \leq (0.6 + 110\rho_w)\sqrt{f'_c} \leq 2.25\sqrt{f'_c} \qquad (1.11)$$

In 1984, Bazant and Kim (17) introduced an expression for cracking shear based on fracture mechanics concepts:

$$v_c = \frac{10\sqrt[3]{\rho_w}}{\sqrt{1 + 0.04\frac{d}{d_a}}}\left[\sqrt{f'_c} + 3000\sqrt{\frac{\rho_w}{(\frac{a}{d})^5}}\right] \qquad (1.12)$$

in which d_a = maximum size aggregate.

With some sacrifice of simplicity, Eq. 1.12 improves on the accuracy of Eq. 1.8 and appears to accurately capture the "size effect". Bazant and Kim proposed a design expression equal to 80% of Eq. 1.12.

Due to the insufficient shear capacity of lightly reinforced beams and also because of wholly inadequate data on the effects of shear reinforcement on these members, Palaskas,

Attiogbe and Darwin (11,34,35) tested 15 simply supported T-beams with low values of flexural and shear reinforcement. The tests included 11 beams with stirrups and 4 beams without stirrups. The shear span-to-depth ratio, a/d was 4 and the flexural reinforcement ratio, ρ_w, ranged from 0.5% to 1%. Well anchored, non-prestressed, prestressing strands were used as flexural reinforcement to prevent a flexural failure. As found in earlier research, their experimental data shows that the ACI Building Code (3) shear design provisions for v_c are unconservative for members with ρ_w less than one percent. Palaskas et al. (11,34,35) observed that, for their beams, the stirrup shear contributions were about 50% greater than predicted by the ACI Building Code design equation, Eq. 1.4. The added strength was due to the fact that the critical shear cracks were flatter than 45 degrees, the value used in the development of Eq. 1.4, and thus intercepted more stirrups. Based on their experiments, Palaskas et al. (11,34,35) came to the conclusion that, despite the low test values of v_c, the shear provisions of the ACI Building Code (3) are safe for lightly reinforced beams, mainly because of 1) significantly higher values of steel shear capacity actually obtained, and 2) beams with $V_u > \phi V_c/2$ must have minimum shear reinforcement as defined by the code. Largely because of this research, ACI Committee 318 did not adopt Eq. 1.11.

To account for the behavior of continuous beams, Rodrigues and Darwin (38,39,40), extended the research of Palaskas et al. (11,34,35) to lightly reinforced T-beams subjected to negative bending. Test data from nine T-beams with ρ_w equal to 0.47% or 0.70% and with a/d equal to 4 provided further evidence that the ACI (3) equations for V_c and V_s are inaccurate for lightly reinforced beams. In the positive moment regions, the shear cracking load was 13% lower and the stirrup contribution was 50% higher than predicted by the ACI (3) equations, while in the negative moment regions, the shear cracking load 29% lower and the stirrup contribution was 20% higher than the ACI (3) predicted values. In all, the ACI Building Code overestimated the value of the total shear strength in the positive moment regions and

underestimated the total shear strength in the negative moment regions. Rodrigues and Darwin inferred that the smaller effective concrete section at the negative moment region, caused by cracking of the flanges, and lower bond strength for negative flexural reinforcement, due to the top-bar effect, were the causes of the lower shear cracking loads in the negative moment regions. The lower shear reinforcement effectiveness was due to the fact that critical shear cracks were steeper in the negative moment regions and thus intercepted fewer stirrups than in positive moment regions. Rodrigues and Darwin (38,39,40) observed that similar conclusions also could be made about the more heavily reinforced members tested by Haddadin, Hong and Mattock (25).

Al-Nahlawi and Wight (7) tested 25 lightly reinforced, simply supported beams using two point and four point loading systems. Concrete compressive strength ranged from 5600 psi to 10600 psi, with transverse reinforcement, $\rho_v f_{vy}$, varying from 0 to 170 psi. Stirrup spacings of d, 0.75d, 0.5d and 0.33d were used. They observed that for a longitudinal reinforcement ratio, ρ_w, below 1%, Eqs. 1.2 and 1.3 were unconservative. They observed that the conservativeness of Eq. 1.4 for beams with $\rho_v f_{vy}$ = 50 psi decreases as concrete strength increases. The reduced conservativeness of Eq. 1.4 was mainly attributed to diminished aggregate interlock due to smooth failure planes for high strength concrete. Based on their analysis, they recommended a minimum stirrup reinforcement value of:

$$\frac{A_v f_{vy}}{b_w s} \geq \frac{f'_c}{100} \text{ psi} \geq 50 \text{ psi} \qquad (1.13)$$

to counter the effect of diminished aggregate interlock in high strength concrete, and an increase in the maximum stirrup spacing to $0.75d_v$, where d_v is the distance between top and bottom longitudinal steel. The recommendation in Eq. 1.13 closely matches the new provisions in ACI

318-89 for increased minimum shear reinforcement, as described following Eq. 1.5.

1.5 Modified Compression Field Theory

The predictive equations for diagonal tension cracking and shear strength of reinforced concrete beams presented in the preceding sections are based on experimental results. These equations cannot predict the full shear response of a general reinforced concrete member subjected to combined shear and bending, since their use is limited to specific classes of members and they provide only limit loads, with no consideration of member deformation. Obtaining the complete shear response of a member requires a method that accounts for the full range of material and member behavior. The modified compression field theory, presented by Vecchio and Collins (43) in 1986, is the basis of such a method. This theory was expanded from the compression field theory for reinforced concrete in torsion and shear, introduced by Collins and Mitchell (21,22,23).

The modified compression field theory (22,43) uses average stresses and average strains to satisfy equilibrium and compatibility conditions and to formulate stress-strain relationships. It takes into account tensile stresses in the concrete between cracks, and treats the concrete as a new material once cracks form. Experimentally verified average stress-average strain relationships are used for the cracked concrete.

A square membrane element of uniform thickness and relatively small size, representing a part of a reinforced concrete member (Fig. 1.1), is used as an analytical model to predict the shear response (22,43). Reinforcement for the membrane element consists of an orthogonal grid of reinforcement, coinciding with the longitudinal, x, and transverse, y, axes. Loads acting at the element's edges are assumed to consist of uniform axial stresses, f_x and f_y, and uniform shear stress, v_{xy} (Fig. 1.1). The deformed shape of the element is defined by

normal strains, ε_x and ε_y, and the shear strain, γ_{xy} (Fig. 1.2). The complete response of the element is obtained by predicting the three strain values and relating them to the corresponding stresses.

The following assumptions are made while predicting the response of the element, although, in practice, they need all not be completely satisfied to successfully apply the method:

1. For every strain state there exists only one state of stress.

2. Stresses and strains can be considered in terms of average values when areas are large enough to include several cracks.

3. The concrete and the reinforcing bars are perfectly bonded together at the boundaries of the element with no overall slip.

4. The longitudinal and transverse reinforcement is uniformly distributed over the element.

Based on these assumptions, strain compatibility, stress equilibrium and stress-strain relations of steel and concrete are developed. A brief explanation of the stress and strain equations used to predict the shear response of a beam at any state of loading follows (22,43):

Prior to cracking, most of the shear is carried by the concrete by equal diagonal tensile and compressive stresses acting at 45 degrees. After cracking, the tensile stress is substantially reduced, and it varies from zero at the cracks to a peak value between cracks. The average value of the tensile stress is used to formulate the stress equilibrium equations. The principal tensile stress in the concrete acting perpendicular to the crack plane, f_1 (Fig. 1.3), is given by the following equations:

$$f_1 = E_c \varepsilon_1, \qquad \text{if } \varepsilon_1 \le \varepsilon_{cr} \tag{1.14}$$

$$f_1 = \frac{\alpha_1 \alpha_2 f_{cr}}{1 + \sqrt{500\varepsilon_1}}, \quad \text{if } \varepsilon_1 \geq \varepsilon_{cr} \tag{1.15}$$

$$f_1 = v_{ci} \tan\theta + \frac{A_v}{sb_v}(f_{vy} - f_v) \tag{1.16}$$

in which E_c is the modulus of elasticity of concrete; ε_{cr} is the cracking strain of concrete; ε_1 is the principle tensile stress; α_1 and α_2 are factors accounting for the bond characteristics of the reinforcement and taken as unity for deformed bars; f_{cr} is the cracking strength of concrete; v_{ci} is the local shear stress on the crack surface; s is the stirrup spacing; θ is the crack angle; A_v is the area of stirrup reinforcement within a length, s, of the beam; f_{vy} is the yield stress of the stirrup reinforcement; and f_v is the stress in the stirrup reinforcement. The smallest value of f_1 is taken from Eqs. 1.14, 1.15 and 1.16. The ability of the concrete to carry a tensile stress after diagonal cracking is the key difference between the modified compression theory (22,43) and compression field theory (21,22,23,31).

The principal compressive stress in the concrete, f_2 (Fig. 1.3), is derived from the following relationship:

$$f_2 = (\tan\theta + \cot\theta)v - f_1 \tag{1.17}$$

in which v is given by $V/(b_w jd)$; b_w is the web width of the beam; jd is the internal flexural moment arm; and θ is the crack angle. The value of f_2 cannot exceed $f'_c/(0.8+170\varepsilon_1)$.

The unbalanced vertical component of diagonal compressive stresses and diagonal tensile stresses is carried by tension in the web reinforcement. This equilibrium requirement can be expressed as:

$$A_v f_v = (f_2 \sin^2\theta - f_1 \cos^2\theta) b_w s \qquad (1.18)$$

Substituting f_2 from Eq. 1.17 in Eq.1.18 and expressing v in Eq. 1.17 as $V/(b_w jd)$ gives an equation for shear force V for a given principal tensile stress, f_1, and crack angle, θ, as:

$$V = f_1 b_w jd \cot\theta + A_v f_v jd \cot\theta / s \qquad (1.19)$$

Eq. 1.19 expresses the shear resistance of a member as the sum of a concrete contribution and a steel contribution, and, in that way, is similar to the ACI (3,5) nominal shear capacity equation, $V_n = V_c + V_s$. However, it expresses shear resistance as a function of the principal tensile stress in concrete, f_1, the tensile stress in stirrup, f_v, and the crack angle θ, rather than $\sqrt{f'_c}$, and f_y, and an assumed horizontal projection of the crack.

The principal compressive strain, ε_2, is given by the equation:

$$\varepsilon_2 = \varepsilon'_c \left(1 - \sqrt{1 - f_2/f_{2max}} \right) \qquad (1.20)$$

in which ε'_c is the concrete compressive strain at its crushing strength; and f_{2max} represents the peak compressive strength of the concrete under combined biaxial tension-compression and is given by $f'_c/(0.8 + 170\varepsilon_1)$.

The longitudinal strain in the web, ε_x, is given by the equation:

$$\varepsilon_x = \frac{\varepsilon_1 \tan^2\theta + \varepsilon_2}{1 + \tan^2\theta} \qquad (1.21)$$

The strain in the web reinforcement, ε_t, is given by the equation:

$$\varepsilon_t = \frac{\varepsilon_1 + \varepsilon_2 \tan^2\theta}{1 + \tan^2\theta} \qquad (1.22)$$

The stress in the stirrup is checked for yield.

To obtain the shear force in a section at a certain bending moment, equilibrium of forces must be satisfied along the longitudinal axis of the member. The unbalanced longitudinal component of the diagonal concrete stresses, for a certain crack angle and principal tensile stress, is balanced by tensile stresses in the longitudinal reinforcement and compressive stresses in the concrete resulting from bending. This equilibrium condition can be expressed by:

$$A_x f_s + A_c f_c = (f_2 \cos^2\theta - f_1 \sin^2\theta) b_w j d \qquad (1.23)$$

in which $A_x f_s$ is the force in the longitudinal steel and $A_c f_c$ is the force in the concrete (Fig. 1.4). (Note: Tensile stresses are taken as positive, and compressive stresses are taken as negative.) Substituting for the principal compressive stress, f_2, from Eq. 1.17 in Eq. 1.23 gives:

$$A_x f_x + A_c f_c = V \cot\theta - f_1 b_w j d \qquad (1.24)$$

To obtain the forces $A_x f_x$ and $A_c f_c$, the longitudinal strain in the web, ε_x from Eq. 1.21, is assumed to occur at a specific level through the depth of the member. The strain distribution corresponding to the value and location of ε_x and the moment acting at the section is determined using plane section analysis. For members with web reinforcement, ε_x is assumed to occur at

the midheight of the cross section, which results in higher tensile strains at the level of the longitudinal steel and higher compressive strains at the compressive face of the member. The midheight of the section is chosen because of the load redistribution capacity of such members, which results in the shear stresses being transferred from high strain regions of the cross-section to low strain regions. Members that do not contain any web reinforcement have less capacity for redistribution of load, and hence it is reasonable to assume that ε_x occurs at the level of the flexural steel, resulting in smaller tensile and compressive strains.

To obtain the shear, V, and crack angle, θ, for a given moment to shear ratio, at a particular principal tensile strain, ε_1, an estimate of θ is made first. Using Eq. 1.14-1.16, the smallest value of principal tensile stress, f_1, is calculated. The tensile stress in the stirrup reinforcement, f_v, is estimated. The shear, V, corresponding to the chosen ε_1 is then obtained from Eq. 1.19. The principal compressive stress, f_2, is then calculated from Eq. 1.17. The calculated value of f_2 gives the principal compressive stress, ε_2, using Eq. 1.20. The longitudinal strain in the web, ε_x, and the tensile strain in the stirrups, ε_t, are obtained from Eqs. 1.21 and 1.22, respectively. The estimated value of f_v is checked using the calculated value of ε_t and a new estimate is made, if necessary. With the calculated value of ε_x, the strain distribution for the moment corresponding to the given moment to shear ratio is found using plane section analysis. The longitudinal forces at the section $A_x f_x$ and $A_c f_c$ corresponding to this moment are used in Eq. 1.24 to check for equilibrium. A new estimate of θ is made, if required, and the process is repeated. The shear response of the section is obtained by plotting shear, V, versus the principal tensile stress, ε_1. The shear capacity of the section, V_{max}, is the maximum value of shear obtained from this plot.

Detailed procedures for predicting shear capacity and obtaining a shear response of a reinforced concrete member using modified compression field theory are presented in Chapter 3.

1.6 Object and Scope

The purpose of the proposed research is to study the shear strength of truly continuous, lightly reinforced concrete flexural members with deformed bars as flexural steel and to investigate possible modifications to the current design provisions (3). The research includes tests of 6, continuous two-span T-beams, with beam-girder connections, to identify the effects of flexural and shear reinforcement on shear capacity. Flexural reinforcement ratios of 0.75% and 1% and levels of shear reinforcement ranging from 0 psi to 82 psi are used. The results of these tests are compared with predictive equations developed in previous studies and used to evaluate present shear design methods. These tests extend the work of Palaskas et al. (11,34,35) and Rodrigues and Darwin (38,39,40).

Chapter 2

EXPERIMENTAL INVESTIGATION

2.1 General

The experimental investigation was carried out to study the shear strength of continuous T-beams with light flexural reinforcement. Primary emphasis was given to the behavior of the negative moment regions of the beams. Since the ACI Building Code (3) appears to underestimate the shear strength of beams having flexural reinforcement below 1%, negative moment region flexural reinforcement was chosen to be less than or equal to 1%. Shear reinforcement with nominal strengths between 0 psi to 82 psi, i.e. up to 60% above the minimum required by the ACI Building Code, was used. The details of the experimental work are described in the following sections.

2.2 Test Specimens

The specimens were two-span continuous T-beams; each span was 20.5 ft long. To simulate conditions in actual structures, a simply supported transverse girder with a span of 41 in. was provided as the middle support. The test regions in the beams extended from the faces of the transverse girder to the points of maximum positive bending in both spans. The flanges of the T-beams were 24 in. wide and 4 in. thick. The beams were 18 in. deep, with a web thickness of 7.5 in. Concrete cover for the reinforcement followed the provisions of the ACI Code (3). The depth of the transverse girder was increased by 1 in. to provide adequate cover for the bottom steel of that member. Beam dimensions and properties are shown in Figs. 2.1 through 2.3 and Table 2.1.

There were two series of beams, I and J, with negative moment region reinforcement

ratios based on the area of the web, ρ_w, of 1.0% and 0.75%, respectively. For the I series beams, the top longitudinal steel consisted of two No.6 bars and one No.5 bar. For the J series beams, the top longitudinal steel consisted of two No.6 bars. The beams were designed to fail in shear in the negative moment region and, in some cases, to yield in negative bending. To prevent the formation of a mechanism prior to shear failure, adequate bottom steel was provided to insure that the beams did not fail in positive bending. The I series had equal steel at the bottom and the top. The J series had positive moment region ρ_w values of 0.75%, 1%, and 1.83% for beams J-1, J-2 and J-3, respectively. Positive moment region ρ_w values of 0.75% and 1% were provided by the same bars as used in the negative moment regions at the same values of ρ_w, while ρ_w of 1.83% was provided by four No.6 bars and one No.5 bar. In beams I-2, J-2 and J-3, this combination of top and bottom steel allowed for moment redistribution after the formation of a plastic hinge at the middle support.

Class A splices (3) were used to splice the longitudinal steel. Top bars had a splice length of 27 in. and were staggered as far away from the face of the transverse girder as possible to limit congestion of steel in the test region. For the I series, the top-bar splices started 44 in. and, for the J series, 74 in. from the face of the transverse girder.

Bottom bars had a splice length of 19 in. For the I series, the two No. 6 bars were spliced 41 in. and 161 in. from the face of the transverse girder, while the No. 5 bar was spliced 13 in. from the face of the transverse girder. No. 6 bars for beams J-1 and J-2 were spliced 41 in. and 161 in. from the face of the transverse girder. The No. 5 bar of beams J-2 was spliced 13 in. from the face of the transverse girder. The bottom bars for beam J-3 were placed in two layers, with two No. 6 bars and one No. 5 bar in the lower layer and two No. 6 bars in the upper layer. The splices in the lower layer were identical to the splices used for the bottom bars of beam J-2, while those in the upper layer were identical to the splices used for the bottom bars of beam J-1.

Two loading configurations were used for the tests: a single point load per span or two point loads per span. Beams I-1, I-2 and J-1 were subjected to the single point span loading, while beams I-3, J-2 and J-3 were subjected to the two point span loading. The loading systems are described later in the chapter. Typical M/Vd ratios in the negative moment regions of the beams ranged from 3.2 to 3.8. The higher values of M/Vd were obtained in beams tested under single point span loading.

Smooth low carbon steel wire stirrups were used at a spacing of 7 in. to provide nominal shear reinforcement values of 34, 57 and 82 psi and satisfy the ACI Code (3) maximum stirrup spacing requirement of one-half the effective depth of the beam. These stirrups were used only in the test regions. To prevent a shear failure outside of the test region, No. 3 bar stirrups were provided at a spacing of 7 in. The shear force between the two point loads, in case of the beams with two point loads per span, did not require stirrups to carry the shear. In this region, three No. 3 bar stirrups were provided at a spacing of 17.5 in. to hold the longitudinal steel in place. The flanges of the beams were reinforced transversely with No.3 bars spaced at 7 in.

2.3 Materials

2.3.1 Concrete

The air-entrained concrete mixture used to cast the beams was supplied by a local ready-mix plant and was made using Type I portland cement and 3/4 in. nominal maximum size coarse aggregate. Kansas River sand was used as fine aggregate. During casting, air content and slump were measured. The air content ranged between 3 and 4% and the slump measured about 3 in. Standard 6 x 12 in. ASTM C 31-88 (9) compressive test cylinders were cast with each beam

specimen and tested for compressive strength, as per ASTM C 39-86 (10). The compressive strength of the concrete, f'_c, ranged between 4400 psi and 4600 psi. Concrete mixture proportions and properties are presented in Table 2.2.

2.3.2 Steel

ASTM A 615 (8) Grade 60 No. 3, No. 5, and No. 6 deformed billet steel bars were used to reinforce the specimens, except for the shear reinforcement in the test region.

Shear reinforcement in the test region was provided by low carbon smooth wires with diameters of 0.165 and 0.222 in. The targeted values of $\rho_v f_{vy}$ were 25, 50 and 75 psi. Two different types of 0.165 in. diameter wire were used. One of these had to be annealed to lower its yield strength and gave a $\rho_v f_{vy}$ value to 34 psi. As done in a previous research at the University of Kansas (11,34,38), preyielding was necessary to give the other two wires a distinct yield point. However, preyielding results in an increase in the yield strength of the wires with time, due to strain aging. To obtain the actual yield strength of these wires on the day the beams were tested, three specimens of each wire were tested after failure of the beams. The values of $\rho_v f_{vy}$ obtained were 57 and 82 psi. Preyielding was not required for the annealed wires, as they already had a sharp yield point after the annealing processes. Typical stress versus strain curves for test stirrup steel and flexural steel are shown in Fig. 2.4.

2.4 Specimen Preparation

The test stirrups were fabricated in a jig and welded at the top over a lap length equal to the width of the stirrup. The No. 3 bar stirrups were fabricated with 90 degree hooks in a reinforcing bar bender. Typical reinforcement cages used for beams with and without test

stirrups are shown in Figs. 2.1 through 2.3.

Micro-Measurements Type EA-06-060LZ-120 strain gages were used to measure strains in the stirrups and flexural steel. These gages were installed following the procedures used by Palaskas and Darwin (34) and polysulfide encapsulated with Micro-Measurements Type M-Coat J protective coating for protection against water. The gages were located at the mid-height on the test stirrups and at points of maximum bending on the flexure steel. Gage locations are shown in Fig. 2.5.

Waterproof BB plyform was used to construct the forms, which were supported on tables made of 2x4 in. studs. The forms were lacquered before casting each specimen to prevent water damage. After the reinforcing cage was fabricated in place using commercially available ties and steel chairs, and the strain gages were installed, the forms were oiled with form release agent and bolted in place. The lead wires from the strain gages were bound with plastic ties and passed out through holes in the sides of the forms.

A one cubic yard bucket was used to cast the beams in two lifts; first the web and then the flanges. Each layer was vibrated using internal vibrators. The initial and final discharge of concrete from the concrete truck was used to pour the ends of the beams, away from the test region. The test region was poured using concrete from the middle portion of the discharge. The beams were hand screeded longitudinally after which the surface was floated, in the transverse direction, using a magnesium bull float. Concrete samples were taken as per ASTM C 31-88 (9).

Care was taken not to over-finish the surface of the beam so that minimum bleed water was worked into the surface. About an hour was allowed to let the bleed water evaporate from the surface of the beams, after which the beams and the 6 x 12 in. compressive test cylinders were covered with polyethylene sheets. The forms were stripped when the concrete attained a compressive strength of 3000 psi. The beams and the test cylinders were kept moist until a

compressive strength of 4000 psi was attained. The concrete was then allowed to air dry until it attained the test strength of about 4500 psi. Tests were conducted 11 to 19 days after casting.

Diluted white latex paint was applied within the test regions on one side of the beams. All reinforcement locations were marked within this region to aid in establishing where the cracks intersected the reinforcing steel. Stirrup locations were marked in beams without test stirrups for the purpose of providing coordinates for comparison with beams with stirrups.

To measure concrete strains, Precision Type W240-120 paper-backed strain gages were installed on the top and bottom surfaces of the beams, following the procedure used by Palaskas and Darwin (34). Gage locations are shown in Figs. 2.5a and 2.5b..

2.5 Loading System

The test beams were supported at the ends by rollers. The transverse girder, which served as the middle support for the beams, rested on pins at each end. These pins were oriented longitudinally for the transverse girder, thus performing as pin supports for the test beams and partially restrained supports for the girder. A view of the transverse girder with its supports is presented in Fig. 2.6. Two layers of 1/32 in. thick teflon sheets were used between the bearing surfaces of the pin supports to reduce friction.

Two configurations of the loading system were used; one point load per span and two point loads per span. The two point loading system was used on beams I-3, J-2 and J-3. The two point loading was used to reduce positive moment without reducing the shear near the supports. With this lower moment, less positive flexural reinforcement was required to insure that flexural strength would not govern for the beams reinforced with the stronger test stirrups. The two point span loading system also had the advantage of producing M/Vd ratios very close to

that obtained under uniform loading.

The loading systems are shown in Fig. 2.7. Four 1.5 in. diameter steel rods were used to load the beam; two for each span. The rods were strain gaged with full bridges to serve as load cells. Each load rod had a loading capacity of 60 kips.

Two cylindrical compression load cells were used below the supports of the transverse beam to measure reactions. The compression load cells were strain gaged with a full bridge using eight strain gages instead of the usual four. To compensate for eccentric loading, gages diametrically opposite to each other on the load cells were connected in series, and located on each arm of the full bridge.

Hydraulic jacks, located below the structural floor and powered by an Amsler hydraulic testing machine, were used to pull down on the four load rods, which transferred the load to short transverse loading beams. In the single point load system, load was transferred directly to the test beam (Fig. 2.7), but in case of the two point load system, the transverse loading beams rested on bolsters fixed to longitudinal loading beams. The loads were transmitted from the longitudinal loading beam to the test beam by a bolster and a roller (Fig. 2.7).

2.6 Instrumentation

Midspan deflections were monitored using linear variable differential transformers (LVDTs). Concrete and steel strain gage readings and midspan deflections were recorded by a Hewlett-Packard data acquisition system which was remotely controlled by a Hewlett-Packard Vectra PC. The PC also controlled a Hewlett-Packard plotter which recorded the average load versus midspan deflection on a continuous basis. Load and deflection readings were recorded in a disc file and printed out at every load step.

2.7 Test Procedure

The test procedure included an initial elastic test to determine if all equipment was in working order. In this elastic test, the beam was loaded up to 30% of the cracking load, approximately 6 kips total load, and then unloaded. The actual test was then started by taking initial readings of all strain gages and LVDTs at zero total load and then taking the total load up to 6 kips, after which the total load was incremented in steps of 2 kips until failure occurred in the weaker span. At each load step, load, strain and deflection readings were taken while keeping the load constant. Cracks were also marked at each load step, and the total load inscribed at the end of each crack. This was done as quickly as possible to limit the effects of creep.

With the exception of beam I-2, after failure of one of the spans, the beams were unloaded and external stirrups were used to clamp the failed span. The test was then continued. The load was taken up to the load at which the weaker span failed and then incremented in steps of 2 kips until failure of the second span. A test took about three hours. Fig. 2.8 shows the external stirrups.

After completion of the beam test, the concrete cylinders and the stirrup tension specimens were tested.

2.8 Results and Test Observations

Plots of average span load versus average midspan deflection for the beams are shown in Figs. 2.9a-2.9i. The load point and load cell forces at failure are presented in Table 2.3. The values do not account for the weight of the beam but do account for the weight of the load system. The nominal shear forces, V_n(test), and stresses, v_n(test), at failure are presented in Table 2.4. The failure shears correspond to the shear at the face of the middle support at the peak

recorded loads. Typical load-stirrup strain and load-concrete strain plots are shown in Figs. 2.10 and 2.11. Crack patterns for the beams are shown in Fig. 2.12. The bending moment and shear force diagrams for all beams at failure are presented in Figs. 2.13a-2.13m.

As the load was increased, flexure cracks appeared first in sections of maximum bending moment, at the load points and at the center support. At higher loads, the cracks appeared further away from these sections. The cracks began as flexure cracks and, as they were subjected to increasing shear, travelled toward the load points and supports. The angle of crack inclination was flatter, the greater the distance of the starting point from the point of maximum bending. All beams experienced shear failures in the negative shear span, near the girder. The crack patterns for the test beams are shown in Fig. 2.12. Summaries of the loading and failure sequences of the beams follow:

1. Beam I-1: A single point load was used per span. Neither span had shear reinforcement. No positive shear span failures occurred. The east negative shear span failed first, at a shear of 15.3 kips. After clamping the east span with external stirrups, the test was continued. The west negative shear span failed at a shear of 14.9 kips.

2. Beam I-2: A single point load was used per span. Both spans had shear reinforcement, $\rho_v f_{vy}$, of 34.1 psi. The beam failed in shear in the east negative shear span at a shear of 23.5 kips. The test was not continued.

3. Beam I-3: Two point loads were used per span. The west span had shear reinforcement, $\rho_v f_{vy}$, of 33.9 psi, while the east span had no shear reinforcement. The east negative shear span failed at a shear of 16.7 kips. External stirrups were installed on the east span and upon reloading, the west negative shear span failed at a shear of 21.0 kips.

4. Beam J-1: A single point load was used per span. Neither span had shear reinforcement. This beam underwent four shear failures, as external stirrups were used following each of the first three failures. The east positive shear span failed first, at a shear of

12.0 kips. This was followed by failure of the west negative shear span at a shear of 15.0 kips. The third shear failure occured at the west positive shear span at a shear of 14.5 kips. The last shear failure occurred at the east negative shear span at a shear of 14.9 kips.

5. Beam J-2: Two point loads were used per span. The east span had no shear reinforcement, while the west span had shear reinforcement, $\rho_v f_{vy}$, of 34.0 psi. This beam underwent two shear failures. The east shear span failed first, at a shear of 15.5 kips. External stirrups were added and, upon reloading, the west negative shear span failed at a shear of 21.6 kips.

6. Beam J-3: Two point loads were used per span. The east span had shear reinforcement of 57.3 psi, while the west span had shear reinforcement of 82.0 psi. Two shear failures occured. The east negative shear span failed at a shear of 24.6 kips. External stirrips were added and, upon reloading, the west negative shear span failed at a shear of 31.2 kips.

Fewer cracks appeared in the negative shear spans than in the positive shear spans. The initial cracks in the negative shear spans were flexure cracks, which appeared at the top of the flange near the face of the transverse beam and travelled vertically downwards. At higher loads, cracks appeared further away from the face of the transverse beam, extended vertically downwards until they met the web, and then propagated at an angle until they met the face of the transverse girder near the level of the bottom flexural steel. The angle of inclination of the cracks changed gradually and became flatter as a crack approched the face of the transverse girder. When the beams were near shear failure in the negative moment region, a crack would propagate along the bottom of the flange, moving away from the face of the transverse beam, intersecting two or three stirrups before passing diagonally through the flange, causing a shear failure. This is amply illustrated in the east negative shear span of beam J-1 (Fig. 2.12).

Shear failure in a positive shear span was observed only in beam J-1, although shear cracking was observed in positive moment regions on all beams. Cracks in this region first

appeared in the positive moment region at the bottom of the beam. As the loads increased, more cracks appeared at the bottom of the beam. The cracks near the maximum positive moment region propagated vertically and stopped at the base of the flange. The cracks further away propagated at an angle, and moved towards the point of maximum moment, stopping at the base of the flange. The shear cracking loads for the positive moment regions were identified using the same criteria as used for the negative moment regions (discussed in detail in chapter 3). Like the shear failure cracks in the negative shear spans, the failure cracks in the positive shear spans were cracks which started away from the point of maximum positive bending and propagated at a flat angle. After reaching the base of the flange in the maximum moment region, failure crack travelled horizontally and intersected two or three stirrups before passing through the flange to cause failure. This can be seen in the east positive shear span of beam J-1 (Fig. 2.12). Just before shear failure in the positive shear span, some short inclined parallel cracks formed away from the load points at the level of the bottom steel. These cracks can be seen at the positive shear spans of beams J-1 (Fig. 2.12).

From Fig. 2.12, it can be seen that the negative moment regions had fewer cracks than the positive moment regions. The lower number of cracks may be due to lower bond strength of the top-cast flexural reinforcement compared to that of the bottom-cast flexural reinforcement.

Fig. 2.10 shows a typical total load versus stirrup strain curve. Load versus stirrup strain curves initially show no strain, but as cracks appear, the curves show progressively more stirrup strain. The increase in stirrup strain is gradual for flexure cracks, but as the flexure cracks turn into shear cracks, the curves show a sharp increase in strain.

A typical total load versus concrete compressive strain curve is presented in Fig. 2.11. The curve shows low strains initially, but as cracks appear, the slope of the curve increases. The increase results from a reduction in the effective concrete compressive area due to

cracking. At shear cracking, the curves show a reversal in concrete strain as the stresses are redistributed in response to the change in the configuration of the member.

Chapter 3

ANALYSIS OF TEST RESULTS

3.1 General

This chapter contains an analysis of the shear cracking loads and stresses determined from the test results described in Chapter 2. Based on the analysis, the effectiveness of stirrups in carrying shear is estimated. Member shear cracking stresses and failure loads are compared to values predicted by ACI 318-89 (3), ACI-ASCE Committee 426 (6), Batchelor and Kwun (14), Bazant and Kim (16), Rajagopalan and Ferguson (37), and Zsutty (44). Modified compression field theory (18,22,23,43), as introduced in Chapter 1, is used to predict the shear capacity of the test members. Comparisons are made between the predicted values from the modified compression field theory and the measured capacities of the members.

3.2 Determining the Shear Cracking Load

The shear cracking load is often described by investigators (11,28,30,34,35,36,38, 39,40,41) as the load at which diagonal cracks, caused by shear and flexural stresses, cause significant changes in the load carrying mechanisms of a member, resulting in a redistribution of stresses within the beam. Three techniques are used to determine the loads at which shear cracking occurs. The techniques are based on the crack patterns, the stirrup strain, and the concrete strain at the top and bottom of the section. These three techniques are described individually in the following sections.

3.2.1 Crack Pattern Analysis

Several definitions have been proposed to define the shear cracking load based on crack patterns. Haddadin, Hong, and Mattock (25) defined the shear cracking load as the load at which the diagonal tension crack makes an angle of 45 degrees with the transformed neutral axis of the beam. Batchelor and Kwun (14) described the shear cracking load as the load at which an inclined crack extends from the longitudinal tension reinforcement into the compression zone and makes an angle of 45 degrees with the flexural reinforcement.

Palaskas, Attiogbe, and Darwin (11,34,35) defined the shear cracking load as the load at which a shear crack makes an angle of 45 degrees or flatter at, or above, the transformed neutral axis of the beam. Rodrigues and Darwin (38,39,40) extended this definition to continuous beams and defined the shear cracking load as the load at which a diagonal tension crack first makes an angle of 45 degrees or less, at or above the neutral axis in the positive moment region, or at or below the neutral axis in the negative moment region. The current research uses the definition of shear cracking load presented by Rodrigues and Darwin (38,39,40). The crack patterns for the test specimens are shown in Figs. 2.12a and 2.12b.

In the current study, cracks first appeared as flexure cracks at locations of maximum bending moment. These cracks formed first at the top of the flange at the beam-girder intersection in the negative moment region and at the bottom of the web underneath a load point in the positive moment region. As the load was increased, cracks began to form progressively further away from the point of maximum moment. These cracks would then propagate toward the load point in the positive moment region, or toward the support in the negative moment region. For cracks that initiated at points progressively removed from points of maximum moment, the cracks became flatter as they grew due to shear. More cracks were observed in the positive moment region than in the negative moment region. Usually, the negative moment

region would contain only one flexure crack until the time this crack turned flatter than 45 degrees, becoming a shear crack. After this initial shear crack formed, more cracks would appear in the negative moment region. For beams containing stirrups, more load could be carried than in beams without stirrups, resulting in an increase in cracking compared to beams without stirrups. The added cracks in the negative moment region were longer and generally flatter than the initial shear crack.

During a test, the crack locations were marked on the exterior of the beam after each load step, along with the corresponding total load. After failure of the specimen, photographs were taken of the crack patterns. The photographs were used to determine the load at which shear cracking occurred. The shear cracking stress, v_c, was determined by setting v_c equal to $V_c/(b_w d)$. Shear cracking loads and stresses are listed in Tables 3.1 and 3.2, respectively.

3.2.2 Stirrup Strain Analysis

The shear cracking load based on stirrup strain is taken from the load-stirrup strain curves; a typical load-stirrup strain curve is shown in Fig. 2.10. The shear cracking load is defined as the load at which a sharp increase in stirrup strain is observed, indicating that the load carrying mechanisms have changed.

A review of test data typically shows relatively small strains in the stirrups until either a flexure crack or a shear crack intercepts the stirrup. A sharp increase in stirrup strain indicates that a shear crack has intercepted the stirrup, while a gradual increase in stirrup strain indicates that a flexure crack has intercepted the stirrup. A sharp increase is seen because the diagonal tension crack transfers more force to the stirrup than a flexure crack due to the flatter angle of inclination of the diagonal tension crack. Load-stirrup strain curves from gages located in the regions of high moment and shear are analyzed using the above

criterion to determine if shear cracking has occurred.

The method described above to determine the shear cracking load from stirrup strain was used by Rodrigues and Darwin (38,39,40). They found that the shear cracking load obtained from stirrup strain was higher than that obtained from crack patterns for all negative moment cases in their study. However, as shown in Tables 3.1 and 3.2, the current research shows that the shear cracking load obtained from stirrup strain data is lower in eleven out of twelve cases, in both positive and negative moment regions, than that obtained using crack patterns.

3.2.3 Concrete Strain Analysis

The shear cracking load determined using concrete strain data is obtained from strain gages located along the compressive face of the beam. Strain gage locations are shown in Figs. 2.5a and 2.5b. A typical load-concrete strain curve is shown in Fig. 2.11. As the beam is loaded, the concrete strain on the compressive face increases until shear cracking occurs and there is a change in the load carrying mechanisms within the beam. When these load carrying mechanisms change, the stresses are redistributed within the section and stress along the face of the member decreases sharply, sometimes even changing from compression to tension. Because of this, the shear cracking load is taken as the load at which a reduction in the concrete compressive strain occurs. The shear cracking load for a particular region of the beam is based on the strain gage readings from the locations of maximum moment in that region.

This method was used with success by both Rodrigues and Darwin (38,39,40) and Palaskas, Attiogbe, and Darwin (11,34,35). Rodrigues and Darwin observed that the shear cracking load obtained from the concrete strain was greater than or equal to that obtained using crack patterns in ten out of seventeen cases. In the current study, the shear cracking load from

concrete strain is greater than or equal to the shear cracking load obtained from crack patterns in ten out of 22 cases, as is shown in Tables 3.1 and 3.2.

3.3 Comparison of Measured and Predicted Strengths

The results obtained from the current research were combined with the results obtained by Rodrigues and Darwin (38,39,40) and Palaskas, Attiogbe, and Darwin (11,34,35) to have a broader data base from which to work. Values for nominal shear stress and shear cracking stress will be compared with predicted values obtained using equations from other investigators, as well as the current design code, ACI 318-89 (3). Because the beams tested by Rodrigues and Darwin and Palaskas et al. did not use deformed bars for flexural reinforcement, the beams in those studies are expected to have relatively lower shear cracking stresses and shear strengths than the beams in the current study, which use deformed bars as flexural reinforcement. The use of prestressing strands as flexural reinforcement results in a decreased bond strength between the reinforcement and the concrete. This decrease in bond strength causes fewer cracks to form. This is especially true in the negative moment region where the top-bar effect causes the reinforcement to have a lower bond strength than is obtained for bottom-cast bars.

The six beams tested in the present study produced thirteen shear failures, of which eleven were in the negative moment region. Combining this data with the previous research, a total of 35 failures are studied in all. Seventeen of these failures occurred in a negative moment region.

Shear cracking stresses are given in Table 3.2. Rodrigues and Darwin (38,39,40) found that the shear cracking stresses obtained using the crack patterns were lower in most cases than those obtained using the other two methods. They also found that the shear cracking

stresses obtained from crack patterns were higher in the positive moment region than in the negative moment region for five out of eight beams. In the current study, the shear cracking stresses from crack patterns are higher in the positive moment region in half of the twelve cases. In three of these cases, no shear cracking was observed in the positive moment regions. Averaging the shear cracking stresses obtained from crack patterns shows a difference of less than 1% between the average shear cracking stresses in the positive moment regions and negative moment regions. Thus, the current research shows no trend in the level of cracking stress based on the sign of the bending moment. The previous research used prestressing strands for reinforcement, and the earlier analysis results were thought to be conservative because of the lower bond strength of strands compared to deformed reinforcement.

Shear cracking stresses calculated using equations in ACI 318-89 (3), and by ACI-ASCE Committee 426 (6), Batchelor and Kwun (14), Bazant and Kim (16), Rajagopalan and Ferguson (37), and Zsutty (44) are given in Table 3.3. Zsutty's equation, Eq. 1.8, and Bazant and Kim's equation, Eq. 1.12, require a value for the shear span-to-depth ratio. The shear span, a, is approximated by the ratio of the maximum moment to the maximum shear, M/V, in a moment region. Thus, M/(Vd) is used to approximate the shear span-to-depth ratio, a/d. Values for the shear spans in the current research, as well as shear span-to-depth ratios are given in Tables 3.4 and 3.5, respectively. Shear cracking stresses obtained in this study using the three methods are compared with the values obtained from the equations in Tables 3.6 through 3.8 and Figs. 3.1 through 3.6.

The calculated values of the shear cracking stresses are compared with the measured values of the positive moment region shear cracking stresses obtained from the three analysis techniques in Tables 3.6a, 3.7a, and 3.8a. The shear cracking stress, normalized against concrete compressive strength, $v_c/\sqrt{f'_c}$, is plotted versus the longitudinal reinforcement ratio in Figs. 3.1, 3.2, and 3.3. These figures include lines representing the equations in ACI 318-

89 (3), and by ACI-ASCE Committee 426 (6), Batchelor and Kwun (14), and Rajagopalan and Ferguson (37). The comparisons with the lowest coefficients of variation in the positive moment region were those comparisons made using crack pattern analysis to determine the shear cracking load. Therefore, the comparisons that follow are taken from Table 3.6a, which compares shear cracking stresses obtained from crack patterns to various predictive equations described in Chapter 1.

For the positive moment regions, the average measured shear cracking stress is 90% of the value predicted by ACI 318-89 (3) in Eq. 1.2. The coefficient of variation is 20.8%. The average measured cracking stress is 87%, 90%, and 93% of the values predicted by Zsutty (44), ACI-ASCE 426 (6), and Bazant and Kim (16), respectively. The corresponding coefficients of variation are 11.7%, 12.9%, and 12.4%. The average cracking stress is 101% and 103% of the stresses predicted by Rajagopalan and Ferguson (37) and Batchelor and Kwun (14), respectively, with coefficients of variation of 14.0% and 11.0%.

For the negative moment regions, the calculated values of the shear cracking stresses are compared to the measured values of the shear cracking stresses obtained from the three analysis techniques in Tables 3.6b, 3.7b, and 3.8b. The concrete shear cracking stress in the negative moment regions, normalized against concrete compressive strength, $v_c/\sqrt{f'_c}$, is plotted versus reinforcement ratio, ρ_w, for the three methods of shear crack analysis in Figs. 3.4, 3.5, and 3.6. The comparisons made using the shear cracking load determined from crack patterns once again have the lowest coefficients of variation. Therefore, the comparisons that follow are taken from Table 3.6b, which compares shear cracking stresses in the negative moment regions obtained from crack patterns to the predicted results.

For the negative moment region, the average measured shear cracking stress is 91% of the value predicted by ACI 318-89 (3) in Eq. 1.2. The coefficient of variation is 8.4%. The average measured cracking stress is 93% and 99% of the values predicted by Zsutty (44) and

ACI-ASCE 426 (6), respectively, with coefficients of variation of 7.8% and 12.4%. The average cracking stress is 109%, 117%, and 102% of the stresses predicted by Rajagopalan and Ferguson (37), Batchelor and Kwun (14), and Bazant and Kim (16), respectively. The corresponding coefficients of variation are 12.0%, 12.9%, and 8.8%.

The ratios of measured cracking stresses to calculated cracking stresses are averaged for both the negative and positive moment regions in Tables 3.6b, 3.7b, and 3.8b. Overall, the average measured cracking stress is 91% of the stress predicted by ACI 318-89 (3) in Eq. 1.2. The coefficient of variation is 14.5%. The average cracking stress is 90%, 95%, and 98% of the values predicted by Zsutty (44), ACI-ASCE 426 (6), and Bazant and Kim (16), respectively, with coefficients of variation of 9.6%, 13.1%, and 10.9%. The average cracking stress is 105% and 111% of the values predicted by Rajagopalan and Ferguson (37) and Batchelor and Kwun (14), respectively, with coefficients of variation of 13.0% and 13.5%.

The comparisons made using shear cracking stresses obtained from crack patterns in Tables 3.6a and 3.6b show that comparisons made in the negative moment regions have lower coefficients of variation than the same comparisons made in the positive moment regions. Higher coefficients of variation in the positive moment regions indicate more scatter with respect to the predictive equations. The greater scatter is likely due to the widely varying shear span-to-depth ratios in the positive moment regions, which are not accounted for by Eqs. 1.2, 1.7, 1.10, and 1.11. Eqs. 1.8 and 1.12 do account for varying M/(Vd) ratios, but are not valid for the full range of M/(Vd) ratios, 1.60 to 3.83, obtained in the positive moment regions. The values for shear span-to-depth ratios in the negative moment regions ranged only from 3.28 to 3.81. Another interesting contrast between the positive and negative moment regions is that in the positive moment region, comparisons to the ACI 318-89 (3) equation, Eq. 1.2, show the highest coefficients of variation for any comparison made. This is true for all methods of determining shear cracking load in the positive moment regions. In the negative moment

regions, however, the coefficients of variation for comparisons made to Eq. 1.2 are lower than almost all other comparisons, regardless of the method used to determine the shear cracking load. For the combined negative and positive moment regions, the coefficient of variation for comparisons to Eq. 1.2 is the highest of any comparison. The comparison with the lowest coefficient of variation for the combined moment regions is the comparison made to Zsutty's Eq. 1.8.

3.3.1 Stirrup Effectiveness

As the load is increased above the shear cracking load, additional load is carried by the stirrups. Thus, the increase in total shear stress, v_n, beyond the shear cracking stress, v_c, can be used as a measure of the effectiveness of the shear reinforcement. The shear reinforcement effectiveness, $v_n - v_c$, includes the shear stress carried by the stirrups, as well as the shear stress carried by dowel action and aggregate interlock. The values of shear reinforcement effectiveness from this study, as well as those from Rodrigues and Darwin (38,39,40) and Palaskas, Attiogbe, and Darwin (11,34,35), are presented in Table 3.9.

The evaluation of stirrup effectiveness for beams in the current study is based on failures in the negative moment region, because only two failures were observed in the positive moment region and both of these failures occurred in beam J-1 which had no stirrups. The shear reinforcement effectiveness is plotted versus the nominal stirrup capacity, $\rho_v f_{vy}$, for the current research, in Fig. 3.7. Using regression analysis, the relationship for shear reinforcement effectiveness in terms of nominal stirrup capacity is:

$$v_n - v_c = 1.35\rho_v f_{vy} + 12.26 \qquad (3.1)$$

with a correlation coefficient, r, of 0.87. This relationship is obtained considering only those beams which contained stirrups.

Rodrigues and Darwin (38,39,40) performed a regression analysis on the negative moment region data from their research and found the following relationship:

$$v_n - v_c = 1.19\rho_v f_{vy} + 4.70 \qquad (3.2)$$

with a correlation coefficient, r, of 0.96.

The test results for the eleven negative moment region failures are combined with the negative moment region failure results obtained by Rodrigues and Darwin (38,39,40). This data is plotted in Fig. 3.8. A regression analysis of the combine data yields the following relationship:

$$v_n - v_c = 1.28\rho_v f_{vy} + 8.28 \qquad (3.3)$$

with a correlation coefficient, r, of 0.89.

It can be seen from this analysis that, overall, the contribution of shear reinforcement to shear strength is approximately 30% greater in the negative moment regions of the beams studied than predicted by Eq. 1.4 from ACI 318-89 (3).

Care must be taken when grouping these two sets of results together because of the differences in the two studies. The correlation coefficients from the regression analyses show that the scatter in the data was small. The line which is fit for the data from Rodrigues and Darwin (38,39,40) has a lower slope than the line based on the results from the current study. This shows that the study by Rodrigues and Darwin did indeed give conservative results compared to regular reinforced concrete members. This is expected because of the differences

in the two studies. The use of lower reinforcement ratios and prestressing strands as flexural reinforcement by Rodrigues and Darwin cause the section to experience more flexural tensile strain than if a higher reinforcement ratio and deformed bars had been used. The higher strain results in steeper shear cracks. The steeper cracks intercept fewer stirrups, and thus the stirrup contribution to shear strength is less.

For the positive moment region, the test results of Rodrigues and Darwin (38,39,40) and Palaskas, Attiogbe, and Darwin (11,34,35) were combined. The linear regression analysis for the combined data shows that the web reinforcement in the positive moment region was 59% more effective than predicted by ACI 318-89 (3) using Eq. 1.4. The higher than predicted stirrup contribution was obtained for beams using prestressing strands as flexural reinforcement which yields a more conservative shear strength. Rodrigues and Darwin (38,39,40) concluded this difference in shear reinforcement contribution between the positive and negative moment regions could be due to the top bar effect. It is not clear if this behavior would be observed for the beams in the current study since no beams with stirrups failed in the positive moment region.

3.3.2 Horizontal Crack Projection

The differences observed in the stirrup contributions in the negative and positive moment regions are due to the differences in the horizontal projection of the critical shear crack, defined as the shear crack which causes the failure of the beam. ACI 318-89 (3) predicts the stirrup contribution to shear strength in Eq. 1.4 based on the assumption that the horizontal crack projection is equal to the effective depth of the beam, d. Table 3.10 shows that the horizontal projection of the critical shear crack is greater in the positive moment region than in the negative moment region for the combined results of Rodrigues and Darwin

(38,39,40), Palaskas, Attiogbe, and Darwin (11,34,35) and the current study.

The average horizontal projection of the critical shear crack in the negative moment region from the current research is 1.38d. Rodrigues and Darwin (38,39,40) observed an average horizontal projection of the critical shear crack in the negative moment region of 1.0d. Differences in the type of flexural reinforcement used, as well as differing shear span-to-depth ratios likely caused the differences in the horizontal crack projections. When the results of the current research are combined with results from the research of Rodrigues and Darwin (38,39,40), the average horizontal projection of the critical shear crack in the negative moment region is 1.23d. The average horizontal critical shear crack projection in the positive moment region from Rodrigues and Darwin (38,39,40) and Palaskas, Attiogbe, and Darwin (11,34,35) (the current research did not experience any positive moment region failures in beams containing stirrups) is 1.74d.

Rodrigues and Darwin (38,39,40) observed that the positive moment region had a longer horizontal crack projection due to a shallower crack angle and the fact that the crack propagates along the underside of the flange before it enters the flange. Because of this longer horizontal crack projection, more stirrups are intercepted by the critical crack. Therefore, the stirrups take more load, and the stirrup effectiveness, $v_n - v_c$, is greater in the positive moment region. In the current study, the critical shear cracks in the negative moment region also propagated along the flange-web intersection as the beam approached failure. This explains the relatively greater negative moment region stirrup effectiveness observed in the current research than observed in the research of Rodrigues and Darwin (38,39,40).

The increase in shear stress at ultimate above the shear cracking stress, $v_n - v_c$, measures the amount of shear carried by dowel action and aggregate interlock, as well as that carried by the stirrups. The shear stress carried by the stirrups alone can be expressed as

$$v_{si} = nA_v f_{vy}/b_w d \qquad (3.4)$$

in which n = number of stirrups intercepted by the critical shear crack. It is the number of stirrups intercepted, not the horizontal projection of the crack, that actually determines the stirrup contribution to shear strength.

Because the number of stirrups which the critical shear crack intercepts is known based on the crack maps, Figs. 2.12a and 2.12b, it is possible to calculate the shear carried by the stirrups, v_{si}. These values are presented in Table 3.10.

A regression analysis performed on the negative moment results from the current research gives the relationship between v_{si} and nominal stirrup capacity, $\rho_v f_{vy}$ as:

$$v_{si} = 1.23\rho_v f_{vy} + 7.97 \qquad (3.5)$$

with a correlation coefficient, r, of 0.97. These results are illustrated in Fig. 3.9.

Eq. 3.5 contrasts with the results obtained by Rodrigues and Darwin (38,39,40) in the negative moment region:

$$v_{si} = 1.00\rho_v f_{vy} - 6.00 \qquad (3.6)$$

with a correlation coefficient, r, of 0.96.

The regression analysis performed by Rodrigues and Darwin (38,39,40) based on their data for the positive moment region resulted in a relationship:

$$v_{si} = 1.41\rho_v f_{vy} - 4.2 \qquad (3.8)$$

with a correlation coefficient, r, of 0.99.

The relationship for the positive moment region in Eq. 3.8 shows that approximately 40% more stirrups were intercepted by the critical shear crack than predicted by Eq. 1.4, ACI 318-89 (3). The relationship from the results of Rodrigues and Darwin (38,39,40) show that the number of stirrups intercepted by the critical shear crack in the negative moment region is approximately equal to the number predicted by Eq. 1.4. The relationship from the current study shows that approximately 23% more stirrups were intercepted in the negative moment region than predicted by Eq. 1.4. These percentages contrast with what might be higher expected values based on the horizontal projections of the cracks. Clearly, crack projection alone is not a reliable guide to the contribution of shear reinforcement to shear strength.

3.3.4 Nominal Shear Stress

The measured nominal shear stresses, v_n(test), from the current research and for the six beams with negative moment region shear failures from the study by Rodrigues and Darwin (38,39,40) are compared to the calculated nominal shear stresses based on ACI 318-89 (3), v_n(ACI), in Table 3.11 and Figs. 3.10 and 3.11. ACI 318-89 (3) is unconservative in approximately half of the comparisons in the negative moment region. Of the beams with stirrups, four out of ten had a nominal shear capacity below that predicted by ACI 318-89 (3). The four spans with the measured nominal shear strength in the negative moment region less than that predicted by ACI 318-89 (3) for those beams with stirrups were all tested by Rodrigues and Darwin (38,39,40). All beams with stirrups in the current study failed at a higher load than predicted by ACI 318-89 (3). This contrast once again points to the differences between the current study and the study performed by Rodrigues and Darwin (38,39,40). In addition to the use of deformed bars as flexural reinforcement for the current

research compared to the use of prestressing strands by Rodrigues and Darwin (38,39,40), the beams in the current study were statically indeterminate with a varying shear span-to-depth ratio due to moment redistribution, while Rodrigues and Darwin tested statically determinate beams with a constant shear span-to-depth ratio. Rodrigues and Darwin also tested beams with lower flexural reinforcement ratios, which should give even lower nominal shear strengths.

For the negative moment region, Rodrigues and Darwin (38,39,40) obtained an average of $v_n(test)/v_n(ACI)$ equal to 0.91, with a coefficient of variation of 8.4%. The average value of $v_n(test)/v_n(ACI)$ in the negative moment region for beams from the current study is 1.04 with a coefficient of variation of 9.5%. For beams with stirrups, the average of $v_n(test)/v_n(ACI)$ in the negative moment region is 1.13 with a coefficient of variation of 7.0% for beams in the current study, and 0.89 with a coefficient of variation of 11.0% for beams tested by Rodrigues and Darwin (38,39,40). The results of the current study indicate that ACI 318-89 (3) adequately predicts the nominal shear capacity of the beams studied. However, ACI 318-89 (3) does not appear to adequately predict the nominal shear capacity in the negative moment regions of the beams tested by Rodrigues and Darwin (38,39,40). This disagreement is due to the differences between the two studies, discussed previously. The beams with the lowest relative strengths in the Rodrigues and Darwin study had reinforcement ratios, ρ_w, of only 0.47%, considerably lower than the low value of 0.75% used in the current study.

Rodrigues and Darwin (38,39,40) found that the average value of $v_n(test)/v_n(ACI)$ in the positive moment region for all beams was 1.04, with a coefficient of variation of 9.3%. Rodrigues and Darwin (38,39,40) found that the ACI provisions were conservative for twelve of the eighteen beams with positive moment region shear failures. For those beams with stirrups, Rodrigues and Darwin (38,39,40) found that the ACI provisions were conservative in eleven of fourteen positive moment region cases. The average value of $v_n(test)/v_n(ACI)$ in the positive moment region for those beams with stirrups was 1.07 with a coefficient of variation

of 8.4%.

Both positive and negative moment regions with $\rho_w \leq 1.0\%$ have been shown to have a shear cracking stress that is less than that predicted by ACI 318-89 (3) in Eq. 1.2. However, the actual stirrup contribution determined from testing is greater than that predicted by ACI 318-89 (3) in Eq. 1.4 due to a critical shear crack that is flatter than assumed. This higher-than-predicted stirrup contribution appears to compensate for the lower concrete shear capacity in both the negative and positive moment regions.

3.3.5 Other Observations

In order to visualize the effects of ρ_w on the nominal shear capacity of reinforced concrete beams in the negative moment region, v_n is normalized to eliminate the effects of concrete strength using the following equation (38):

$$v_n(norm) = v_c(test)\sqrt{(4000/f'_c)} + [v_n(test) - v_c(test)] \qquad (3.9)$$

Eq. 3.9 normalizes the portion of v_n which is dependent of concrete strength, v_c, to a concrete compressive strength of 4000 psi.

$v_n(norm)/\sqrt{4000}$ is plotted versus $\rho_v f_{vy}$ in Fig. 3.12. This figure illustrates that, for each beam configuration and failure region, stirrup effectiveness increases with increasing ρ_w. This is seen by observing that the slopes of the best fit lines for each group of tests increase with increasing reinforcement ratio. The nominal shear strengths of the beams increase with increasing ρ_w. The best fit lines for the current research lie well above the best fit lines obtained using the negative moment region data of Rodrigues and Darwin (38,39,40).

Fig. 3.12 can be used to evaluate the ACI minimum shear reinforcement requirements

($\rho_v f_{vy}$ = 50 psi). The lines shown on Fig. 3.12 are best fit lines for the normalized data of each group of specimens representing different reinforcement ratios from the tests of the current study and the combined results of Palaskas, Attiogbe, and Darwin (11,34,35) and Rodrigues and Darwin (38,39,40). Fig. 3.12 illustrates that beams without stirrups have a nominal shear capacity of less than $2\sqrt{f'_c}$. However, the nominal shear capacity of beams with no stirrups is above $\sqrt{f'_c}$, the effective usable shear strength of beams without stirrups (3). The results in Fig. 3.12 indicate that the use of as little as 26 psi of shear reinforcement will raise the nominal shear capacity, v_n, to $2\sqrt{f'_c}$ for all beams with $\rho_w \geq 0.47\%$. Fig. 3.12 shows that if minimum shear reinforcement, $\rho_v f_{vy}$ = 50 psi, is used, the nominal shear capacity of the concrete, v_c, is safely predicted by ACI 318-89 for both the negative and the positive moment regions.

To look at the overall ability of ACI 318-89 (3) to predict the nominal shear capacity of the test specimens, the best fit lines from Fig. 3.12 are divided by the nominal shear strength predicted by ACI 318-89 (3) and plotted versus the nominal stirrup capacity, $\rho_v f_{vy}$, in Fig. 3.13. The first observation made about Fig. 3.13 is that for the beams with ρ_w = 0.47% in the negative moment region (38), ACI 318-89 (3) will never predict an adequate shear strength, no matter how much shear reinforcement is used. This is also true for ρ_w = 0.70% in the negative moment region. These two reinforcement ratios come from the test results of Rodrigues and Darwin (38,39,40) which have already been shown to behave differently than the beams in the current research. The negative moment region data from the current research shows that ACI 318-89 (3) safely predicts the shear capacity when shear reinforcement is provided. This is seen quite easily by observing the upward slope of the curve for the beams with reinforcement ratios of 0.75% and 1.0%. These curves cross the line representing $v_n(\text{norm}) = v_n(\text{ACI})$ at $\rho_v f_{vy} < 10$ psi.

3.4 Modified Compression Field Theory

Two procedures were developed using the modified compression field theory (18,22,23,43), MCFT, to predict the shear capacity of the test beams. These procedures are outlined in this section. The first procedure, called the response procedure, gives the full force-stress-strain response of the member subjected to moment and shear. The procedure uses an iterative process to reach a solution. The second procedure, called the design procedure, is based on the response procedure; however, simplifying assumptions are made which allow the use of design tables presented by Collins and Mitchell (22) to obtain the shear capacity of the member. The design procedure is also iterative, but is simpler than the response procedure.

3.4.1 Response Procedure Using MCFT

The relationships from the modified compression field theory, presented in Chapter 1, are used to obtain the shear response of a member. The shear response is expressed in terms of principal tensile strain, ε_1, and the shear force corresponding to ε_1. Values of ε_1 are gradually increased to obtain the behavior. With the exception of those steps marked with an asterisk, *, the iterative procedure used to obtain the response is as outlined by Collins and Mitchell (22). The additions to the steps outlined in reference 22 were made because additional information was needed to perform the analysis, which was not specifically addressed in the steps outlined (22). The procedure is :

Step 1: Choose a value of ε_1 at which to find the corresponding shear, V.

Step 2: Make an estimate of the crack angle, θ.

Step 3: Calculate crack width, w, from:

$$w = \varepsilon_1 s_{m\theta} \tag{3.10}$$

in which $s_{m\theta}$ is the crack spacing parameter, defined as:

$$s_{m\theta} = 1/\left(\frac{\sin\theta}{s_{mx}} + \frac{\cos\theta}{s_{mv}}\right) \tag{3.11}$$

in which s_{mx} and s_{mv} are crack spacings along the longitudinal and shear reinforcement and are defined as:

$$s_{mx} = 2\left(c_x + \frac{s_x}{10}\right) + 0.25k_1\frac{d_{bx}}{\rho_x} \tag{3.12}$$

$$s_{mv} = 2\left(c_v + \frac{s}{10}\right) + 0.25k_1\frac{d_{bv}}{\rho_v} \tag{3.13}$$

in which c_x is the vertical distance from the neutral axis of the uncracked section to the inside edge of the tension steel,

c_v is the horizontal distance from the center of the web to the inside edge of the stirrup,

d_{bx} is the diameter of the longitudinal steel,

d_{bv} is the diameter of the stirrups,

s_x is the horizontal clear space between the longitudinal bars,

s is the stirrup spacing,

$\rho_x = A_s/A_c$, and

k_1 is 0.4 for deformed bars and 0.8 for smooth bars.

Step 4: Estimate the stress in the stirrups, f_v.

Step 5: Calculate the principal tensile stress, f_1, from Eqs. 1.14, 1.15, and 1.16, using the smallest value.

Step 6: Calculate the shear load on the section, V, using Eq. 1.19.

in which the flexural lever arm, jd, is determined from section equilibrium as:

$$jd = \frac{d - (M/jd - V_u \cot\theta)}{1.70 f'_c b} \qquad (3.14)$$

Step 7: Calculate the principal compressive stress, f_2, from Eq. 1.17. If f_2 exceeds f_{2max} presented in Chapter 1, the iteration is terminated because ε_1 is too large.

Step 8: Calculate the principal compressive strain, ε_2, from Eq. 1.20.

Step 9: Calculate the longitudinal strain in the web, ε_x, using Eq. 1.21, and the strain in the web reinforcement, ε_t, using Eq. 1.22. Note, ε_x is calculated at the midheight for members which contain stirrups, and at the level of the tension steel in members which contain no stirrups.

Step 10: Calculate $f_v = \varepsilon_t E_s \leq f_{vy}$

Step 11: Check to see if the calculated value of f_v in step 10 equals the value of f_v estimated in step 4. If it does not, go back to step 4 and revise the estimate of f_v.

Step 12*: Find axial forces due to the moment which occurs at the shear, V, calculated in step 6. This is done using moment-curvature relationships in the following procedure:

Step 12a*: Set moment equal to the shear, V, times the ratio M/V. This ratio will be constant throughout the loading of the beam for these cases, and is dependant upon the loading and beam geometry.

Step 12b*: Assume a linear strain distribution across the concrete section, and choose a strain at the extreme compressive fiber of the concrete, ε_{ct}.

Step 12c*: The distribution of compressive stress in the concrete can be represented by an equivalent stress block with an average stress of $\alpha_1 f'_c$ and a depth of $\beta_1 c$, in which c is the distance from the extreme compressive fiber to the neutral axis of the section. The equations used for β_1 and $\alpha_1\beta_1$ are:

$$\beta_1 = \frac{4 - \frac{\varepsilon_{ct}}{\varepsilon_0}}{6 - 2\frac{\varepsilon_{ct}}{\varepsilon_0}} \qquad (3.15)$$

$$\alpha_1\beta_1 = \frac{\varepsilon_{ct}}{\varepsilon_0} - \frac{1}{3}\left(\frac{\varepsilon_{ct}}{\varepsilon_0}\right)^2 \qquad (3.16)$$

in which ε_0 is the strain at f'_c.

Step 12d*: Calculate the distance from the compression face to the neutral axis, c, using the flexural lever arm, jd, calculated in step 6.

$$c = (d - jd/2) - x \quad \text{(for beams with stirrups)} \qquad (3.17a)$$

$$c = d - x \quad \text{(for beams without stirrups)} \qquad (3.17b)$$

in which x is the distance from the point where ε_x is measured to the neutral axis and is given by:

$$x = \frac{\varepsilon_x(d - jd/2)}{\varepsilon_x + \varepsilon_{ct}} \quad \text{(for beams with stirrups)} \qquad (3.18a)$$

$$x = \frac{\varepsilon_x d}{\varepsilon_x + \varepsilon_{ct}} \quad \text{(for beams without stirrups)} \qquad (3.18b)$$

Step 12e*: Calculate the tension force, T, and compression force, C, in the concrete.

$$T = \varepsilon_s E_s A_s \leq A_s f_y \qquad (3.19)$$

in which ε_s is the strain in the tension steel, which is given by:

$$\varepsilon_s = \varepsilon_{ct}\frac{d - c}{c} \quad \text{(for beams with stirrups)} \qquad (3.20a)$$

$$\varepsilon_s = \varepsilon_x \quad \text{(for beams without stirrups)} \qquad (3.20b)$$

and

$$C = \alpha_1\beta_1 b_w c f'_c \qquad (3.21)$$

Step 12f*: Calculate the moment about the point that is jd/2 from the tensile steel.

$$M = T(jd/2) + C\left(d - jd/2 - \frac{\beta_1 c_1}{2}\right) \qquad (3.22)$$

The moments due to f_1 and V are equal to zero about this point due to the symmetry of these forces in the cross-section.

Step 12g*: Check to see if the moment in step 12f equals the moment obtained in step 12a. If

not, go back to step 12b and choose a new ε_{ct}.

Step 13*: Calculate the net axial load, N, at the cross-section using:

$$N = T + f_1 b_w jd - (C + V\cot\theta) \qquad (3.23)$$

Step 14: Check to see if the section is in equilibrium, N=0. If not, return to step 2 and reestimate θ. If N does equal zero, then the shear calculated in step 6 corresponds to the value of ε_1 chosen in step 1. To obtain the entire response for the member, return to step 1 and choose a new ε_1.

Once a complete response is obtained, the nominal shear capacity of the member is taken as the peak shear attained on the response curve. A typical beam response is given in Table 3.12, and a typical response curve is shown in Fig. 3.14.

3.4.2 Design Procedure Using MCFT

The design procedure is based on the response procedure. As presented by Collins and Mitchell (22), the design procedure uses several assumptions to develop a design table which can be used to predict the capacity of a member. Portions of the design tables developed by Collins and Mitchell are given in Table 3.13. These tables were developed using the assumptions that the maximum size of aggregate, used to calculate v_{si} in Eq. 1.16, is 0.75 inches and, for the beams with stirrups, $s_{m\theta}$ is equal to 12 inches. For all beams, ε_x is taken at the level of the flexural reinforcement. These assumptions are made to give conservative results. The design procedure is an iterative process and proceeds as follows for a fixed value of M/V = r:

Step 1: Estimate the nominal shear capacity, V_n, and the crack angle, θ.

Step 2: Calculate the height of the compressive stress block, a. The following equation is

used for the current study:

$$a = \frac{V_u\left(\frac{r}{jd} - \cot\theta\right)}{0.85f'_c b} \qquad (3.24)$$

in which jd = d - a/2.

Step 3: Calculate ε_x using the equation given by Collins and Mitchell (22):

$$\varepsilon_x = \frac{V_u\left(\frac{r}{jd} - 0.5\cot\theta\right)}{E_s A_s} \qquad (3.25)$$

$$\varepsilon_x \leq f_y/E_s$$

Step 4: For beams with stirrups, calculate v/f'_c, in which $v = V_n/(b_w jd)$.

Step 5: Use the design tables to determine β and θ. Partial listings of the design tables are shown in Table 3.13.

Step 6: Determine the nominal shear capacity of the member using the following equations:

$$V_n = V_c + V_s \qquad (3.26)$$

In which,

$$V_c = \beta\sqrt{f'_c}\, b_w jd \qquad (3.27)$$

$$V_s = \rho_v f_{vy} b_w jd\cot\theta \qquad (3.28)$$

Step 7: Compare the V_n and θ from step 7 to the V_n and θ estimated in step 1. If they are not equal, go back to step 1 and reestimate V_n and θ.

This procedure continues until the V_n and θ estimated match those which are obtained from the tables. This procedure gives the nominal shear capacity of the member, not a full shear response of the member.

3.4.3 Comparison of Results

Tables 3.14 and 3.15 compare the nominal shear capacities of the beams from the current study with the nominal shear capacities predicted using the two MCFT procedures.

When using the response procedure, the average value of $v_n(test)/v_n(MCFT)$ for all beams from the current study is 1.26, with a coefficient of variation of 11.8%. For beams without stirrups the average is 1.31, with a coefficient of variation of 7.6%, while for beams with stirrups, the average value of $v_n(test)/v_n(MCFT)$ is 1.18, with a coefficient of variation of 16.1%. A plot of $v_n(test)$ versus $v_n(MCFT)$ is shown in Fig. 3.15. This plot shows that the difference between the level of the predicted and test strengths is relatively constant for the response procedure, i.e. the data points lie roughly parallel to the $v_n(MCFT)=v_n(test)$ line. The modified compression field theory, as used in the response procedure, appears to be quite conservative when applied to all beams from the current study. Although the response procedure predicts the nominal shear capacities of beams which contain stirrups better than beams which contain no stirrups [in terms of $v_n(test)/v_n(MCFT)$], the predicted values for beams containing stirrups are still quite conservative.

A modification can be made to step 3 of the response procedure by using $k_1 = 0.4$ instead of $k_1 = 0.8$. This represents an increased bond strength between the stirrups and the concrete. Table 3.14 shows the results obtained from the current research using this modification. For beams with stirrups, the average value of $v_n(test)/v_n(MCFT)$ drops slightly with this modification; 1.15 is obtained for $k_1 = 0.4$ compared to 1.18 for $k_1 = 0.8$. Changing the bond strength of the stirrups to the concrete has only a small effect on the predicted results, especially for beams with a flexural reinforcement ratio of 0.75%, as seen in Table 3.14.

The horizontal projection of the critical shear crack predicted by the modified compression field theory is a measure of the predicted stirrup contribution to shear strength.

Fig. 3.16 compares the horizontal projection of the critical shear crack measured after testing (Table 3.10) and the horizontal projection obtained using the response procedure (k_1 = 0.8), listed in Table 3.14. The average experimental horizontal critical shear crack projection for beams containing stirrups in the current study is 1.38d. The average predicted critical shear crack projection for the same beams is 1.11d. As shown in Fig. 3.16, the horizontal projection of the critical shear crack predicted by the response procedure is less than the measured horizontal projection for all but one of the beams (beam I-3, west span) from the current study. The difference between the measured and predicted horizontal projection of the critical shear crack shows that the response procedure underestimated the stirrup contribution for most of the beams in this study.

The results obtained using the response procedure can be compared to the values of nominal shear capacity predicted by ACI 318-89 (3), for the beams in the current study. The values of nominal shear capacity predicted by ACI 318-89, and comparisons of these values to the experimental shear capacities are given in Table 3.16 for all beams in the current study. This table contains the same information as Table 3.11, plus the two positive moment region failures from beam J-1. For all of the beams in the current study, the average value of $v_n(test)/v_n(ACI)$ is 1.01, compared to the average value of $v_n(test)/v_n(MCFT)$, 1.26. The coefficient of variation obtained for $v_n(test)/v_n(ACI)$ is 12.4% compared to 11.8% for $v_n(test)/v_n(MCFT)$. For beams in the current study containing stirrups, the average value of $v_n(test)/v_n(ACI)$ is 1.13, with a coefficient of variation of 7.0%, compared to an average value of $v_n(test)/v_n(MCFT)$ of 1.18, with a coefficient of variation of 16.1%. For beams in the current study which contain no stirrups, the average value of $v_n(test)/v_n(ACI)$ is 0.94, with a coefficient of variation of 9.0%, while the average value of $v_n(test)/v_n(MCFT)$ is 1.31, with a coefficient of variation of 7.6%.

Overall, the comparisons made between the modified compression field theory response

procedure and ACI 318-89 (3) show that ACI 318-89 predicts the nominal shear strength of the beams in the current study better than the MCFT response procedure. It should be noted that the comparisons made above represent only thirteen failures of lightly reinforced beams, and therefore do not represent a comprehensive comparison between ACI 318-89 (3) and the MCFT response procedure.

Next, the results obtained with the MCFT design procedure are compared with the test results. The nominal shear capacities, as well as the horizontal crack projections, predicted by the design procedure for the beams from the current study are listed in Table 3.15.

Comparisons are made between the experimental and predicted nominal shear capacities. A plot of v_n(test) versus v_n(MCFT) is shown in Fig. 3.17. This plot shows that as nominal shear strength increases, the difference between the predicted and test strengths also increases, i.e. as nominal shear strength increases, the data points shift farther above the line representing v_n(MCFT)=v_n(test). The average value of v_n(test)/v_n(MCFT) for all beams in the current study is 1.32, with a coefficient of variation of 9.5%. For beams with no stirrups, the average value of v_n(test)/v_n(MCFT) is 1.27, with a coefficient of variation of 8.4%, and for beams with stirrups, the average value of v_n(test)/v_n(MCFT) is 1.40, with a coefficient of variation of 8.4%. The design procedure appears to present a very conservative prediction of shear capacity for the beams in the current study. The prediction is better for the beams without stirrups than for the beams with stirrups. This could be due, in part, to a lack of sensitivity in Table 3.13 to beams containing stirrups with $v_n/f'_c \leq 0.050$, which covers beams with low reinforcement ratios and low amounts of shear reinforcement, and, in part, to the placement of ε_x at the level of the tension reinforcement rather than at the midheight of the beam, as done in the response procedure. The position of ε_x at the level of the tension reinforcement is conservative when stirrups are not present, and is even more conservative when stirrups are present.

Like the response procedure, the design procedure gives a prediction of the horizontal projection of the critical shear crack. A plot of the experimental horizontal projection of the critical shear crack versus the predicted horizontal projection of the critical shear crack is shown in Fig. 3.18. The average horizontal projection of the critical shear crack predicted by the modified compression field theory for beams with stirrups, using the design procedure, is 1.03d. This compares with the average measured horizontal projection of the critical shear crack, 1.38d. Fig. 3.18 shows that the horizontal projection predicted by the design procedure is less than the measured horizontal projection for all but one of the beams (beam I-3, west span) from the current study. The differences between the predicted and measured horizontal projections show that the procedure underestimates the stirrup contribution to shear strength.

The results obtained using the design procedure (in Table 3.15) are compared with the predicted nominal shear capacities obtained using ACI 318-89 (3) in Table 3.16. The average value of v_n(test)/v_n(MCFT) for all beams in the current study is 1.32 [versus 1.01 for v_n(test)/v_n(ACI)], with a coefficient of variation of 9.5% (versus 12.4%). For beams without stirrups, the average value of v_n(test)/v_n(MCFT) is 1.27 (versus 0.94), with a coefficient of variation of 8.4% (versus 9.0%). For beams with stirrups, the average value of v_n(test)/v_n(MCFT) is 1.40 (versus 1.13), with a coefficient of variation of 8.4% (versus 7.0%). As with the response procedure, the design procedure is not as accurate as ACI 318-89 (3) in predicting the nominal shear capacity of the members in the current study. The average value of v_n(test)/v_n(ACI) is closer to 1.00 than the average value of v_n(test)/v_n(MCFT) for all three combinations. The coefficients of variation, however, are relatively small, and show no clear advantage for either procedure. Once again, it should be noted that these comparisons represent only thirteen failure cases.

Before comparisons can be made between the response procedure and the design procedure, it is necessary to point out the differences between these two procedures. As

mentioned before, the response procedure is the basic application of the modified compression field theory to predict the shear response of a member, while the design procedure includes several assumptions to simplify the process of obtaining the nominal shear capacity. The first assumption made in the design procedure is that the crack spacing parameter, $s_{m\theta}$, is equal to twelve inches, a conservative estimate. No such assumption is required for the response procedure. A second major difference between the design procedure and the response procedure is the level at which ε_x is calculated. The design procedure takes ε_x at the level of the tensile steel in all cases. The response procedure takes ε_x at the level of the tensile steel only for beams without stirrups and at the midheight of the member for beams with stirrups.

When comparing the performance of the two modified compression field theory procedures, it is easiest to begin with the similarities. The obvious similarity is that both procedures are conservative and in some cases very conservative. Perhaps not as obvious, both procedures are particularly time consuming and somewhat confusing to use initially.

When looking at the average values of $v_n(test)/v_n(MCFT)$ for both procedures (Tables 3.14 and 3.15), it is clear that the procedures work better for the beams with the higher value of ρ_w, the I-series beams. For both procedures, the average value of $v_n(test)/v_n(MCFT)$ is closer to 1.00 for the I-series beams than for the J-series beams, 1.16 versus 1.32 for the response method and 1.28 versus 1.34 for the design method.

In terms of differences in performance, the response procedure gives better predictions of the nominal shear capacities of beams with stirrups. The design procedure gives better predictions of the nominal shear capacities of beams without stirrups. As noted previously, the difference between the predicted and measured strengths appears to be nearly constant with increasing shear capacity for the response procedure, while it increases with increasing nominal shear capacity for the design procedure.

For the members tested during the current study, ACI 318-89 (3) provides a better

prediction of nominal shear capacity than either of the modified compression field theory procedures.

Chapter 4

SUMMARY AND CONCLUSIONS

4.1 Summary

The objective of this research is to study the shear strength of continuous lightly reinforced concrete T-beams. Six two-span T-beams with and without web reinforcement were tested. The primary variables in this investigation were the longitudinal reinforcement ratio, ρ_w (0.75% and 1.0%), and nominal stirrup strength, $\rho_v f_{vy}$ (0 to 82 psi). Variations in shear span-to-depth ratio were experienced due to moment redistribution in some test members. Shear cracking loads are determined using three analysis techniques: crack pattern analysis, stirrup strain analysis, and concrete strain analysis. Stirrup effectiveness is evaluated based on the increase in load from shear cracking to failure of the member.

The test results are compared to the shear provisions of ACI 318-89 (3) and with the predictive equations developed by several investigators (6,14,16,37,44). For some comparisons, the results of the current research are combined with the results of Palaskas, Attiogbe, and Darwin (11,34,35) and Rodrigues and Darwin (38,39,40). The results from the current study are also compared to the results predicted by two procedures based on the modified compression field theory.

4.2 Conclusions

The following conclusions are made based on the test results and analyses performed in the current study.

1. ACI 318-89 (3) overpredicts the concrete shear capacity of lightly reinforced

beams without shear reinforcement.

2. There is little difference between shear cracking stresses in the negative and positive moment regions for beams in the current study.

3. Negative moment regions experience fewer cracks at wider spacings than positive moment regions, likely due to the top-bar effect.

4. For both the negative and positive moment regions, the stirrup contribution to shear strength exceeds the value predicted by ACI 318-89 (3).

5. Stirrup contribution to shear strength increases with increasing reinforcement ratio, ρ_w.

6. Because of the requirement to use minimum shear reinforcement when the factored shear is greater than one-half of the design shear capacity of the concrete, the ACI 318-89 (3) shear provisions are conservative for the beams tested in the current study, ρ_w = 0.75% and 1.0%.

7. The two procedures based on the modified compression field theory are conservative for the beams tested in the current study.

8. The MCFT response procedure appears to underpredict the value of nominal shear strength by a consistent margin for the beams tested in the current study.

9. The MCFT design procedure appears to become more conservative as nominal shear strength increases.

10. ACI 318-89 (3) better predicts the nominal shear strength of the beams in the current study than either of the MCFT procedures.

4.3 Future Work

The current study represents the only existing data for the negative moment region

shear strength of lightly reinforced continuous beams using deformed bars as flexural reinforcement. Additional data is needed for beams with reinforcement ratios less than 0.75%. Studies are also needed to further evaluate the effect of shear span-to-depth ratio on the shear strength of similar beams.

Reinforced concrete joist construction deserves special attention. ACI 318-89 (3) allows a 10% increase in concrete shear capacity in joists due to the presumed load-sharing capabilities of multi-stem members. There is no published experimental data to support these provisions. In addition, joists are lightly reinforced members, seldom contain stirrups, and are not covered by the minimum shear reinforcement requirements imposed on reinforced concrete beams with $V_u > \phi V_n/2$. This causes particular concern since the current research demonstrates that the shear provisions in ACI 318-89 (3) are safe for lightly reinforced beams only because of the minimum shear reinforcement criteria. A follow-on study at the University of Kansas will specifically address both the load-sharing capabilities and the concrete contribution to shear strength of multispan joist systems.

REFERENCES

1. ACI Committee 318, *Commentary of Building Code Requirements for Reinforced Concrete (ACI 318-63)*, SP-10 American Concrete Institute, Detroit, 1963, 91 pp.

2. ACI Committee 318, "Proposed Revisions to: Building Code Requirements for Reinforced Concrete (ACI 318-77) and Commentary on Building Code Requirements for Reinforced Concrete," *Concrete International*, V. 4, No. 12, December 1982, pp. 38-127.

3. ACI Committee 318, *Building Code Requirements for Reinforced Concrete (ACI 318-89) and Commentary - ACI 318R-89*, American Concrete Institute, Detroit, 1989, pp.140-144.

4. ACI-ASCE Committee 326, "Shear and Diagonal Tension," ACI Journal, *Proceedings* V. 59, No. 2, February, 1962, pp. 277-333.

5. Joint ACI-ASCE Committee 426 on shear and Diagonal Tension, "The Shear Strength of Reinforced Concrete Members," *Journal of the Structural Division*, ASCE, V. 99, No. ST6, June 1973, pp. 1091-1187.

6. ACI-ASCE Committee 426, "Suggested Revisions to Shear Provisions of ACI Code 318-71," ACI Journal, *Proceedings* V. 74, No. 9, September 1977, pp. 458-469.

7. Al-Nahlawi, M. K. A., and Wight, J. K., "An Experimental and Analytical Study of Shear Strength of Lightly Reinforced Concrete Beams," *Report* No. UMCE 89-7, Ann Arbor, Michigan, July 1989, 232 pp.

8. ASTM. "Standard Specification for Deformed and Plain Billet-Steel Bars for Concrete Reinforcement," (ASTM A 615-89) *1990 Annual Book of ASTM Standards*, Vol. 1.04, American Society for Testing and Materials, Philadelphia, PA, pp. 388-391.

9. ASTM. "Standard Practice for Making and Curing Concrete Test Specimens in the Field" (ASTM C 31-90) *1990 Annual Book of ASTM Standards*, Vol. 4.02, American Society for Testing and Materials, Philadelphia, PA, pp. 5-9.

10. ASTM. "Standard Test Method for Compressive Strength of Cylindrical Concrete Specimens," (ASTM C 39-86) *1990 Annual Book of ASTM Standards*, Vol. 4.02, American Society for Testing and Materials, Philadelphia, PA, pp. 20-24.

11. Attiogbe, E. K., Palaskas, M. N., and Darwin, D., "Shear Cracking and Stirrup Effectiveness of Lightly Reinforced Concrete Beams," *SM Report* No.1, University of Kansas Center for Research, Lawrence, Kansas, July 1980, 138 pp.

12. Baldwin, J. W., and Viest, I. M., "Effect of Axial Compression on Shear Strength of Reinforced Concrete Frame Members," ACI Journal, *Proceedings* V. 55, No. 5, November 1958, pp. 635-654.

13. Baron, M. J., and Siess, C. P., "Effect of Axial Load on the Shear Strength of Reinforced Concrete Beams," *Structural Research Series* No. 121, Civil Engineering Studies, University of Illinois at Urbana, Champaign, June 1956.

14. Batchelor, B. deV., and Kwun, M. K., "Shear in RC Beams Without Web Reinforcement," *Journal of the Structural Division*, ASCE, V. 107, No. ST5, May 1981, pp. 907-921.

15. Bazant, Z. P., "Size Effect in Blunt Fracture: Concrete, Rock, Metal," *Journal of Engineering Mechanics*, ASCE, V. 110, No. 4, April 1984, pp. 518-535.

16. Bazant, Z. P., and Kim, J. K., "Size Effect in Shear Failure of Longitudinally Reinforced Beams," ACI Journal, *Proceedings* V. 81, No. 5, September-October 1984, pp. 456-468.

17. Bernaert, S., and Siess, C. P., "Strength in Shear of Reinforced Concrete Beams under Uniform Load," *Structural Research Series*, No.120, Civil Engineering Studies, University of Illinois at Urbana, Champaign, June 1956.

18. Bhide, S. B., and Collins, M. P., "Influence of Axial Tension on the Shear Capacity of Reinforced Concrete Members" ACI Structural Journal, V. 86, No. 5, September-October 1989, pp. 89-101.

19. Bower, J. E., and Viest, I. M., "Shear Strength of Restrained Concrete Beams without Web Reinforcement," ACI Journal, *Proceedings* V. 57, No. 1, July 1960, pp. 73-98.

20. Bresler, B., and Scordelis, A. C., "Shear Strength of Reinforced Concrete Beams," ACI Journal, *Proceedings* V. 60, No. 1, January 1963, pp. 51-72.

21. Collins, M. P., "Towards a Rational Theory for Reinforced Concrete Members in Shear," *Journal of the Structural Engineering Division*, ASCE, V. 104, No. ST4, April 1978, pp. 649-666.

22. Collins, M. P., and Mitchell, D., (1990), *Prestressed Concrete Structures*, Prentice Hall, Englewood Cliffs, New Jersey 07632, 751 pp.

23. Collins, M. P., and Mitchell, D., "A Rational Approach to Shear Design-The 1984 Canadian Code Provisions," ACI Journal, *Proceedings* V. 83, No. 6, November-December 1986, pp. 925-933.

24. Diaz de Cossio, R., and Siess, C. P., "Behavior and Strength in Shear of Beams and Frames Without Web Reinforcement," ACI Journal, *Proceedings* V. 56, No. 8, February 1960, pp. 695-735.

25. Haddadin, M. J., Hong, S., and Mattock, A. H., "Stirrup Effectiveness in Reinforced Concrete Beams with Axial Force," *Journal of the Structural Division*, ASCE, V. 97, No. ST9, September 1971, pp. 2277-2297.

26. Hanson, J. W., "Square Openings in Webs of Continuous Joists," *Research and Development Bulletin* RD 001.01D, Portland Cement Association, Skokie, IL, 1969, 14 pp.

27. Kani, G. N. J., "Basic Facts Concerning Shear Failure," ACI Journal, *Proceedings* V. 63, No. 63, June 1966, pp. 675-692.

28. Krefeld, W. J., and Thurston, C. W., "Studies of the Shear and Diagonal Tension of Strength of Simply Supported Reinforced Concrete Beams," *Report*, Columbia University, New York, NY, June 1962, 96 pp.

29. MacGregor, J. G., and Gergely, P., "Suggested Revision to ACI Building Code Clauses Dealing with Shear in Beams," ACI Journal, *Proceedings* V. 74, No. 10, October 1977, pp. 493-500.

30. Mathey, R. G., and Watstein, D., "Shear Strength of Beams Without Web Reinforcement Containing Deformed Bars of Different Yield Strengths," ACI Journal, *Proceedings* V. 60, No. 2, February 1963, pp. 183-208.

31. Mitchell, D., and Collins, M. P., "Diagonal Compression Field Theory-A Rational Model for Structural Concrete in Pure Torsion," ACI Journal, *Proceedings* V. 71, No. 8, Aug. 1974, pp. 396-408.

32. Moody, K. G., Viest, I. M., Elstner, R. C., and Hognestad, E., "Shear Strength of Reinforced Concrete Beams-Parts 1 and 2," ACI Journal, *Proceedings* V. 51, No. 4, December 1954, pp. 317-332, No. 5, January 1955, pp. 417-434.

33. Morrow, J., and Viest, I. M., "Shear Strength of Reinforced Concrete Frame Members Without Web Reinforcement," ACI Journal, *Proceedings* V. 53, No. 9, March 1957, pp. 833-869.

34. Palaskas, M. N., and Darwin, D., "Shear Strength of Lightly Reinforced T-Beams," *SM Report* No.3, University of Kansas Center for Research, Lawrence, Kansas, September 1980, 198 pp.

35. Palaskas, M. N., Attiogbe, E. K., and Darwin, D., "Shear Strength of Lightly Reinforced Concrete Beams," ACI Journal, *Proceedings* V. 78, No. 6, November-December 1981, pp. 447-455.

36. Placas, A., and Regan, P. E., "Shear Failure of Reinforced Concrete Beams," ACI Journal, *Proceedings* V. 68, No. 10, October 1971, pp. 763-773.

37. Rajagopalan, K. S., and Ferguson, P. M.,"Exploratory Shear Tests Emphasizing Percentage of Longitudinal Steel," ACI Journal, *Proceedings* V. 65, No. 8, August 1968, pp. 634-638.

38. Rodrigues, C. P., and Darwin, D., "Negative Moment Region Shear Strength of Lightly

Reinforced T-Beams," *SM Report* No. 13, University of Kansas Center for Research,Lawrence, Kansas, June 1984, 111 pp.

39. Rodrigues, C. P., and Darwin, D., "Shear Strength of Lightly Reinforced T-Beams in Negative Bending," *ACI Structural Journal*, V. 84, No. 1, January-February 1987, pp. 77-85.

40. Rodrigues, C. P., and Darwin, D., Closure to discussion, "Shear Strength of Lightly Reinforced T-Beams in Negative Bending," *ACI Structural Journal*, V. 84, No. 6, November-December 1987, pp. 548-550.

41. Rodriguez, J. J., Bianchini, A. C., Viest, I. M., and Kesler, C. E., "Shear Strength of Two-Span Continuous Reinforced Concrete Beams," ACI Journal, *Proceedings* V.55, No.10, April 1959, pp.1089-1130.

42. Somes, N. F., and Corley, W. G., "Circular Openings in Webs of Continuous Beams," *Shear and Reinforced Concrete,* SP 42, V. 1, American Concrete Institute, Detroit, MI, 1974, pp. 359-398.

43. Vecchio, F. J., and Collins, M. P., "The Modified Compression-Field Theory for Reinforced Concrete Elements Subjected to Shear," ACI Journal, *Proceedings* V. 83, No. 2, March-April 1986, pp. 219-231.

44. Zsutty, T. C., "Beam Shear Strength Prediction by Analysis of Existing Data," ACI Journal, *Proceedings* V. 65, No. 11, November 1968, pp. 943-951.

Table 2.1 Beam Properties

Positive Moment Region

West Span

Beam	d	A_s	$\rho_w=A_s/b_wd$	$\rho_v=A_v/b_ws$	ρ_vf_{vy}
	in.	in.^{2}			psi
I-1	16.05	1.19	0.0099	0.0000	00.0
I-2	15.92	1.19	0.0100	0.0008	34.1
I-3	15.99	1.19	0.0099	0.0008	33.9
J-1	16.00	0.88	0.0073	0.0000	00.0
J-2	16.02	1.19	0.0099	0.0008	34.0
J-3	15.03	2.07	0.0184	0.0015	82.0

East Span

Beam	d	A_s	$\rho_w=A_s/b_wd$	$\rho_v=A_v/b_ws$	ρ_vf_{vy}
	in.	in.^{2}			psi
I-1	16.05	1.19	0.0099	0.0000	00.0
I-2	15.96	1.19	0.0099	0.0008	34.1
I-3	16.08	1.19	0.0099	0.0000	00.0
J-1	16.00	0.88	0.0073	0.0000	00.0
J-2	16.02	1.19	0.0099	0.0000	00.0
J-3	15.16	2.07	0.0182	0.0008	57.3

Negative Moment Region

West Span

Beam	d	A_s	$\rho_w=A_s/b_wd$	$\rho_v=A_v/b_ws$	ρ_vf_{vy}
	in.	in.^{2}			psi
I-1	15.52	1.19	0.0102	0.0000	00.0
I-2	15.89	1.19	0.0100	0.0008	34.1
I-3	15.89	1.19	0.0100	0.0008	33.9
J-1	15.50	0.88	0.0076	0.0000	00.0
J-2	15.88	0.88	0.0074	0.0008	34.0
J-3	15.75	0.88	0.0074	0.0015	82.0

East Span

Beam	d	A_s	$\rho_w=A_s/b_wd$	$\rho_v=A_v/b_ws$	ρ_vf_{vy}
	in.	in.^{2}			psi
I-1	15.52	1.19	0.0102	0.0000	00.0
I-2	15.89	1.19	0.0100	0.0008	34.1
I-3	15.89	1.19	0.0100	0.0000	00.0
J-1	15.50	0.88	0.0076	0.0000	00.0
J-2	15.88	0.88	0.0074	0.0000	00.0
J-3	15.63	0.88	0.0075	0.0008	57.3

Table 2.2 Concrete Properties

Beam	Mix. Prop. per yard* lbs.	Slump in.	Air %	Temp. F	f'_c** psi	Age at test days
I-1	517:267:1490:1490	$3^1/_4$	3.3	66	4620	11
I-2	517:267:1490:1490	$3^1/_4$	3.8	64	4420	11
I-3	517:267:1490:1490	$3^1/_2$	3.5	67	4470	13
J-1	517:267:1490:1490	$4^1/_2$	4.3	62	4510	15
J-2	517:267:1490:1490	$3^1/_4$	4.6	56	4490	19
J-3	517:267:1490:1490	$2^1/_2$	4.0	80	4430	12

* Cement : water : fine aggregate : coarse aggregate

** Compressive strength of 12 x 6 in. test cylinders

Table 2.3 Point Loads and Middle Support Reaction at Failure

Beam	Failure region	Load points per span	Total load per span, kips West	East	Middle support reaction reaction, kips**
I-1	east negative	1	18.79	18.61	24.23
I-1	west negative	1	18.29	18.11	23.58
I-2	east negative	1	30.60	30.55	39.90
I-3	east negative	2	21.53	20.55	26.15
I-3	west negative	2	27.37	26.54	33.44
J-1	east positive	1	17.15	16.83	23.20
J-1	west negative	1	17.81	17.54	24.02
J-1	west positive	1	20.70	20.56	27.32
J-1	east negative	1	18.08	17.94	24.60
J-2	east negative	2	19.35	18.85	23.68
J-2	west negative	2	28.15	28.22	34.42
J-3	east negative	2	38.13	37.97	46.92
J-3	west negative	2	51.49	50.58	61.35

Table 2.4 Measured Shear Strength

Beam	V_n(test) kips	v_n(test) psi	Failure region
I-1	15.3	131	east negative
I-1	14.9	128	west negative
I-2	23.5	197	east negative
I-3	16.7	140	east negative
I-3	21.0	176	west negative
J-1	12.0	100	east positive
J-1	15.0	129	west negative
J-1	14.5	121	west positive
J-1	14.9	128	east negative
J-2	15.5	130	east negative
J-2	21.6	181	west negative
J-3	24.6	208	east negative
J-3	31.2	266	west negative

Table 3.1 Shear Cracking loads, V_c (kips)

Positive Moment Region

West Span

Beam	Crack Patterns	Stirrup Strain	Concrete Strain
I-1	12.9	--	xx
I-2	17.3	11.5	12.8
I-3	xx	12.4	xx
J-1	12.2	--	11.9
J-2	14.3	11.0	13.4
J-3	17.7	17.4	17.7

East Span

Beam	Crack Patterns	Stirrup Strain	Concrete Strain
I-1	xx	--	12.1
I-2	12.8	8.7	12.1
I-3	xx	--	xx
J-1	11.4	--	10.8
J-2	12.1	--	12.7
J-3	17.6	14.7	17.1

Negative Moment Region

West Span

Beam	Crack Patterns	Stirrup Strain	Concrete Strain
I-1	14.3	--	14.3
I-2	14.9	11.5	13.9
I-3	15.1	15.0	15.8
J-1	12.3	--	13.0
J-2	15.5	15.5	13.5
J-3	15.9	15.3	18.4

East Span

Beam	Crack Patterns	Stirrup Strain	Concrete Strain
I-1	14.9	--	12.9
I-2	13.5	11.5	13.0
I-3	14.2	--	13.5
J-1	12.8	--	13.8
J-2	12.9	--	13.3
J-3	15.8	14.2	17.8

-- no stirrups used
xx method produced no results

Table 3.2 Shear cracking stresses, v_c (psi)

Positive Moment Region

West Span

Beam	Crack Patterns	Stirrup Strain	Concrete Strain
I-1	106.8	--	xx
I-2	144.5	95.9	107.4
I-3	xx	103.1	xx
J-1	101.5	--	98.9
J-2	119.1	91.8	111.9
J-3	157.5	154.2	157.5

East Span

Beam	Crack Patterns	Stirrup Strain	Concrete Strain
I-1	xx	--	100.9
I-2	107.0	72.6	101.4
I-3	xx	--	xx
J-1	95.0	--	89.6
J-2	100.7	--	106.0
J-3	155.0	129.1	150.4

Negative Moment Region

West Span

Beam	Crack Patterns	Stirrup Strain	Concrete Strain
I-1	122.5	--	122.5
I-2	125.2	96.7	116.7
I-3	126.5	126.2	132.6
J-1	105.5	--	111.5
J-2	130.5	130.5	113.4
J-3	134.8	129.4	155.5

East Span

Beam	Crack Patterns	Stirrup Strain	Concrete Strain
I-1	128.0	--	110.6
I-2	113.6	96.7	108.9
I-3	119.2	--	113.1
J-1	110.5	--	119.0
J-2	108.4	--	112.1
J-3	134.9	121.1	151.5

-- no stirrups used
xx method produced no results

Table 3.3 Calculated Shear Cracking Stresses, v_c (psi)

Positive Moment Region

West Span

Beam	Eq. 1.2	Eq. 1.8*	Eq. 1.7	Eq. 1.10	Eq. 1.11	Eq. 1.12*
I-1	135.9	134.9	121.7	135.1	114.8	123.0
I-2	133.0	133.2	119.7	133.0	113.0	122.2
I-3	133.7	**	119.7	132.9	112.9	**
J-1	134.3	120.5	102.7	112.6	94.2	108.2
J-2	134.0	**	119.9	133.2	113.2	**
J-3	133.1	154.2	133.1	153.1	149.8	184.0

East Span

Beam	Eq. 1.2	Eq. 1.8*	Eq. 1.7	Eq. 1.10	Eq. 1.11	Eq. 1.12*
I-1	135.9	135.0	121.7	135.1	114.8	123.6
I-2	133.0	132.4	119.0	132.2	112.3	121.3
I-3	133.7	**	119.7	132.9	112.9	**
J-1	134.3	120.8	102.7	112.6	94.2	108.4
J-2	134.0	**	119.9	133.2	113.2	**
J-3	133.1	152.5	133.1	153.1	149.8	178.5

Negative Moment Region

West Span

Beam	Eq. 1.2	Eq. 1.8*	Eq. 1.7	Eq. 1.10	Eq. 1.11	Eq. 1.12*
I-1	135.9	136.6	123.7	137.6	117.0	126.4
I-2	133.0	135.0	119.7	133.0	113.0	123.3
I-3	133.7	138.6	120.3	133.7	113.7	127.5
J-1	134.3	123.4	104.8	115.0	96.4	111.8
J-2	134.0	126.4	103.2	113.1	94.7	114.2
J-3	133.1	128.9	102.5	112.4	94.1	115.2

East Span

Beam	Eq. 1.2	Eq. 1.8*	Eq. 1.7	Eq. 1.10	Eq. 1.11	Eq. 1.12*
I-1	135.9	136.6	123.7	137.6	117.0	126.2
I-2	133.0	135.1	119.7	133.0	113.0	123.6
I-3	133.7	137.7	120.3	133.7	113.7	126.4
J-1	134.3	122.8	104.8	115.0	96.4	111.3
J-2	134.0	124.9	103.2	113.1	94.7	112.1
J-3	133.1	128.1	103.2	113.1	94.8	115.3

Eq. 1.2 $v_c = 2\sqrt{f'_c}$ — ACI 318-89 (3)

Eq. 1.8 $v_c = 59\left(f'_c \rho_w \frac{d}{a}\right)^{\frac{1}{3}}$ — Zsutty (44)

Eq. 1.7 $v_c = (0.8 + 100\rho_w)\sqrt{f'_c}$ — Rajagopalan and Ferguson

Eq. 1.10 $v_c = (0.8 + 120\rho_w)\sqrt{f'_c}$ — ACI-ASCE 426 (6)

Eq. 1.11 $v_c = (0.6 + 110\rho_w)\sqrt{f'_c}$ — Batchelor and Kwun (14)

Eq. 1.12 $v_c = \frac{10\ (\rho_w)^{\frac{1}{3}}}{\sqrt{1 + 0.04\frac{d}{d_a}}}\left[\sqrt{f'_c} + \sqrt{\frac{\rho_w}{\left(\frac{a}{d}\right)^5}}\right]$ — Bazant and Kim (16)

* use M/Vd from crack pattern analysis (except beam I-1 east, use M/Vd from concrete strain)

** M/Vd < 2.5

Table 3.4 Approximate Shear Span, M/V, inches, at Shear Cracking Load

Positive Moment Region

West Span

Beam	Crack Patterns	Stirrup Strain	Concrete Strain
I-1	61.40	--	xx
I-2	60.48	61.59	61.25
I-3	xx	26.95	xx
J-1	61.73	--	61.80
J-2	28.35	26.84	26.78
J-3	44.47	32.50	44.47

East Span

Beam	Crack Patterns	Stirrup Strain	Concrete Strain
I-1	xx	--	61.29
I-2	61.16	62.75	61.34
I-3	xx	--	xx
J-1	61.23	--	61.42
J-2	25.57	--	25.57
J-3	44.08	34.72	35.06

Negative Moment Region

West Span

Beam	Crack Patterns	Stirrup Strain	Concrete Strain
I-1	58.87	--	58.87
I-2	58.93	58.13	58.72
I-3	54.79	54.79	54.83
J-1	57.97	--	58.23
J-2	53.05	53.05	54.86
J-3	51.08	52.63	44.99

East Span

Beam	Crack Patterns	Stirrup Strain	Concrete Strain
I-1	59.15	--	58.68
I-2	58.69	58.10	58.55
I-3	55.88	--	55.79
J-1	58.81	--	59.04
J-2	55.70	--	55.58
J-3	51.47	55.55	45.17

-- No stirrups used
xx Method produced no results

Table 3.5 Approximation Shear span-to-Depth Ratio, M/(Vd), at Shear Cracking Load

Positive Moment Region

West Span

Beam	Crack Patterns	Stirrup Strain	Concrete Strain
I-1	3.83	--	xx
I-2	3.80	3.87	3.85
I-3	xx	1.68	xx
J-1	3.86	--	3.86
J-2	1.77	1.68	1.67
J-3	2.96	2.16	2.96

East Span

Beam	Crack Patterns	Stirrup Strain	Concrete Strain
I-1	xx	--	3.82
I-2	3.83	3.93	3.84
I-3	xx	--	xx
J-1	3.83	--	3.84
J-2	1.60	--	1.60
J-3	2.91	2.29	2.31

Negative Moment Region

West Span

Beam	Crack Patterns	Stirrup Strain	Concrete Strain
I-1	3.79	--	3.79
I-2	3.71	3.66	3.70
I-3	3.45	3.45	3.45
J-1	3.74	--	3.76
J-2	3.34	3.34	3.45
J-3	3.24	3.34	2.86

East Span

Beam	Crack Patterns	Stirrup Strain	Concrete Strain
I-1	3.81	--	3.78
I-2	3.69	3.66	3.68
I-3	3.52	--	3.51
J-1	3.79	--	3.81
J-2	3.51	--	3.50
J-3	3.29	3.55	2.89

-- no stirrups used
xx method produced no results

Table 3.6a Comparison of test and calculated shear cracking stresses: values represent v_c(test)/v_c(eq) where v_c is calculated from crack patterns

Positive Moment Region

West Span

Beam	Eq. 1.2	Eq. 1.8	Eq. 1.7	Eq. 1.10	Eq. 1.11	Eq. 1.12
I-1	0.79	0.79	0.88	0.79	0.93	0.87
I-2	1.09	1.08	1.21	1.09	1.28	1.18
I-3	xx	xx	xx	xx	xx	xx
J-1	0.76	0.84	0.99	0.90	1.08	0.94
J-2	0.89	**	0.99	0.89	1.05	**
J-3	1.18	0.88	1.18	1.03	1.05	0.86

East Span

Beam	Eq. 1.2	Eq. 1.8	Eq. 1.7	Eq. 1.10	Eq. 1.11	Eq. 1.12
I-1	xx	xx	xx	xx	xx	xx
I-2	0.80	0.81	0.90	0.81	0.95	0.88
I-3	xx	xx	xx	xx	xx	xx
J-1	0.71	0.79	0.92	0.84	1.01	0.88
J-2	0.75	**	0.84	0.76	0.89	**
J-3	1.16	0.87	1.16	1.01	1.03	0.87
mean	0.90	0.87	1.01	0.90	1.03	0.93
standard deviation	0.19	0.10	0.14	0.12	0.11	0.12
coef. of variation, %	20.80	11.68	13.95	12.91	10.97	12.44

Eq. 1.2 $v_c = 2\sqrt{f'_c}$ — ACI 318-89 (3)

Eq. 1.8 $v_c = 59\left(f'_c \rho_w \frac{d}{a}\right)^{\frac{1}{3}}$ — Zsutty (44)

Eq. 1.7 $v_c = (0.8 + 100\rho_w)\sqrt{f'_c}$ — Rajagopalan and Ferguson

Eq. 1.10 $v_c = (0.8 + 120\rho_w)\sqrt{f'_c}$ — ACI-ASCE 426 (6)

Eq. 1.11 $v_c = (0.6 + 110\rho_w)\sqrt{f'_c}$ — Batchelor and Kwun (14)

Eq. 1.12 $v_c = \frac{10\ (\rho_w)^{\frac{1}{3}}}{\sqrt{1 + 0.04\frac{d}{d_a}}}\left[\sqrt{f'_c} + \sqrt{\frac{\rho_w}{\left(\frac{a}{d}\right)^5}}\right]$ — Bazant and Kim (16)

xx no shear cracking observed

** M/Vd < 2.5

Table 3.6b Comparison of test and calculated shear cracking stresses: values represent v_c(test)/v_c(eq) where v_c is calculated from crack patterns

Negative Moment Region

West Span

Beam	Eq. 1.2	Eq. 1.8	Eq. 1.7	Eq. 1.10	Eq. 1.11	Eq. 1.12
I-1	0.90	0.90	0.99	0.89	1.05	0.97
I-2	0.94	0.93	1.05	0.94	1.11	1.02
I-3	0.95	0.91	1.05	0.95	1.11	0.99
J-1	0.79	0.86	1.01	0.92	1.09	0.94
J-2	0.97	1.01	1.26	1.15	1.38	1.14
J-3	1.01	1.05	1.32	1.20	1.43	1.17

East Span

Beam	Eq. 1.2	Eq. 1.8	Eq. 1.7	Eq. 1.10	Eq. 1.11	Eq. 1.12
I-1	0.94	0.94	1.03	0.93	1.09	1.01
I-2	0.85	0.84	0.95	0.85	1.01	0.92
I-3	0.89	0.87	0.99	0.89	1.05	0.94
J-1	0.82	0.90	1.05	0.96	1.15	0.99
J-2	0.81	0.87	1.05	0.96	1.14	0.97
J-3	1.01	1.05	1.31	1.19	1.42	1.17
mean	0.91	0.93	1.09	0.99	1.17	1.02
standard deviation	0.08	0.07	0.13	0.12	0.15	0.09
coef. of variation, %	8.38	7.80	11.95	12.37	12.89	8.83

All beams, both positive and negative moment region

mean	0.91	0.90	1.05	0.95	1.11	0.98
standard deviation	0.13	0.09	0.14	0.12	0.15	0.11
coef. of variation, %	14.53	9.60	13.04	13.06	13.54	10.90

Eq. 1.2 $v_c = 2\sqrt{f'_c}$ — ACI 318-89 (3)

Eq. 1.8 $v_c = 59\left(f'_c \rho_w \frac{d}{a}\right)^{\frac{1}{3}}$ — Zsutty (44)

Eq. 1.7 $v_c = (0.8 + 100\rho_w)\sqrt{f'_c}$ — Rajagopalan and Ferguson

Eq. 1.10 $v_c = (0.8 + 120\rho_w)\sqrt{f'_c}$ — ACI-ASCE 426 (6)

Eq. 1.11 $v_c = (0.6 + 110\rho_w)\sqrt{f'_c}$ — Batchelor and Kwun (14)

Eq. 1.12 $v_c = \frac{10\ (\rho_w)^{\frac{1}{3}}}{\sqrt{1 + 0.04\frac{d}{d_a}}}\left[\sqrt{f'_c} + \sqrt{\frac{\rho_w}{\left(\frac{a}{d}\right)^5}}\right]$ — Bazant and Kim (16)

Table 3.7a Comparison of test and calculated shear cracking stresses: values represent v_c(test)/v_c(eq) where v_c is calculated from stirrup strain

Positive Moment Region

West Span

Beam	Eq. 1.2	Eq. 1.8	Eq. 1.7	Eq. 1.10	Eq. 1.11	Eq. 1.12
I-1	--	--	--	--	--	--
I-2	0.72	0.72	0.80	0.72	0.85	0.78
I-3	0.77	**	0.86	0.78	0.91	**
J-1	--	--	--	--	--	--
J-2	0.69	**	0.77	0.69	0.81	**
J-3	1.16	0.87	1.16	1.01	1.03	0.70

East Span

Beam	Eq. 1.2	Eq. 1.8	Eq. 1.7	Eq. 1.10	Eq. 1.11	Eq. 1.12
I-1	--	--	--	--	--	--
I-2	0.55	0.55	0.61	0.55	0.65	0.60
I-3	--	--	--	--	--	--
J-1	--	--	--	--	--	--
J-2	--	--	--	--	--	--
J-3	0.97	0.72	0.97	0.84	0.86	0.72
mean	0.81	0.72	0.86	0.77	0.85	0.70
standard deviation	0.22	0.13	0.19	0.15	0.12	0.07
coef. of variation, %	27.03	18.29	21.79	20.23	14.64	10.69

Eq. 1.2 $v_c = 2\sqrt{f'_c}$ — ACI 318-89 (3)

Eq. 1.8 $v_c = 59\left(f'_c \rho_w \frac{d}{a}\right)^{\frac{1}{3}}$ — Zsutty (44)

Eq. 1.7 $v_c = (0.8 + 100\rho_w)\sqrt{f'_c}$ — Rajagopalan and Ferguson

Eq. 1.10 $v_c = (0.8 + 120\rho_w)\sqrt{f'_c}$ — ACI-ASCE 426 (6)

Eq. 1.11 $v_c = (0.6 + 110\rho_w)\sqrt{f'_c}$ — Batchelor and Kwun (14)

Eq. 1.12 $v_c = \frac{10\ (\rho_w)^{\frac{1}{3}}}{\sqrt{1 + 0.04\frac{d}{d_a}}}\left[\sqrt{f'_c} + \sqrt{\frac{\rho_w}{\left(\frac{a}{d}\right)^5}}\right]$ — Bazant and Kim (16)

- - no stirrups present
* * M/Vd < 2.5

Table 3.7b Comparison of test and calculated shear cracking stresses: values represent $v_c(test)/v_c(eq)$ where v_c is calculated from stirrup strain

Negative Moment Region

West Span

Beam	Eq. 1.2	Eq. 1.8	Eq. 1.7	Eq. 1.10	Eq. 1.11	Eq. 1.12
I-1	--	--	--	--	--	--
I-2	0.73	0.72	0.81	0.73	0.86	0.78
I-3	0.94	0.91	1.05	0.94	1.11	0.99
J-1	--	--	--	--	--	--
J-2	0.97	1.03	1.26	1.15	1.38	1.14
J-3	0.97	1.00	1.26	1.15	1.38	1.12

East Span

Beam	Eq. 1.2	Eq. 1.8	Eq. 1.7	Eq. 1.10	Eq. 1.11	Eq. 1.12
I-1	--	--	--	--	--	--
I-2	0.73	0.72	0.81	0.73	0.86	0.78
I-3	--	--	--	--	--	--
J-1	--	--	--	--	--	--
J-2	--	--	--	--	--	--
J-3	0.91	0.95	1.17	1.07	1.28	1.05
mean	0.88	0.89	1.06	0.96	1.15	0.98
standard deviation	0.11	0.14	0.21	0.20	0.24	0.16
coef. of variation, %	13.09	15.39	19.66	20.30	21.12	16.52

All beams, both positive and negative moment region

mean	0.84	0.82	0.96	0.86	1.00	0.87
standard deviation	0.17	0.16	0.22	0.20	0.24	0.19
coef. of variation, %	20.18	18.95	22.44	22.80	23.94	22.13

Eq. 1.2 $v_c = 2\sqrt{f'_c}$ ACI 318-89 (3)

Eq. 1.8 $v_c = 59\left(f'_c \rho_w \frac{d}{a}\right)^{\frac{1}{3}}$ Zsutty (44)

Eq. 1.7 $v_c = (0.8 + 100\rho_w)\sqrt{f'_c}$ Rajagopalan and Ferguson

Eq. 1.10 $v_c = (0.8 + 120\rho_w)\sqrt{f'_c}$ ACI-ASCE 426 (6)

Eq. 1.11 $v_c = (0.6 + 110\rho_w)\sqrt{f'_c}$ Batchelor and Kwun (14)

Eq. 1.12 $v_c = \frac{10\ (\rho_w)^{\frac{1}{3}}}{\sqrt{1 + 0.04\frac{d}{d_a}}}\left[\sqrt{f'_c} + \sqrt{\frac{\rho_w}{\left(\frac{a}{d}\right)^5}}\right]$ Bazant and Kim (16)

- - no stirrups present

Table 3.8a Comparison of test and calculated shear cracking stresses: values represent v_c(test)/v_c(eq) where v_c is calculated from concrete strain

Positive Moment Region

West Span

Beam	Eq. 1.2	Eq. 1.8	Eq. 1.7	Eq. 1.10	Eq. 1.11	Eq. 1.12
I-1	xx	xx	xx	xx	xx	xx
I-2	0.81	0.81	0.90	0.81	0.95	0.88
I-3	xx	xx	xx	xx	xx	xx
J-1	0.74	0.82	0.96	0.88	1.05	0.91
J-2	0.84	* *	0.93	0.84	0.99	* *
J-3	1.18	0.88	1.18	1.03	1.05	0.86

East Span

Beam	Eq. 1.2	Eq. 1.8	Eq. 1.7	Eq. 1.10	Eq. 1.11	Eq. 1.12
I-1	0.74	0.75	0.83	0.75	0.88	0.82
I-2	0.76	0.77	0.85	0.77	0.90	0.84
I-3	xx	xx	xx	xx	xx	xx
J-1	0.67	0.74	0.87	0.80	0.95	0.83
J-2	0.79	* *	0.88	0.80	0.94	* *
J-3	1.13	0.84	1.13	0.98	1.00	0.84
mean	0.85	0.80	0.95	0.85	0.97	0.85
standard deviation	0.18	0.05	0.12	0.10	0.06	0.03
coef. of variation, %	21.07	6.34	13.13	11.25	6.19	3.69

Eq. 1.2 $v_c = 2\sqrt{f'_c}$ — ACI 318-89 (3)

Eq. 1.8 $v_c = 59\left(f'_c \rho_w \frac{d}{a}\right)^{\frac{1}{3}}$ — Zsutty (44)

Eq. 1.7 $v_c = (0.8 + 100\rho_w)\sqrt{f'_c}$ — Rajagopalan and Ferguson

Eq. 1.10 $v_c = (0.8 + 120\rho_w)\sqrt{f'_c}$ — ACI-ASCE 426 (6)

Eq. 1.11 $v_c = (0.6 + 110\rho_w)\sqrt{f'_c}$ — Batchelor and Kwun (14)

Eq. 1.12 $v_c = \dfrac{10\ (\rho_w)^{\frac{1}{3}}}{\sqrt{1 + 0.04\frac{d}{d_a}}}\left[\sqrt{f'_c} + \sqrt{\dfrac{\rho_w}{\left(\frac{a}{d}\right)^5}}\right]$ — Bazant and Kim (16)

xx no shear cracking observed

* * M/Vd < 2.5

Table 3.8b Comparison of test and calculated shear cracking stresses: values represent $v_c(test)/v_c(eq)$ where v_c is calculated from concrete strain

Negative Moment Region

West Span

Beam	Eq. 1.2	Eq. 1.8	Eq. 1.7	Eq. 1.10	Eq. 1.11	Eq. 1.12
I-1	0.90	0.90	0.99	0.89	1.05	0.97
I-2	0.88	0.86	0.98	0.88	1.03	0.95
I-3	0.99	0.96	1.10	0.99	1.17	1.04
J-1	0.83	0.90	1.06	0.97	1.16	1.00
J-2	0.85	0.90	1.10	1.00	1.20	0.99
J-3	1.17	1.21	1.52	1.38	1.65	1.35

East Span

Beam	Eq. 1.2	Eq. 1.8	Eq. 1.7	Eq. 1.10	Eq. 1.11	Eq. 1.12
I-1	0.81	0.81	0.89	0.80	0.94	0.88
I-2	0.82	0.81	0.91	0.82	0.96	0.88
I-3	0.85	0.82	0.94	0.85	1.00	0.89
J-1	0.89	0.97	1.14	1.04	1.23	1.07
J-2	0.84	0.90	1.09	0.99	1.18	1.00
J-3	1.14	1.18	1.47	1.34	1.60	1.31
mean	0.91	0.94	1.10	1.00	1.18	1.03
standard deviation	0.12	0.13	0.20	0.19	0.23	0.15
coef. of variation, %	13.38	14.15	18.38	18.76	19.42	14.97

All beams, both positive and negative moment region

mean	0.89	0.89	1.03	0.93	1.09	0.96
standard deviation	0.15	0.13	0.19	0.17	0.21	0.15
coef. of variation, %	16.77	14.25	17.97	18.00	18.82	15.45

Eq. 1.2 $v_c = 2\sqrt{f'_c}$ ACI 318-89 (3)

Eq. 1.8 $v_c = 59\left(f'_c \rho_w \frac{d}{a}\right)^{\frac{1}{3}}$ Zsutty (44)

Eq. 1.7 $v_c = (0.8 + 100\rho_w)\sqrt{f'_c}$ Rajagopalan and Ferguson

Eq. 1.10 $v_c = (0.8 + 120\rho_w)\sqrt{f'_c}$ ACI-ASCE 426 (6)

Eq. 1.11 $v_c = (0.6 + 110\rho_w)\sqrt{f'_c}$ Batchelor and Kwun (14)

Eq. 1.12 $v_c = \frac{10\ (\rho_w)^{\frac{1}{3}}}{\sqrt{1 + 0.04\frac{d}{d_a}}}\left[\sqrt{f'_c} + \sqrt{\frac{\rho_w}{\left(\frac{a}{d}\right)^5}}\right]$ Bazant and Kim (16)

Table 3.9 Stirrup effectiveness, v_n-v_c (psi)

Current Study

Beam	$v_n - v_c$ (psi)	$\rho_v f_{vy}$ (psi)	ρ_w
I-1	3.0	0.0	0.0102
I-1	5.5	0.0	0.0102
I-2	83.4	34.1	0.0100
I-3	20.8	0.0	0.0100
I-3	49.5	33.9	0.0100
J-1*	5.0	0.0	0.0073
J-1	23.5	0.0	0.0076
J-1*	19.5	0.0	0.0073
J-1	17.5	0.0	0.0076
J-2	21.6	0.0	0.0074
J-2	50.5	34.0	0.0074
J-3	73.1	57.3	0.0075
J-3	131.2	82.0	0.0074

Results of Rodrigues and Darwin (38,39,40) and Palaskas, Attiogbe, and Darwin (11,34,35)

Beam	$v_n - v_c$ (psi)	$\rho_v f_{vy}$ (psi)	ρ_w
A-0*	13.9	0.0	0.0066
A-25*	55.1	31.8	0.0066
A25a*	67.5	31.8	0.0067
A-50*	103.0	74.0	0.0066
A-50a*	98.3	75.0	0.0066
A-75*	164.0	97.0	0.0066
B-0*	47.1	0.0	0.0049
B-25*	49.1	32.4	0.0049
B-50*	110.4	76.2	0.0050
C-0*	18.8	0.0	0.0094
C-25*	52.0	32.4	0.0095
C-50*	146.0	76.2	0.0094
C-75*	172.0	103.0	0.0093
D-0	18.4	0.0	0.0068
D-20	37.0	21.6	0.0071
D-40	34.7	37.0	0.0070
D-80(1)*	134.6	82.9	0.0069
D-80(2)	99.9	73.1	0.0070
E-0*	19.0	0.0	0.0047
E-20	34.6	22.2	0.0047
E-40*	54.7	36.8	0.0048
E-80	88.6	73.5	0.0048

* Positive Moment Region Failure

Table 3.10 Horizontal Crack Projection and Stirrup Contribution to Shear Strength at Failure

Negative Moment Region

Beam	Location **	# of stirrups intercepted	Horizontal Projection	$v_{si}=nA_vf_{vy}/b_wd$ (psi)	ρ_vf_{vy} (psi)
I-2	east	4	1.6d	60.1	34.1
I-3	west	3	1.0d	44.8	33.9
J-2	west	3	1.5d	45.0	34.0
J-3	east	3	1.5d	77.0	57.3
J-3	west	3	1.3d	109.3	82.0
D-80(2)*	n/a	2	1.1d	66.8	73.1
D-40*	n/a	1	0.9d	16.8	37.0
D-20*	n/a	2	1.1d	20.0	21.6
E-80*	n/a	2	0.9d	68.3	73.5
E-20*	n/a	2	1.4d	20.2	22.2

Positive Moment Region

Beam	Location **	# of stirrups intercepted	Horizontal Projection	$v_{si}=nA_vf_{vy}/b_wd$ (psi)	ρ_vf_{vy} (psi)
A-25*	n/a	3	1.7d	43.4	31.8
A-25a*	n/a	3	2.2d	43.8	31.8
A-50*	n/a	3	1.8d	100.6	74
A-50a*	n/a	3	2.0d	101.7	75
A-75*	n/a	3	1.8d	131.1	97
B-25*	n/a	2	1.8d	29.2	32.4
B-50*	n/a	3	1.5d	104	76.2
C-25*	n/a	3	1.7d	44.4	32.4
C-50*	n/a	3	1.7d	103.4	76.2
C-75*	n/a	3	1.7d	139	103
D-80(1)*	n/a	3	1.4d	116	82.9
E-40*	n/a	3	1.6d	49.7	36.8

* Test results of Rodrigues and Darwin (38,39,40) and Palaskas et al. (11,34,35)

** In order of failure

Table 3.11 Comparison of Test and Calculated Nominal Shear Stresses from Current Study and Results of Rodrigues and Darwin (38,39,40)

Negative Moment Region Failures

Beam	Span	v_n (test) psi	v_n (ACI)** psi	$\frac{v_n \text{ (test)}}{v_n \text{ (ACI)}}$
I-1	east	131	136	0.96
I-1	west	128	136	0.94
I-2	east	197	167	1.18
I-3	east	140	134	1.04
I-3	west	176	168	1.05
J-1	west	129	134	0.96
J-1	east	128	134	0.96
J-2	east	130	134	0.97
J-2	west	181	168	1.08
J-3	east	208	190	1.09
J-3	west	266	215	1.24
D-0*	n/a	138	135	1.02
D-20*	n/a	148	153	0.97
D-40*	n/a	146	167	0.87
D-80(2)*	n/a	200	201	1.00
E-20*	n/a	127	152	0.84
E-80*	n/a	152	200	0.76

Mean (all beams from the current study)	1.04
Coefficient of Variation	9.5%
Mean (beams with stirrups from the current study)	1.13
Coefficient of Variation	7.0%
Mean (all beams from Rodrigues and Darwin)	0.91
Coefficient of Variation	8.4%
Mean (beams with stirrups from Rodrigues and Darwin)	0.89
Coefficient of Variation	11.0%
Mean (all beams from combined results)	1.00
Coefficient of Variation	11.7%
Mean (beams with stirrups from combined results)	1.01
Coefficient of Variation	15.2%

* Test Results of Rodrigues and Darwin (38,39,40)

** $v_n = \rho_v f_{vy} + 2\sqrt{f'_c}$

Table 3.12 Sample Beam Response (using MCFT response procedure on beam I-2)

ε_1 x 10,000	θ degrees	ε_2 x 100,000	ε_x x 10,000	ε_t x 10,000	V kips	M k-in.
5.00	56.9	-2.72	3.43	1.30	13.4	699
5.50	55.6	-2.97	3.65	1.55	13.9	723
6.00	54.5	-3.21	3.87	1.81	14.3	745
6.50	53.4	-3.44	4.07	2.09	14.7	766
7.00	52.4	-3.68	4.26	2.37	15.1	787
7.50	51.6	-3.91	4.45	2.66	15.5	805
8.00	50.7	-4.13	4.62	2.96	15.8	823
8.50	49.9	-4.36	4.79	3.27	16.1	840
9.00	49.2	-4.57	4.96	3.58	16.5	856
9.50	48.5	-4.80	5.11	3.91	16.8	572
10.00	47.8	-5.01	5.26	4.24	17.1	887
10.50	47.2	-5.22	5.41	4.57	17.3	902
11.00	46.6	-5.42	5.56	4.90	17.6	915
11.50	46.1	-5.63	5.70	5.24	17.9	929
12.00	45.6	-5.86	5.83	5.59	18.1	943
12.50	45.1	-6.11	5.96	5.93	18.4	955
13.00	44.6	-6.36	6.09	6.28	18.6	968
13.50	44.2	-6.61	6.21	6.63	18.8	980
14.00	43.8	-6.86	6.34	6.98	19.1	991
14.50	43.4	-7.12	6.46	7.33	19.3	1003
15.00	43.0	-7.38	6.57	7.69	19.5	1015
15.50	42.6	-7.64	6.69	8.05	19.7	1026
16.00	42.3	-7.89	6.81	8.41	19.9	1036
16.50	41.9	-8.16	6.91	8.77	20.1	1048
17.00	41.6	-8.42	7.03	9.13	20.3	1058
17.50	41.3	-8.68	7.14	9.50	20.5	1068
18.00	41.0	-8.96	7.24	9.87	20.8	1079
18.50	40.7	-9.22	7.35	10.23	20.9	1089
19.00	40.1	-9.41	7.34	10.72	20.7	1077
19.50	39.5	-9.61	7.32	11.22	20.5	1065
20.00	39.0	-9.79	7.31	11.71	20.3	1053

Table 3.13 Partial Design Tables from Collins and Mitchell (22)

Beams with Stirrups

v/f'_c		Longitudinal Strain, ε_x x 1000				
		1.00	1.50	2.00	2.50	3.00
0.050	θ	38	41	43	45	46
	β	2.33	1.95	1.72	1.54	1.39
0.075	θ	36	40	42	43	43
	β	2.15	1.90	1.65	1.44	1.25

Beams without Stirrups

d, inches		Longitudinal Strain, ε_x x 1000				
		1.00	1.50	2.00	2.50	3.00
15.0	θ	45	48	50	52	53
	β	1.99	1.67	1.45	1.30	1.17
25.0	θ	51	54	57	59	61
	β	1.70	1.39	1.19	1.05	0.94

Table 3.14 Results Obtained from MCFT Response Procedure

k_1 from Step 3 equal to 0.8 for shear reinforcement

Beam	Span	θ	Hor. Proj.	V_n(MCFT)	v_n(MCFT)	$\frac{v_n(test)}{v_n(MCFT)}$
I-1	east	50	0.84d	12.5	107	1.22
I-1	west	50	0.84d	12.5	107	1.20
I-2	east **	40.7	1.16d	21.1	177	1.11
I-3	east	50.1	0.84d	12.8	107	1.31
I-3	west **	40.4	1.17d	21.7	182	0.97
J-1*	east	57.6	0.63d	10.3	86	1.16
J-1	west	54.1	0.72d	10.8	93	1.39
J-1*	west	57.6	0.63d	10.3	86	1.41
J-1	east	54.1	0.72d	10.8	93	1.38
J-2	east	54.1	0.72d	11.2	94	1.38
J-2	west **	43.4	1.06d	19.2	161	1.12
J-3	east **	41.1	1.13d	20.3	173	1.20
J-3	west **	44.2	1.03d	21.3	180	1.48

$\frac{v_n(test)}{v_n(MCFT)}$

Mean (I-series beams, ρ_w=1.00%): 1.16
Coefficient of Variation: 11.1%

Mean (J-series beams, ρ_w=0.75%): 1.32
Coefficient of Variation: 10.2%

$\frac{v_n(test)}{v_n(MCFT)}$

Mean (all beams): 1.26
Coefficient of Variation: 11.8%

Mean (beams without stirrups): 1.31
Coefficient of Variation: 7.6%

Mean (beams with stirrups): 1.18
Coefficient of Variation: 16.1%

k_1 from Step 3 equal to 0.4 for shear reinforcement

Beam	Span	θ	Hor. Proj.	V_n(MCFT)	v_n(MCFT)	$\frac{v_n(test)}{v_n(MCFT)}$
I-2	east **	39..3	1.22d	22.2	186	1.06
I-3	west **	38.9	1.24d	22.8	191	0.92
J-2	west **	43.2	1.06d	19.3	162	1.12
J-3	east **	41.3	1.14d	20.3	173	1.20
J-3	west **	45	1.00d	21.4	181	1.47

$\frac{v_n(test)}{v_n(MCFT)}$

Mean (beams with stirrups): 1.15
Coefficient of Variation: 17.7%

* positive moment region failure
** beams containing stirrups

Table 3.15 Results Obtained from MCFT Design Procedure

Beam	Span	θ	Hor. Proj.	V_n(MCFT)	v_n(MCFT)	$\frac{v_n(test)}{v_n(MCFT)}$
I-1	east	48	0.90d	12.3	106	1.24
I-1	west	48	0.90d	12.3	106	1.21
I-2	east **	43	1.07d	16.6	139	1.42
I-3	east	49	0.87d	12.6	106	1.32
I-3	west **	43	1.07d	17.0	143	1.23
J-1*	east	50	0.84d	11.5	96	1.04
J-1	west	50	0.84d	11.1	95	1.36
J-1*	west	50	0.84d	11.5	96	1.26
J-1	east	50	0.84d	11.1	95	1.35
J-2	east	50	0.84d	11.5	97	1.34
J-2	west **	45	1.00d	15.6	131	1.38
J-3	east **	45	1.00d	17.5	149	1.40
J-3	west **	45	1.00d	20.2	171	1.56

	$\frac{v_n(test)}{v_n(MCFT)}$
Mean (I-series beams, ρ_w=1.00%):	1.28
Coefficient of Variation:	6.8%
Mean (J-series beams, ρ_w=0.75%):	1.34
Coefficient of Variation:	11.0%

	$\frac{v_n(test)}{v_n(MCFT)}$
Mean (all beams):	1.32
Coefficient of Variation:	9.5%
Mean (beams without stirrups):	1.27
Coefficient of Variation:	8.4%
Mean (beams with stirrups):	1.40
Coefficient of Variation:	8.4%

* - positive moment region failure
** beams containing stirrups

Table 3.16 Comparison of Test and Calculated Nominal Shear Stress from Current Study

Beam	Span	v_n (test) psi	v_n (ACI)** psi	$\frac{v_n \text{ (test)}}{v_n \text{ (ACI)}}$
I-1	east	131	136	0.96
I-1	west	128	136	0.94
I-2	east	197	167	1.18
I-3	east	140	134	1.04
I-3	west	176	168	1.05
J-1*	east	100	134	0.75
J-1	west	129	134	0.96
J-1*	west	121	134	0.90
J-1	east	128	134	0.96
J-2	east	130	134	0.97
J-2	west	181	168	1.08
J-3	east	208	190	1.09
J-3	west	266	215	1.24
			Mean (all beams)	1.01
			Coefficient of Variation	12.4%
			Mean (beams without stirrups)	0.94
			Coefficient of Variation	9.0%
			Mean (beams with stirrups)	1.13
			Coefficient of Variation	7.0%

* positive moment region failure

** $v_n = \rho_v f_{vy} + 2\sqrt{f'_c}$

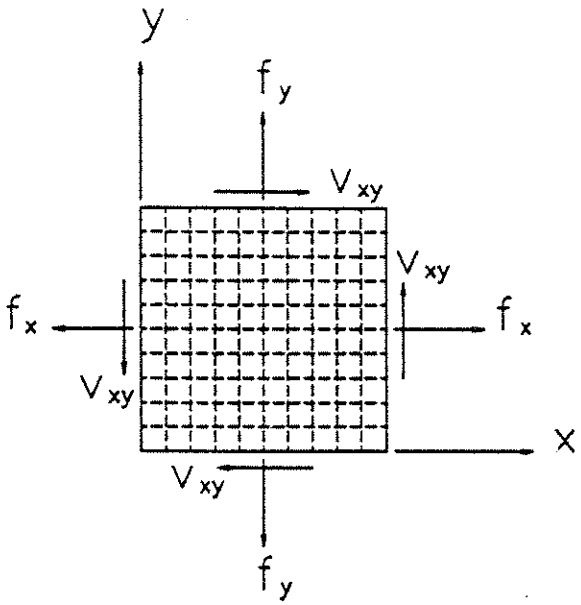

Fig. 1.1 Membrane element - stresses

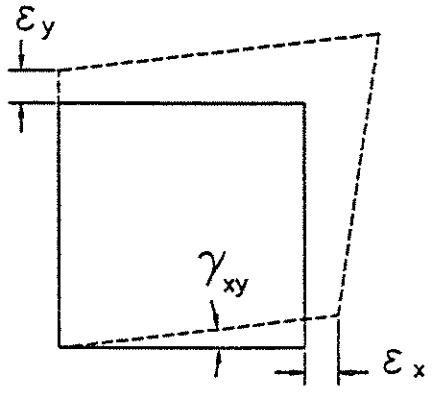

Fig. 1.2 Membrane element - deformation

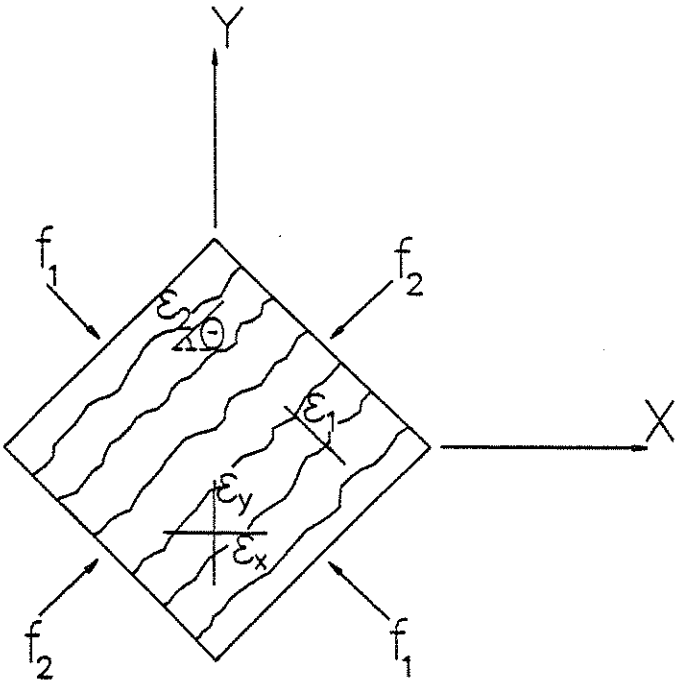

Fig. 1.3 Average stresses and strains in cracked element

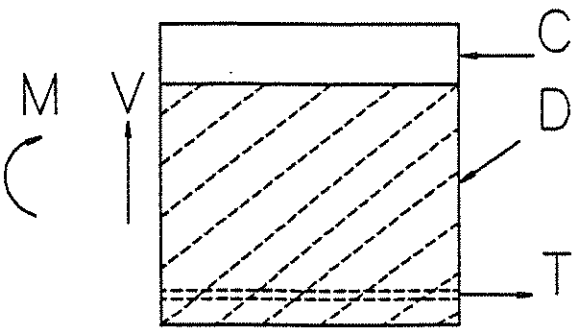

Fig. 1.4 Sectional forces on membrane element

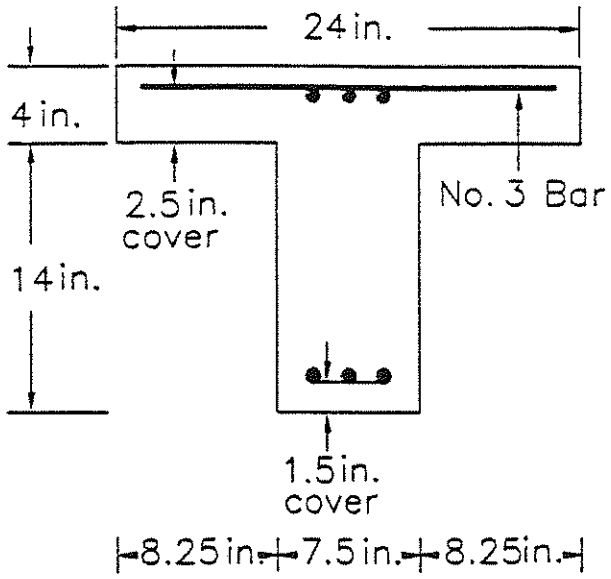

Fig. 2.1 Cross-section of beams without stirrups in test region

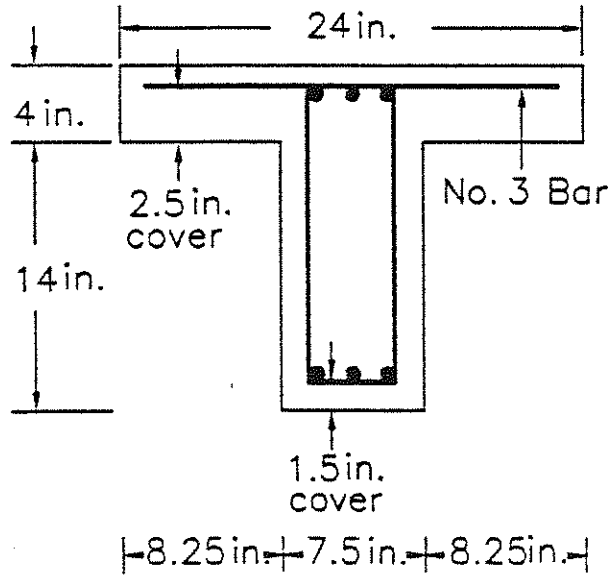

Fig. 2.2 Cross-section of beams with stirrups in test region

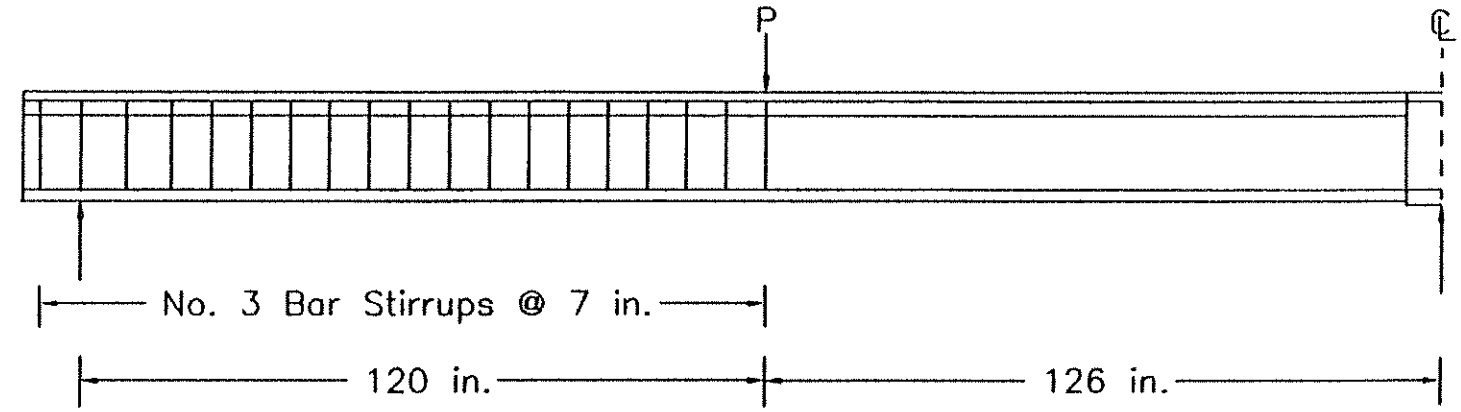

Stirrup Reinforcement For Single Point Load System

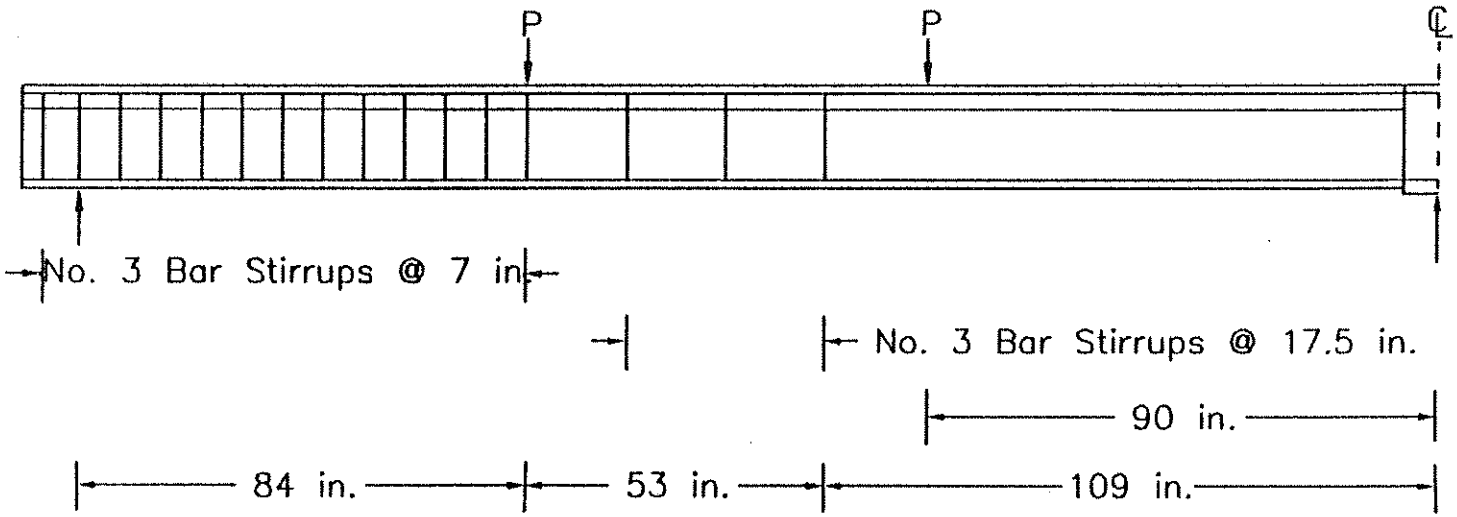

Stirrup Reinforcement For Two Point Load System

Fig. 2.3 a Beams without stirrups in test region

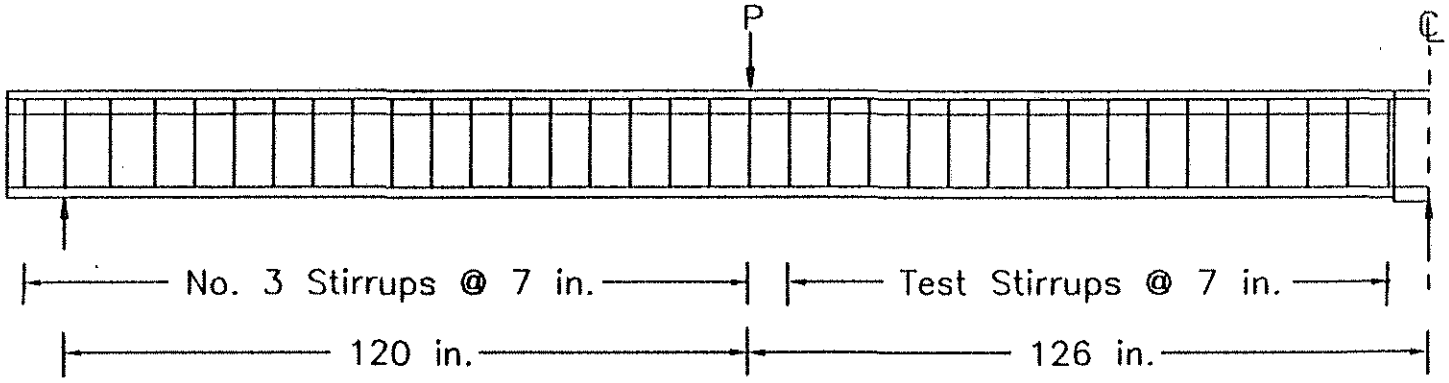

Stirrup Reinforcement For Single Point Load System

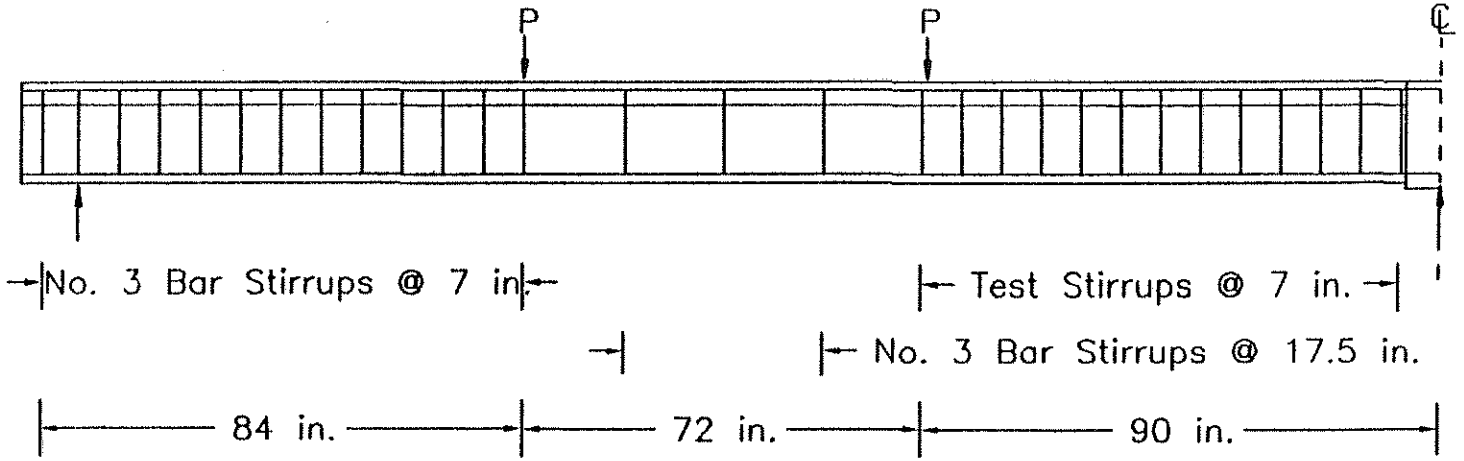

Stirrup Reinforcement For Two Point Load System

Fig.2.3 b Beams with stirrups in test region

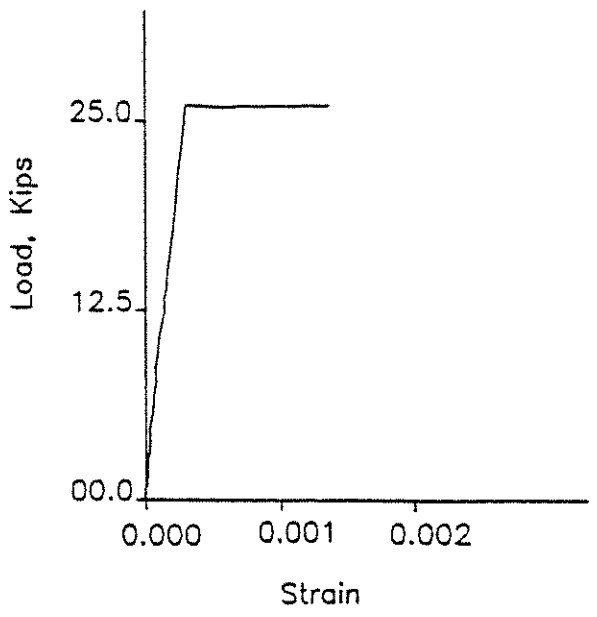

Fig. 2.4 a Load-strain curve for No.5 bar

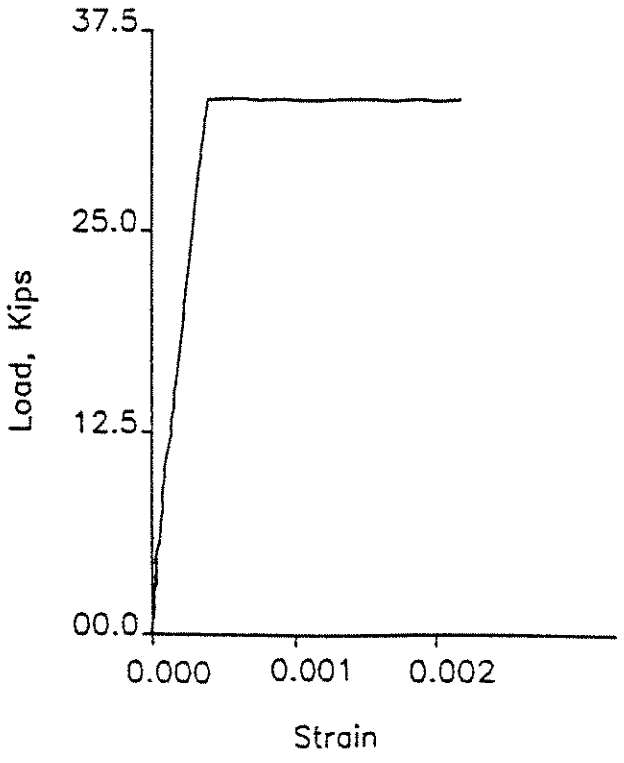

Fig. 2.4 b Load-strain curve for No.6 bar

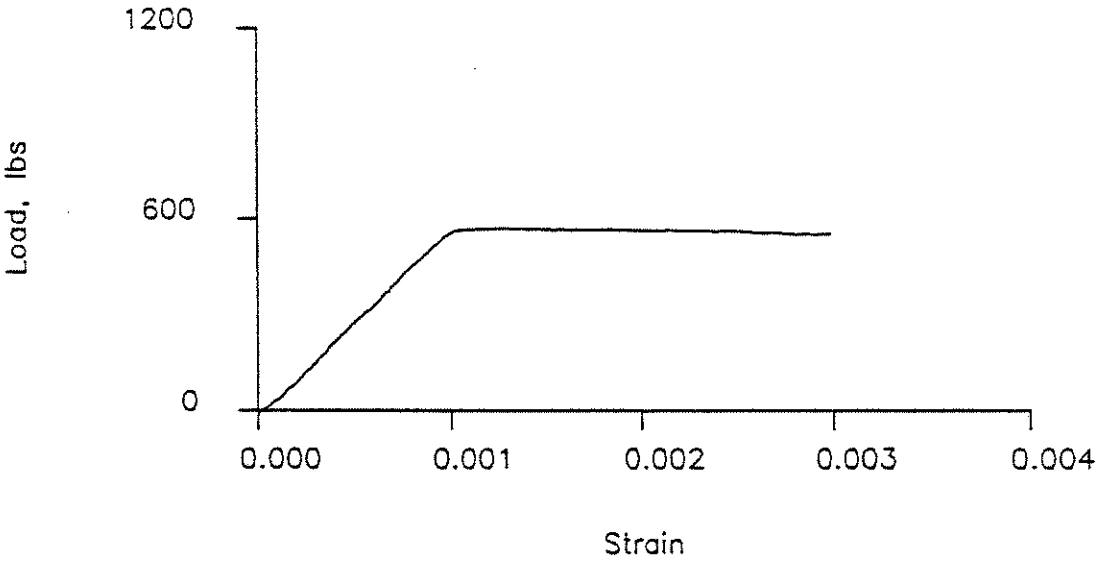

Fig. 2.4 c Load-strain curve for test stirrup, $\rho_v f_{vy}$=34 psi

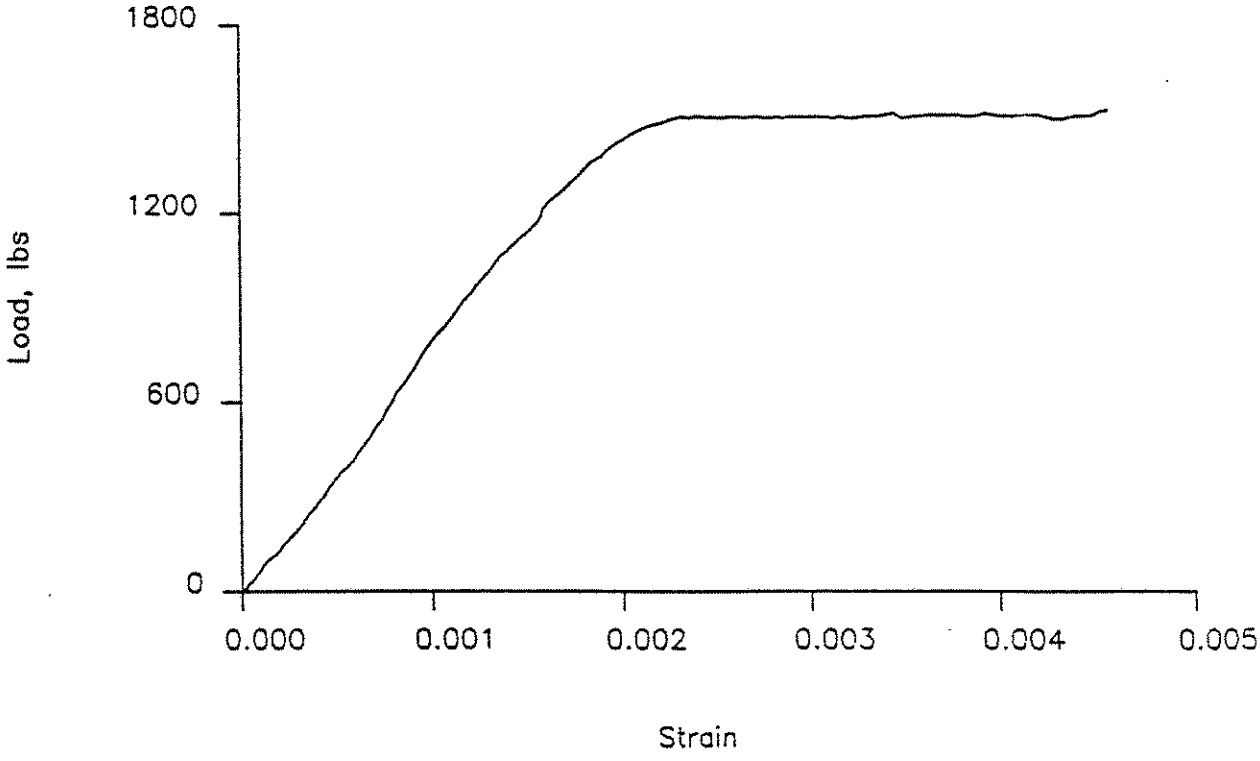

Fig. 2.4 d Load-strain curve for test stirrup, $\rho_v f_{vy}$=57 psi

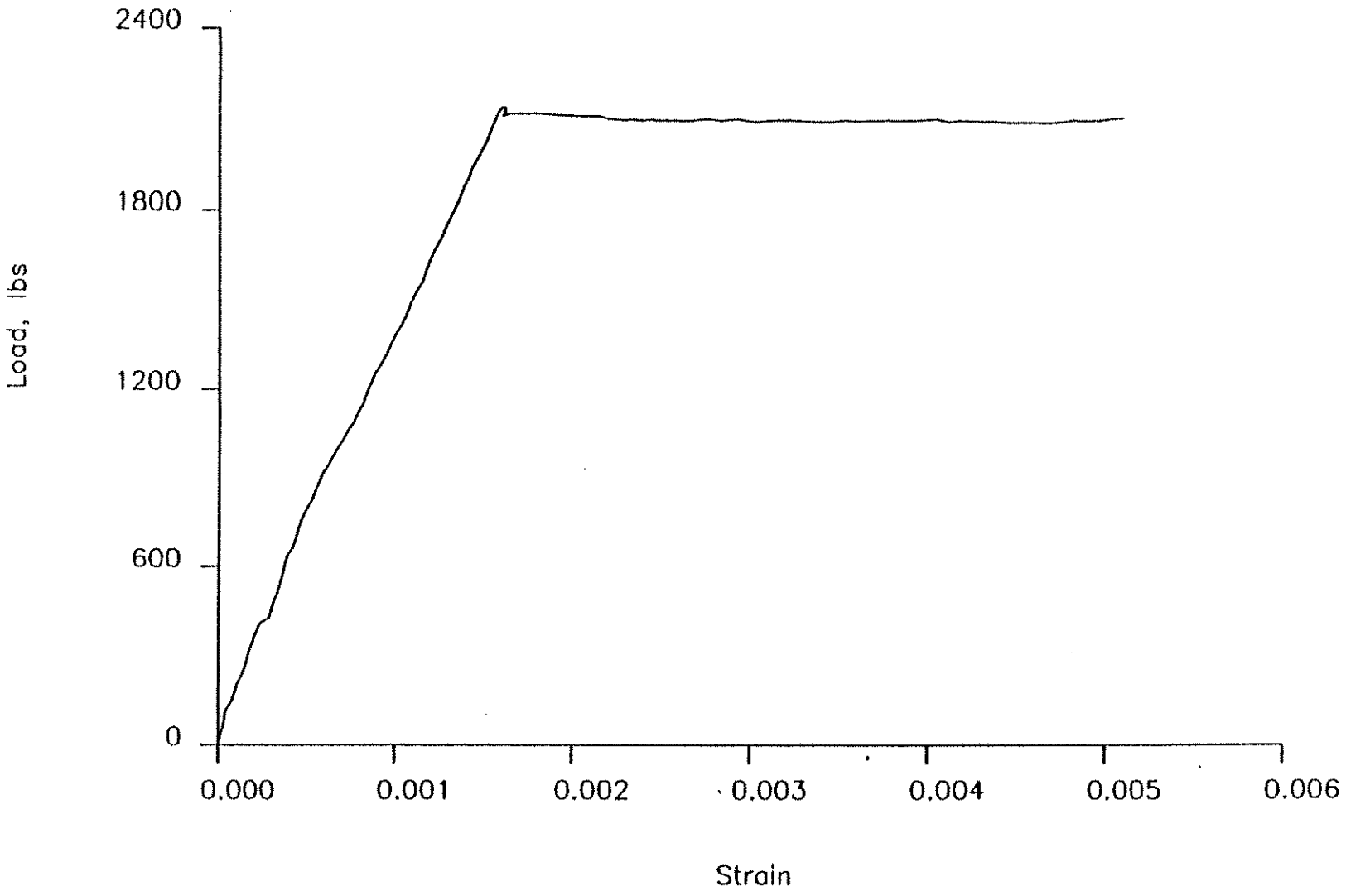

Fig. 2.4 e Load-strain curve for test stirrup, $\rho_v f_{vy}$=82 psi

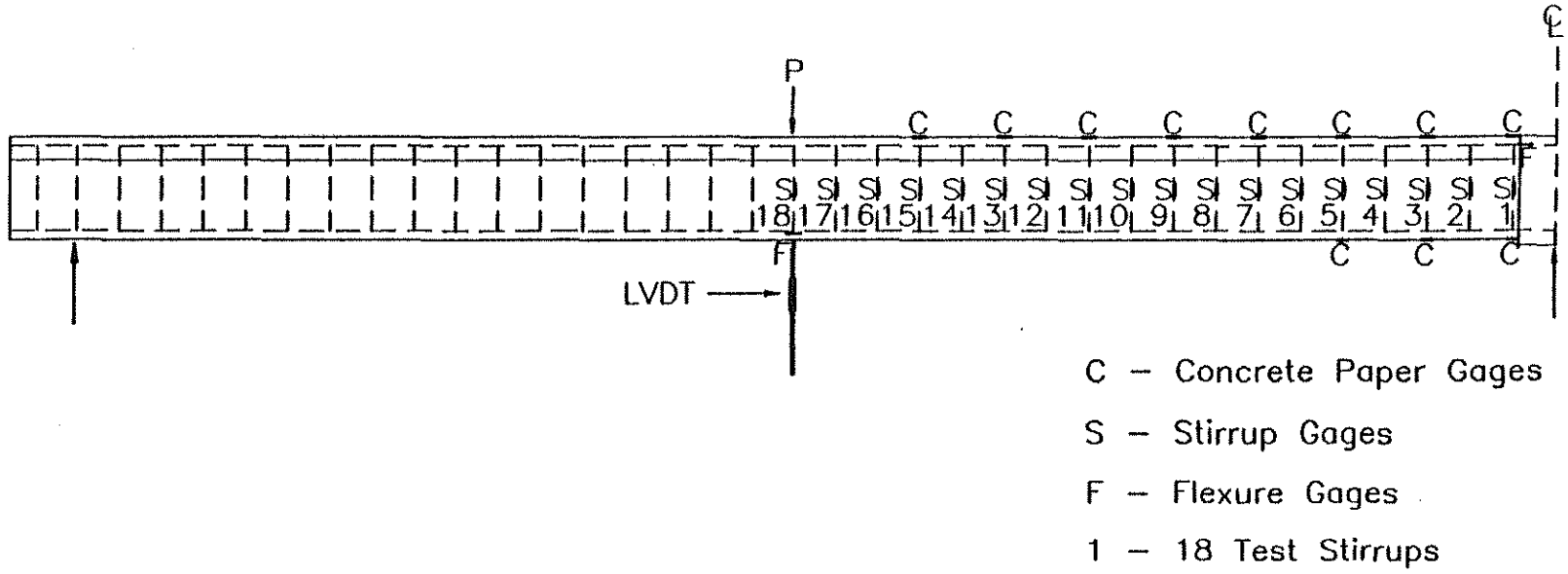

Fig.2.5 a Strain gage locations for beams I-1, I-2, J-1

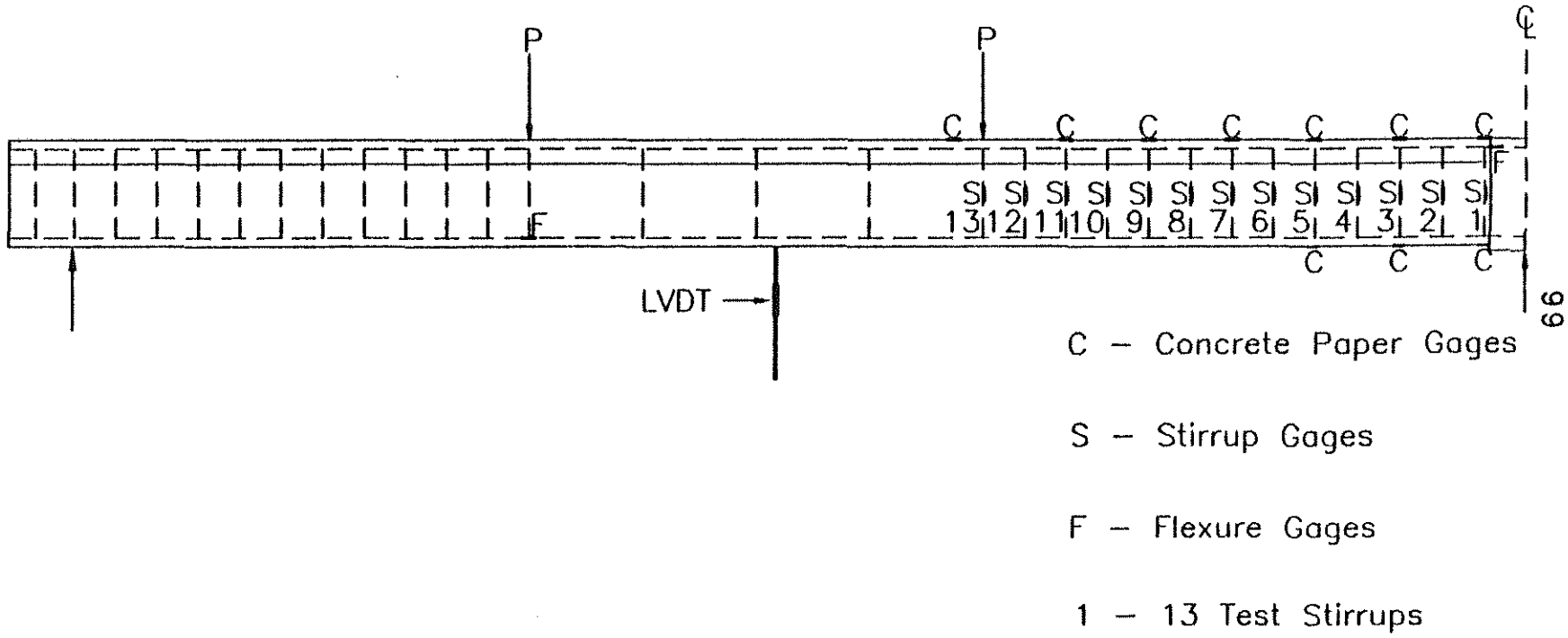

Fig.2.5 b Strain gage locations I-3, J-2, J-3

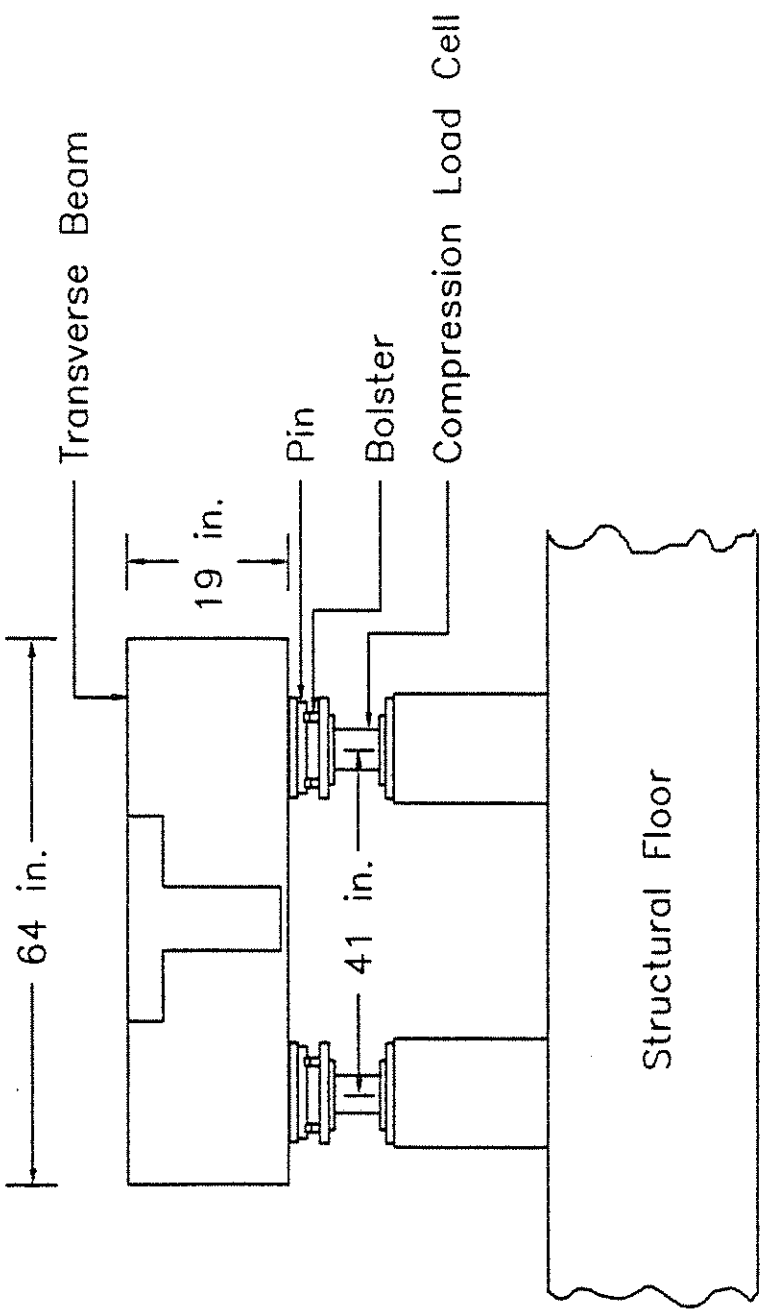

Fig.2.6 Transverse girder

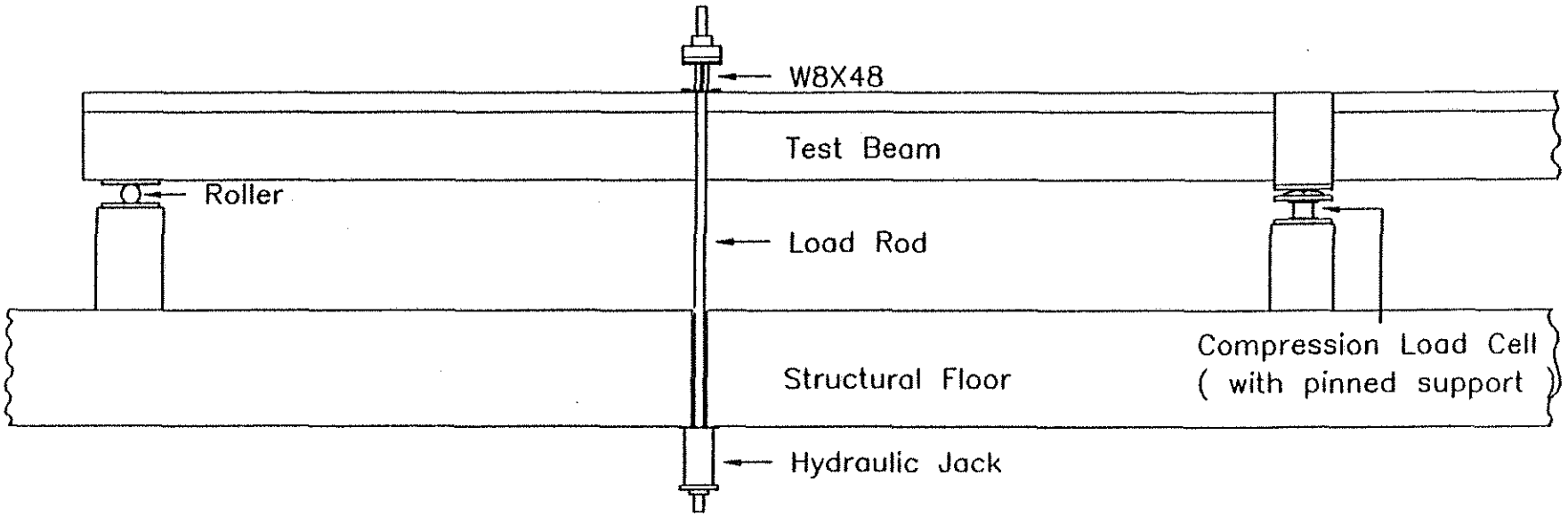

Fig. 2.7 a Single point loading system

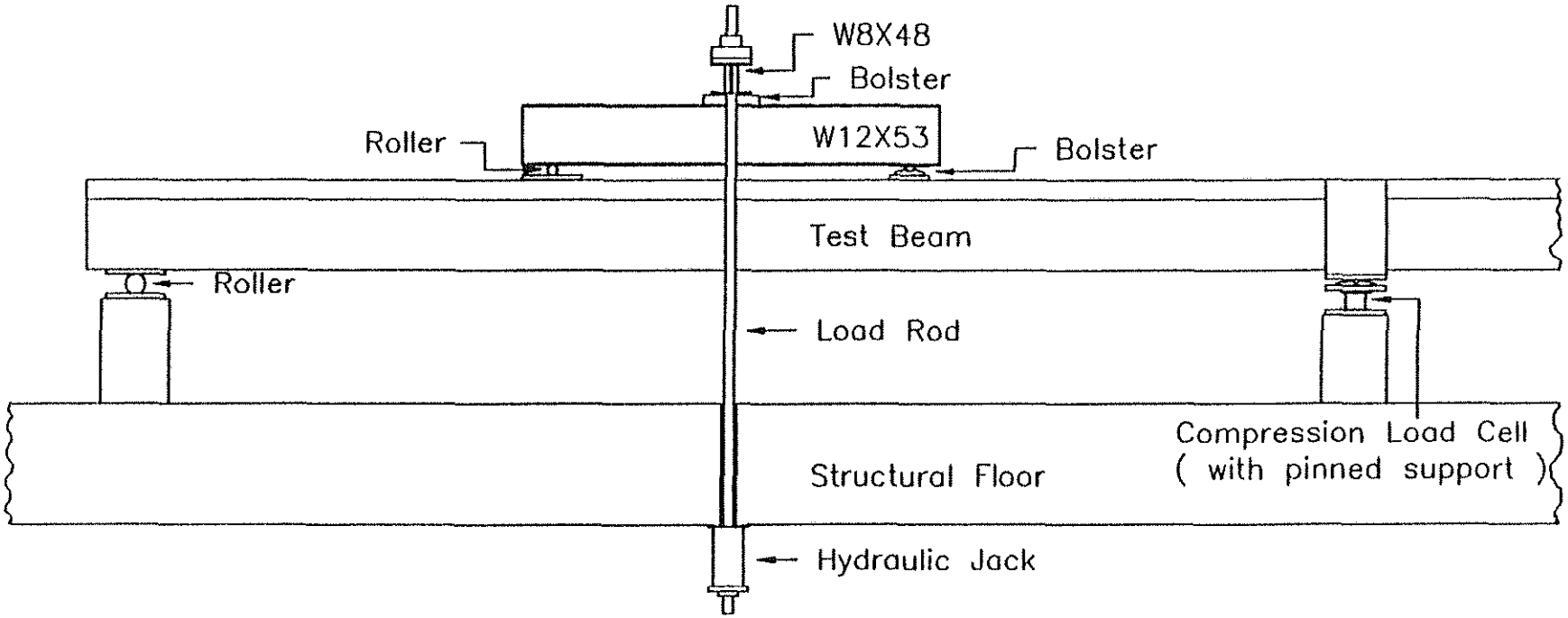

Fig. 2.7 b Two point loading system

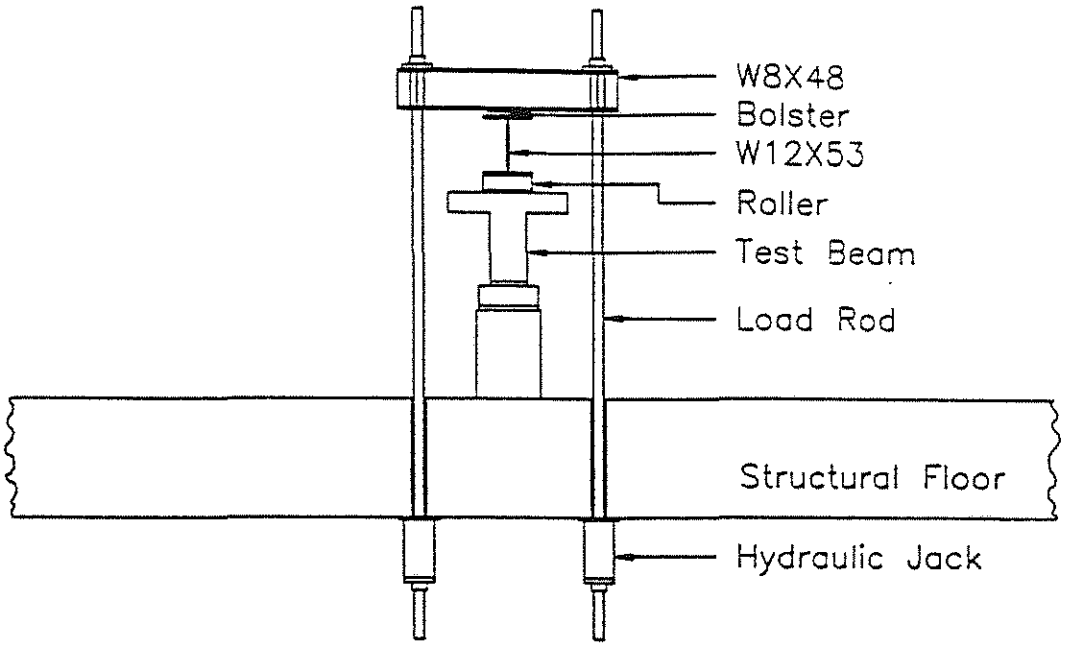

Two point loading system

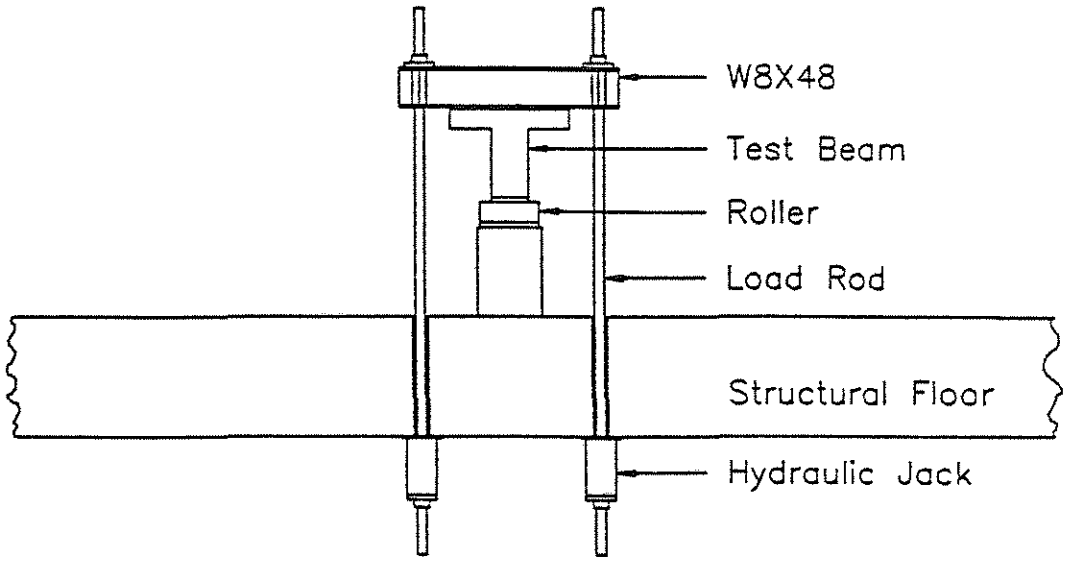

Single point loading system

Fig. 2.7 c Loading system - End view

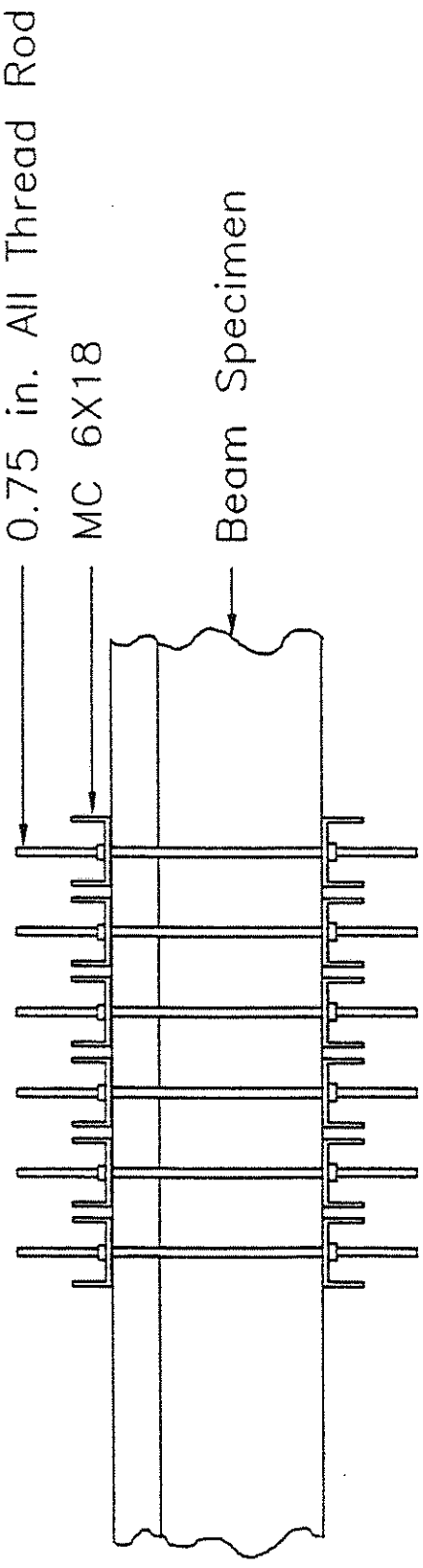

Fig. 2.8 External Stirrups

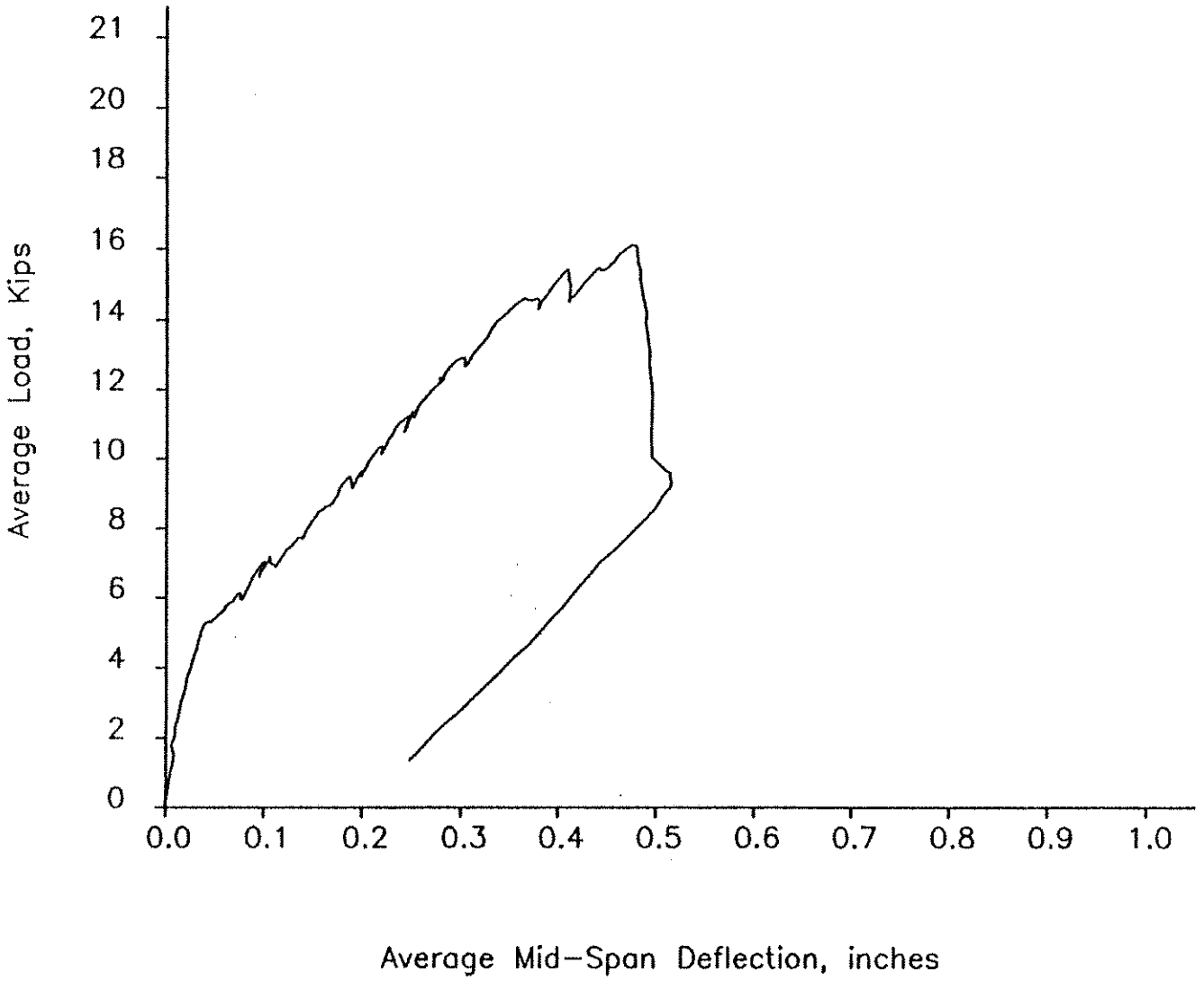

Fig. 2.9 a Average load-average midspan deflection curve for beam I-1

(east negative shear span failure)

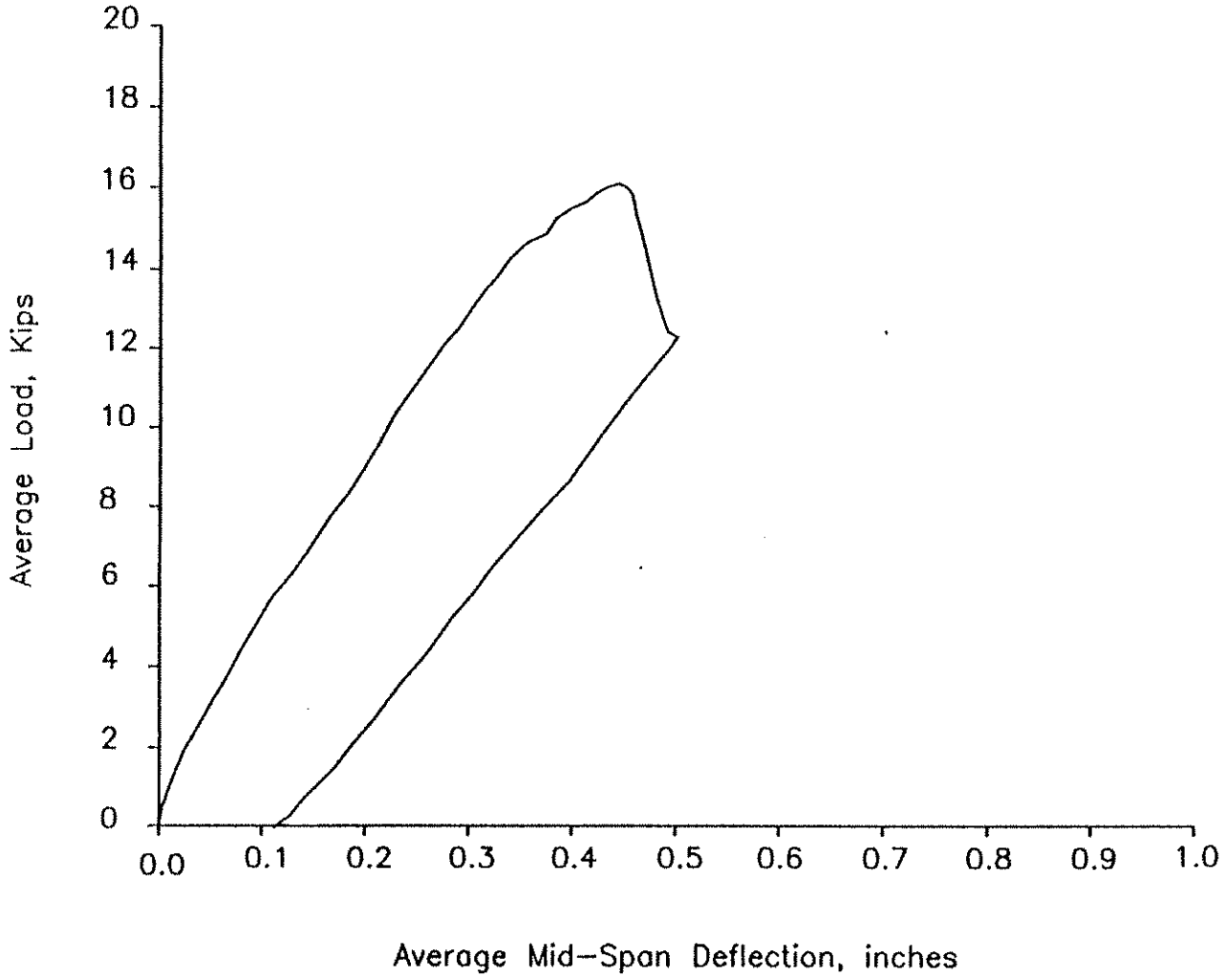

Fig. 2.9 b Average load-average midspan deflection curve for beam I-1

(west negative shear span failure)

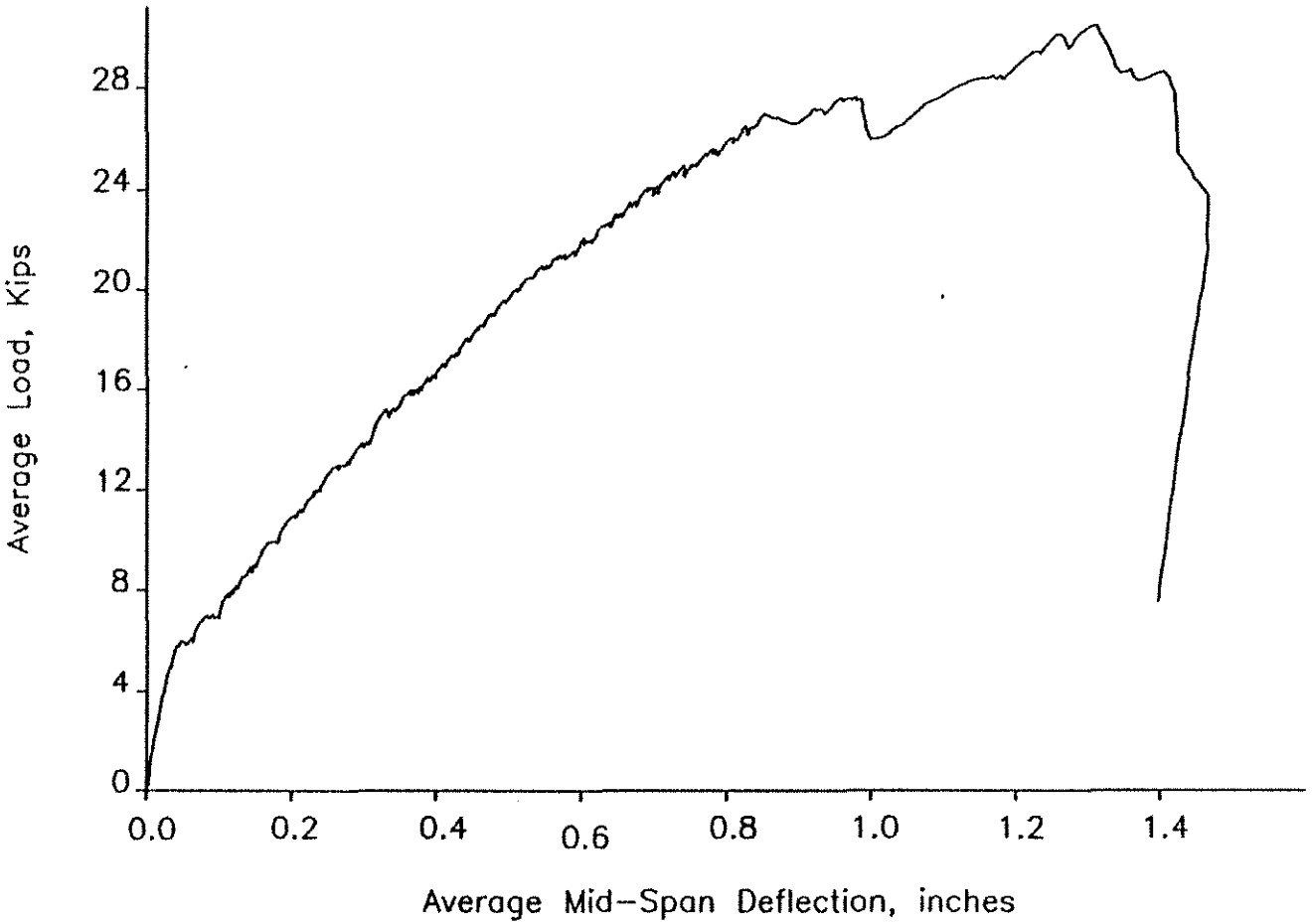

Fig. 2.9 c Average load-average midspan deflection curve for beam I-2

(east negative shear span failure)

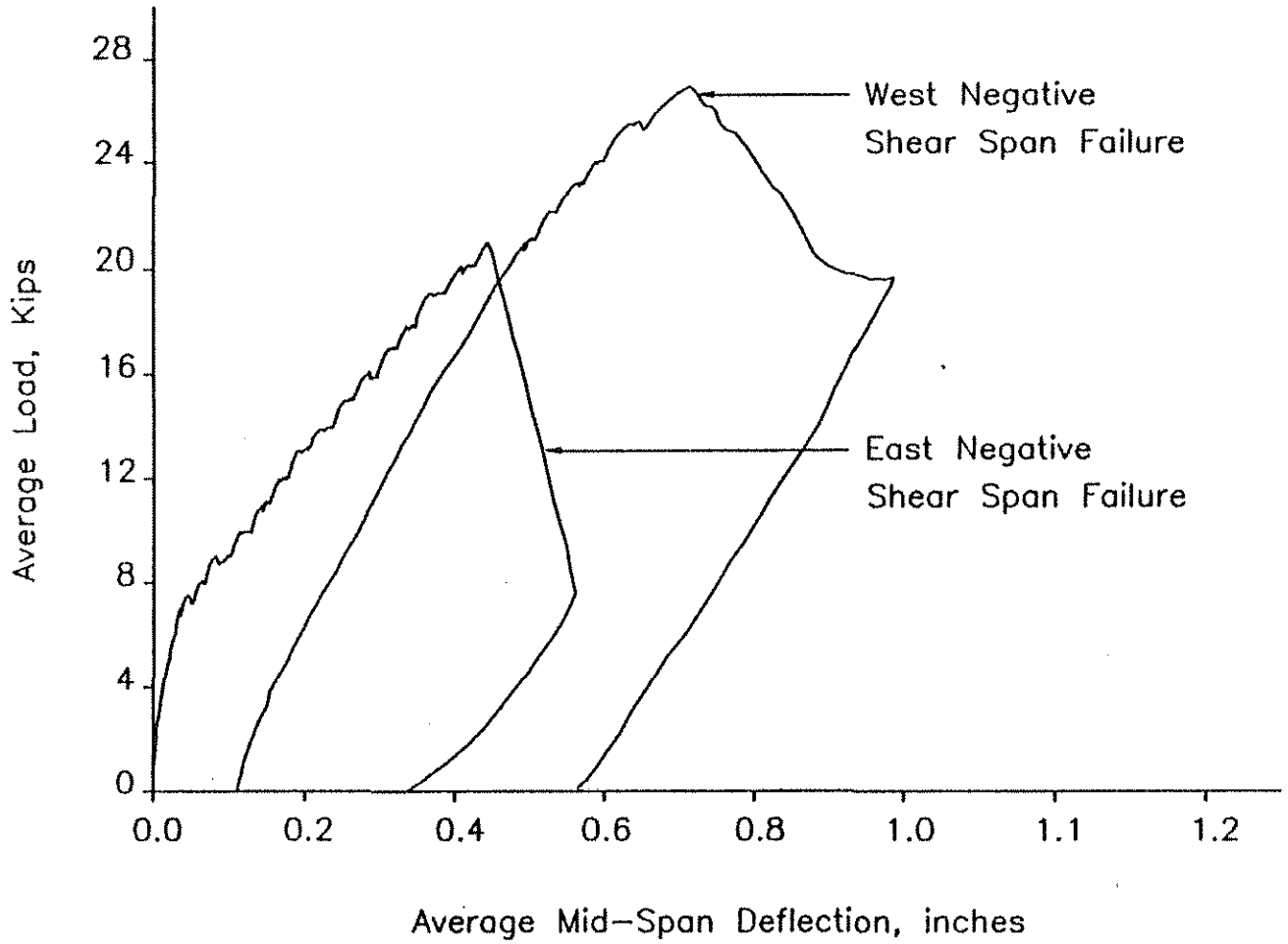

Fig. 2.9 d Average load-average midspan deflection curve for beam I-3

(east and west negative shear span failures)

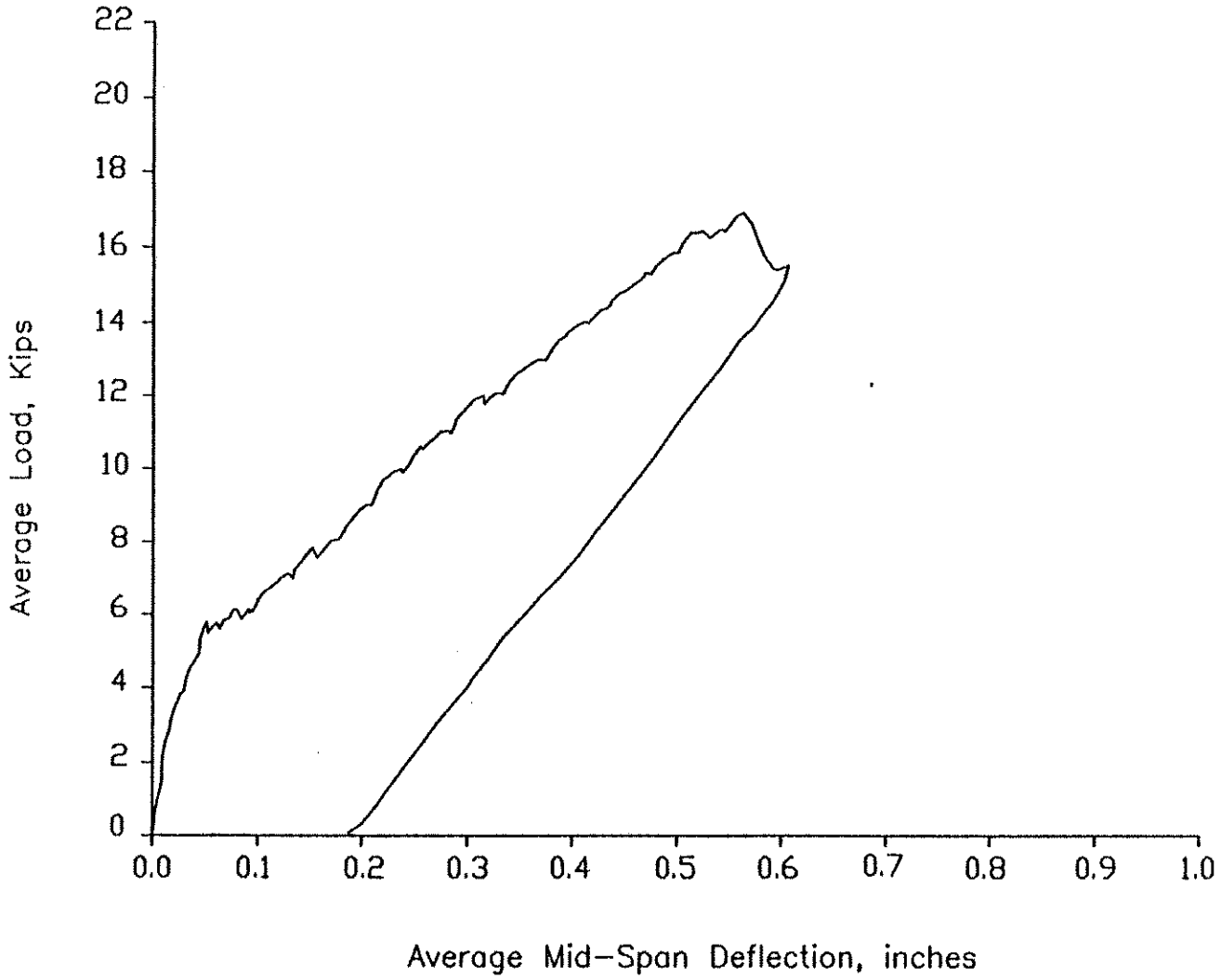

Fig. 2.9 e Average load-average midspan deflection curve for beam J-1

(east positive shear span failure)

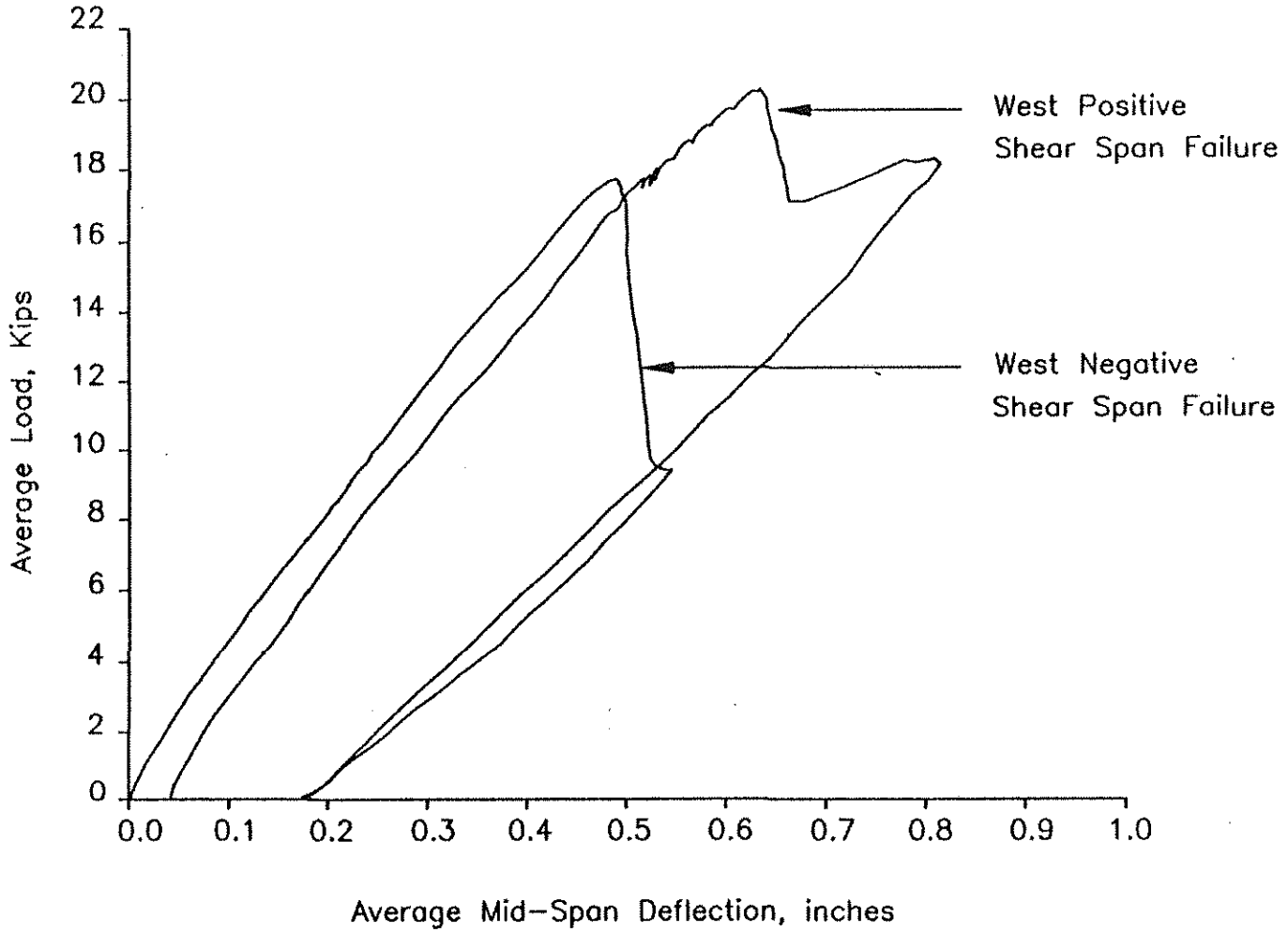

Fig. 2.9 f Average load-average midspan deflection curve for beam J-1

(west positive and negative shear span failure)

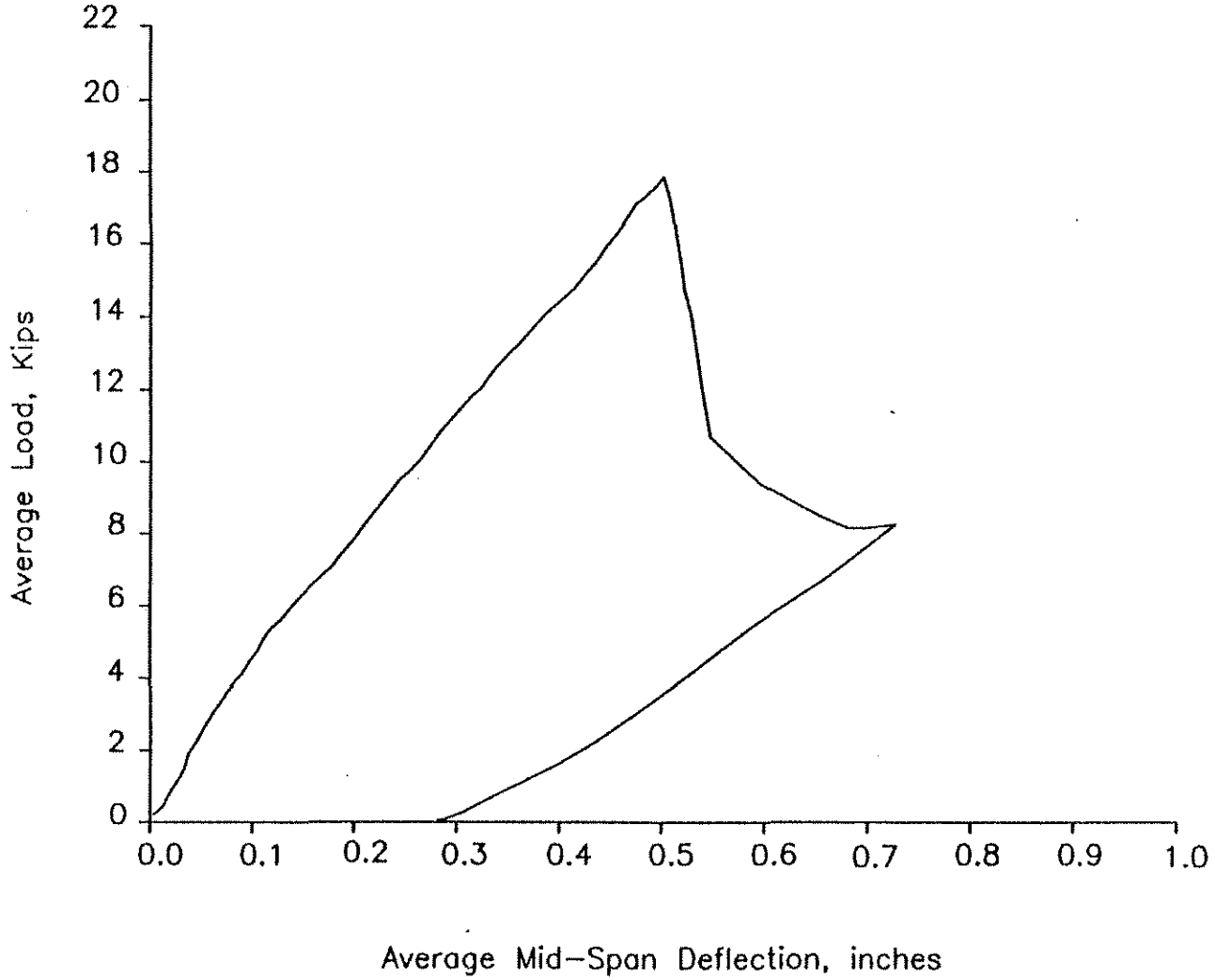

Fig. 2.9 g Average load-average midspan deflection curve for beam J-1

(east negative shear span failure)

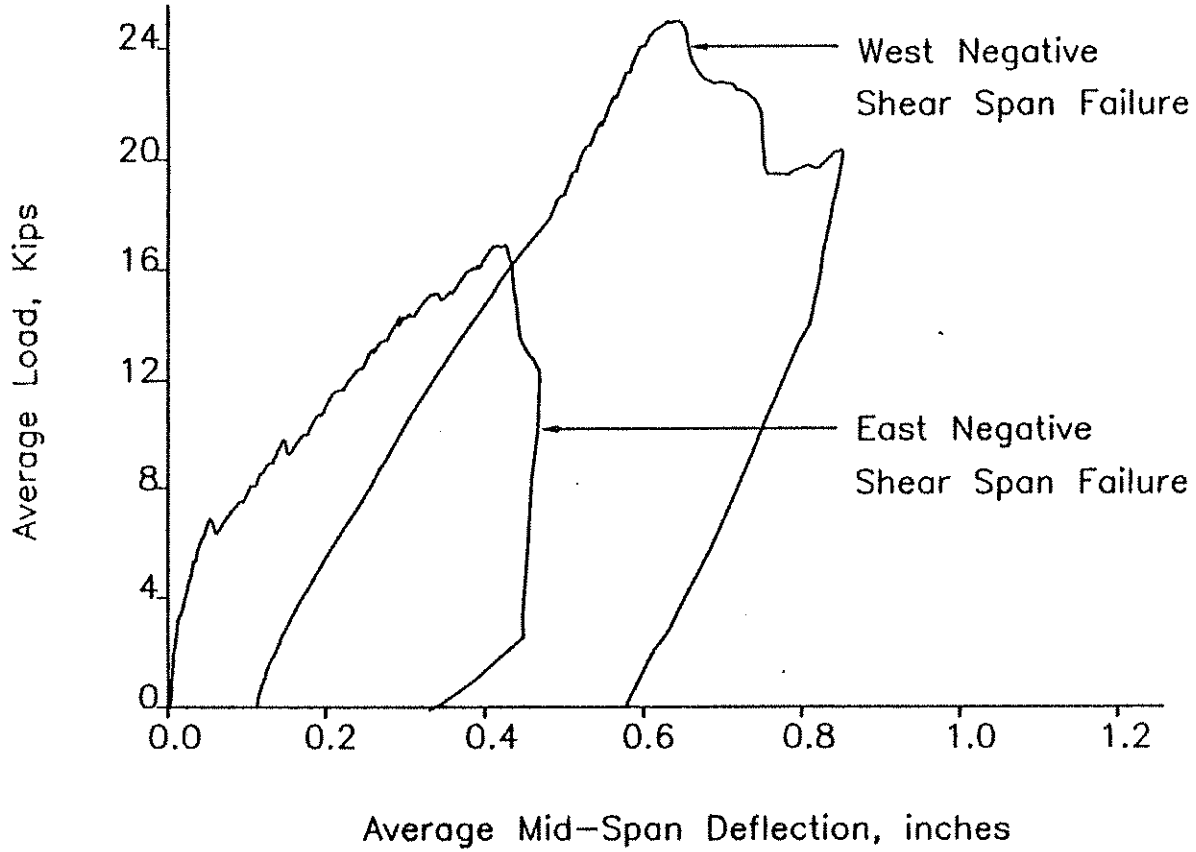

Fig. 2.9 h Average load-average midspan deflection curve for beam J-2

(east and west negative shear span failure)

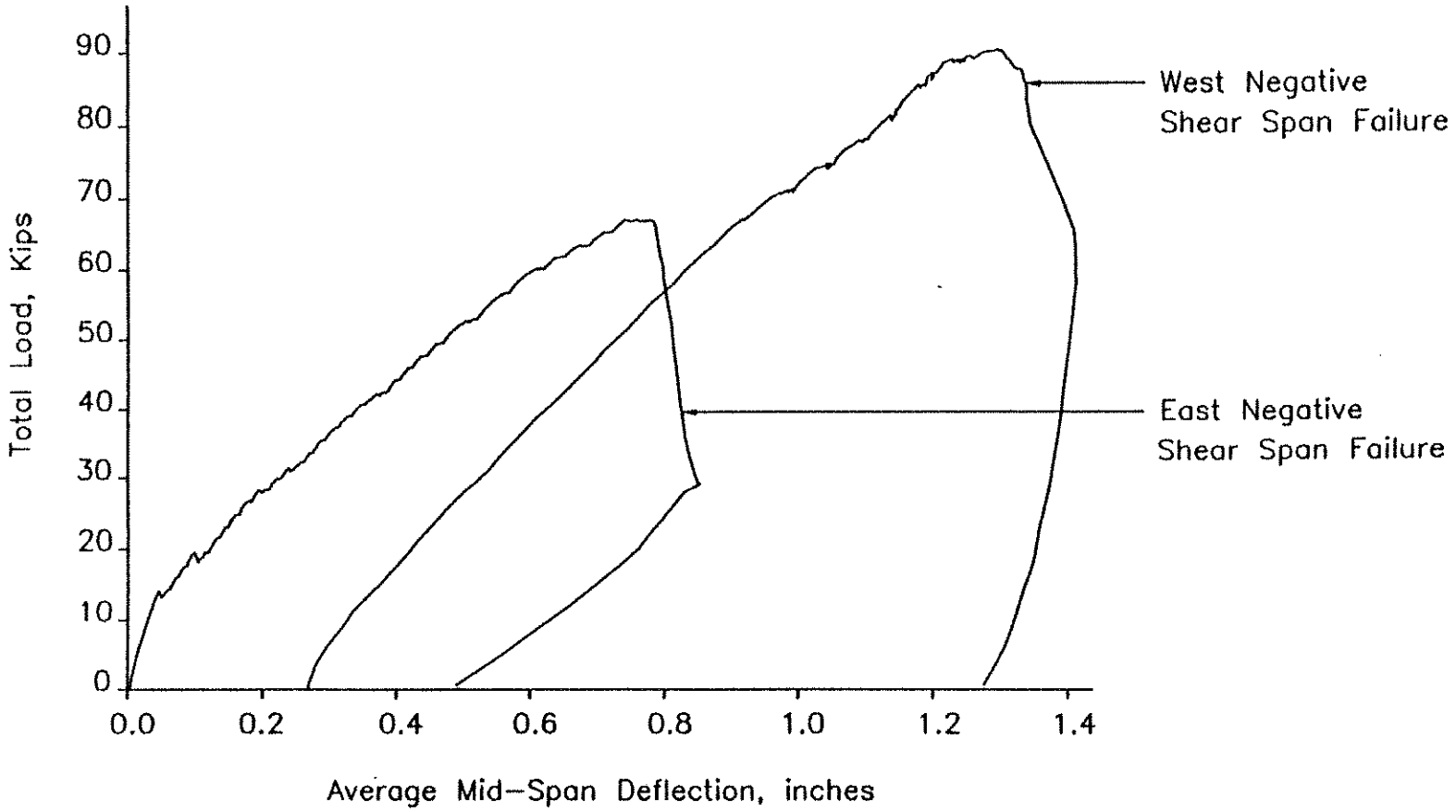

Fig. 2.9 I Average load-average midspan deflection curve for beam J-3

(east positive and negative shear span failure)

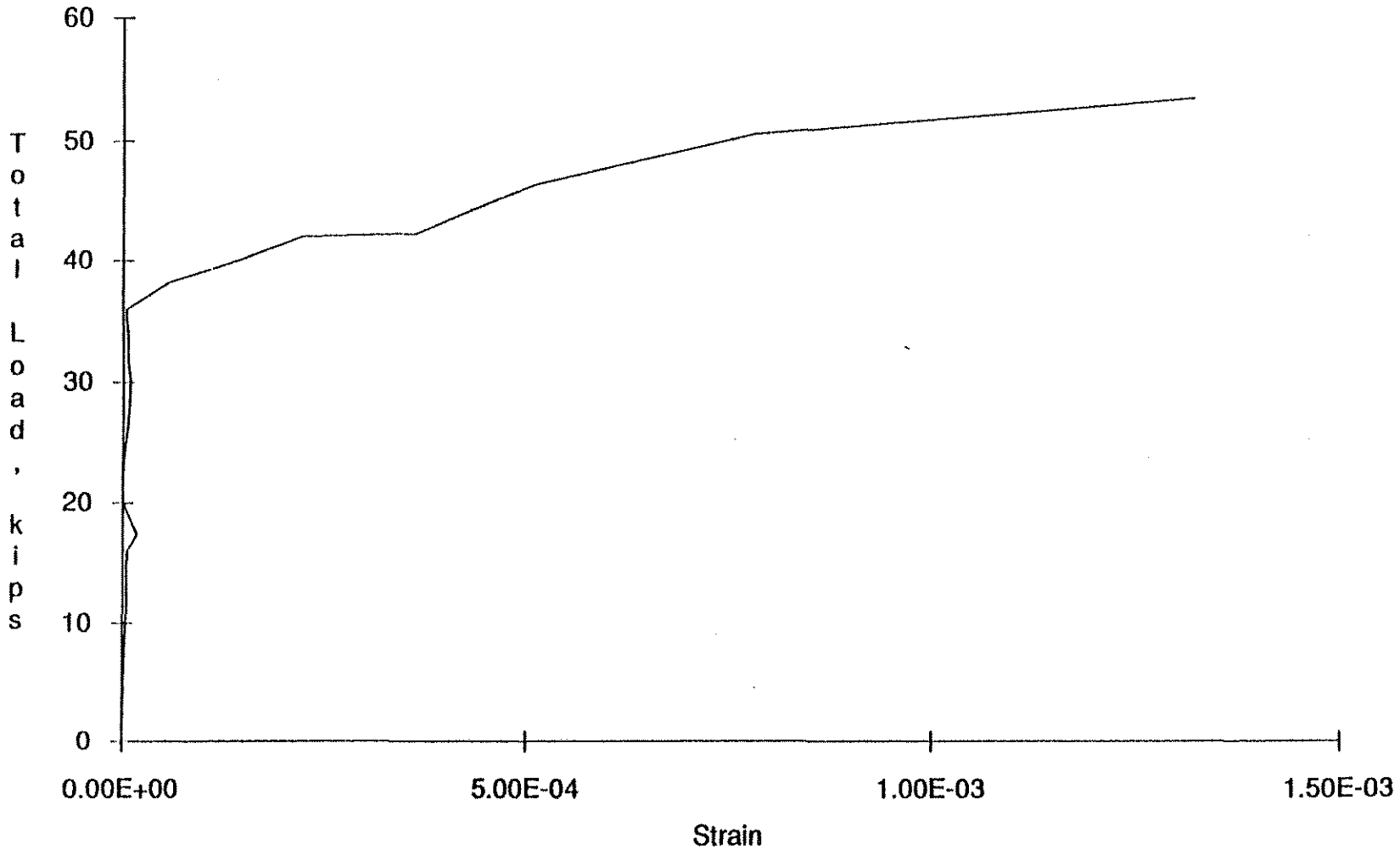

Fig. 2.10 Total Load versus stirrup strain curve

(third stirrup from face of transverse girder in west span of beam I-3)

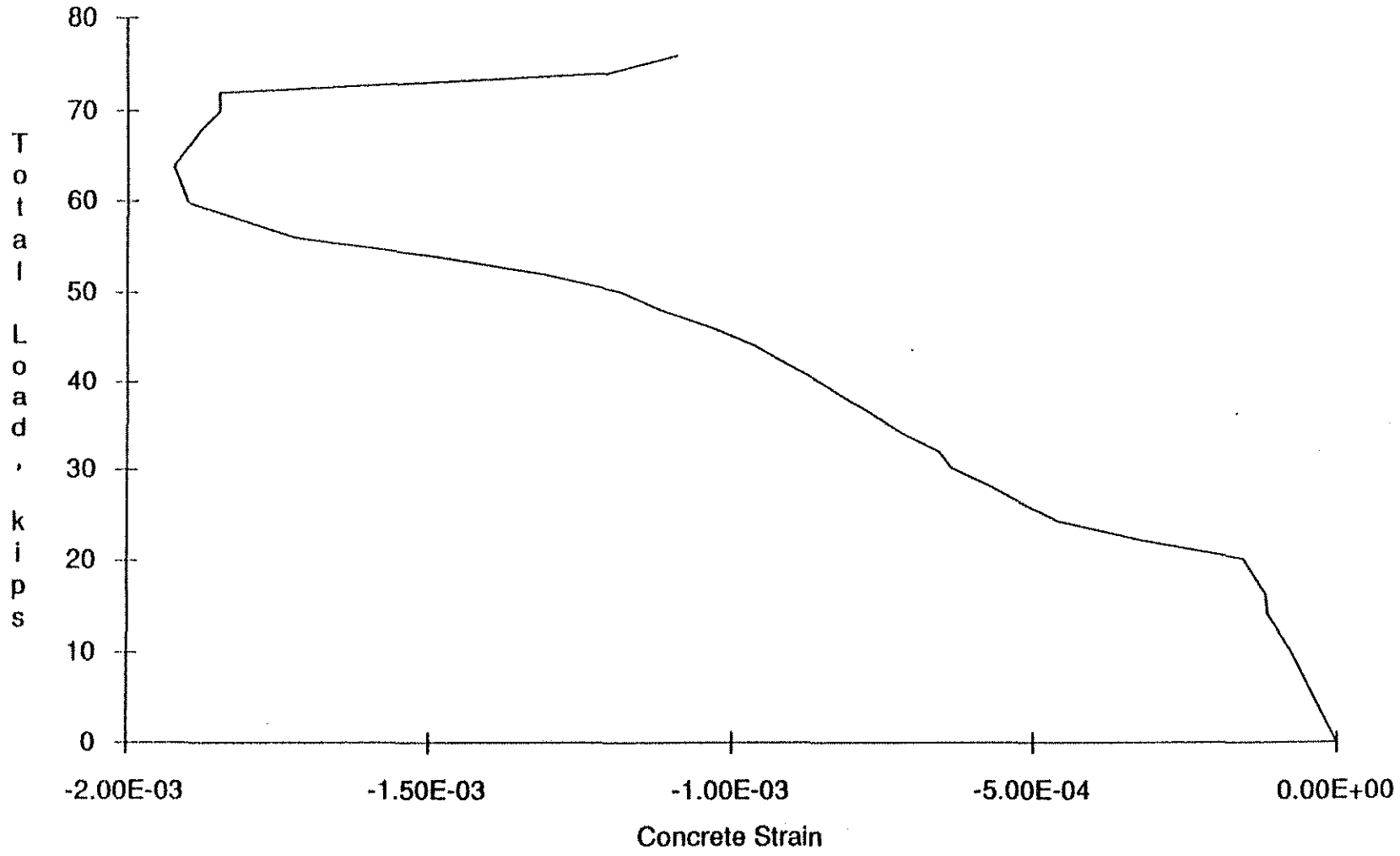

Fig. 2.11 Total Load versus concrete strain curve

(first bottom gage from face of transverse girder in east span of beam J-3)

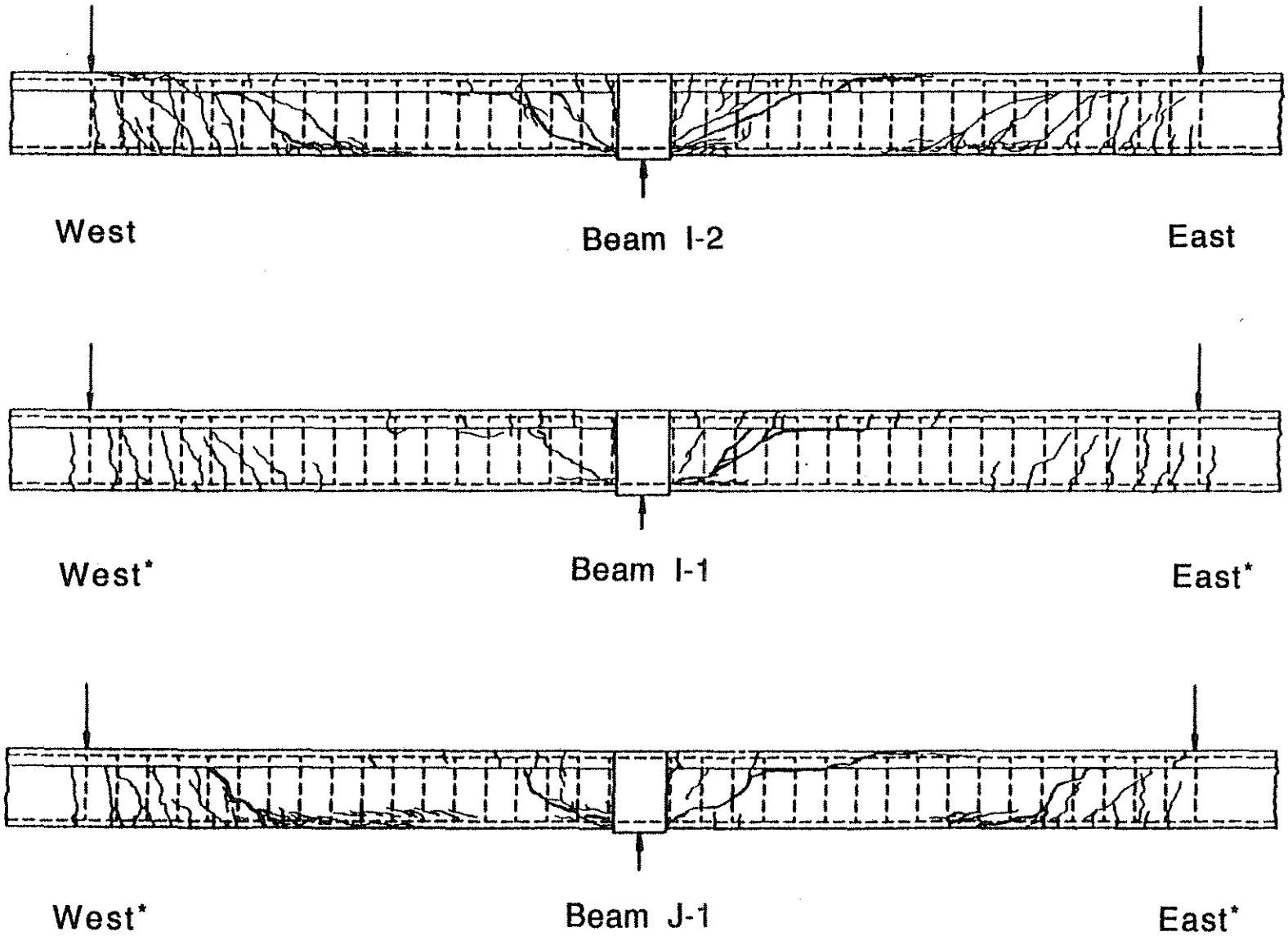

Fig. 2.12 a Crack Patterns, Beams I-1, I-2, J-1 (* Indicates span without stirrups)

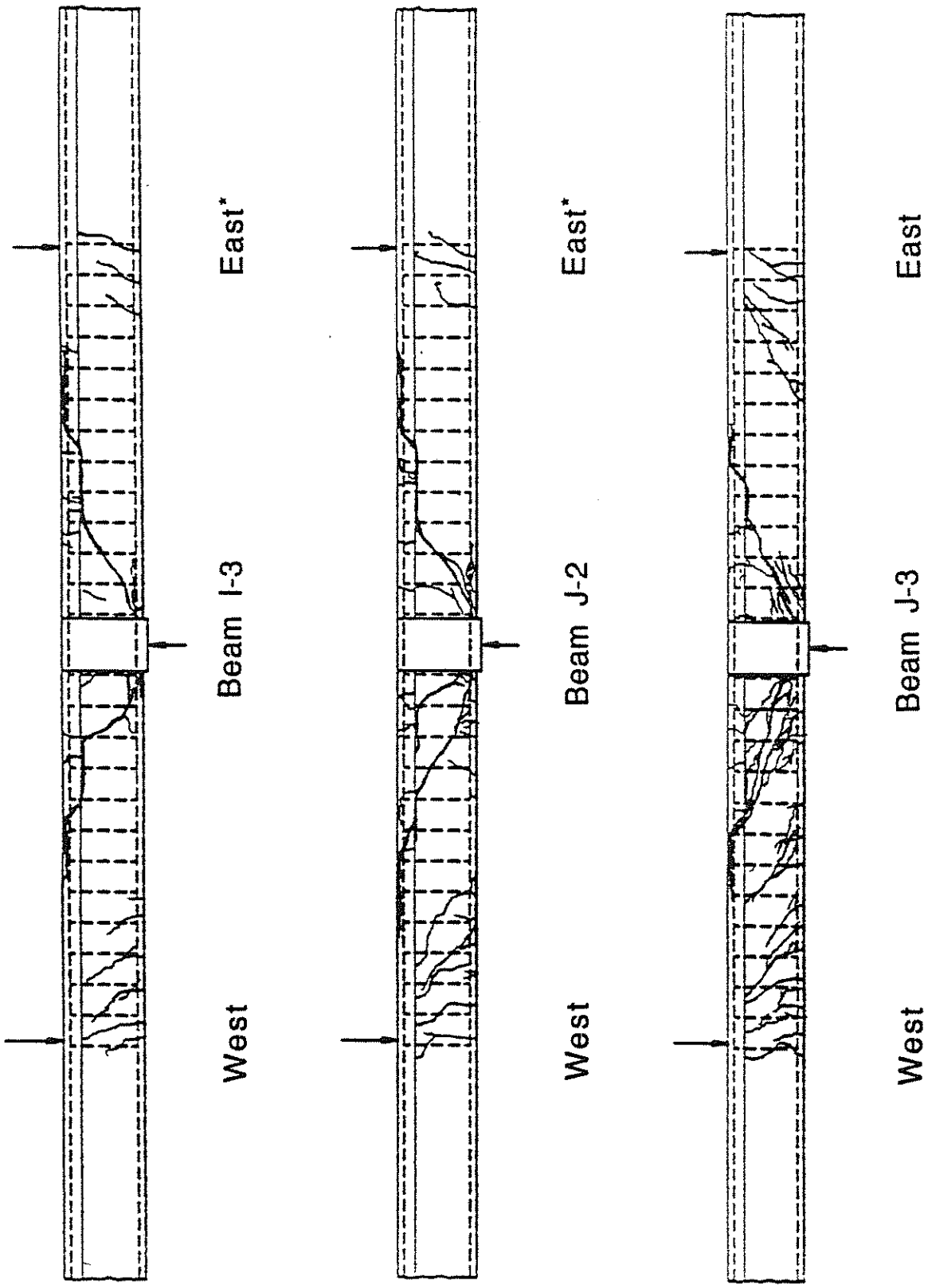

Fig. 2.12 b Crack Patterns, Beams I-3, J-2, J-3 (* indicates span without stirrups)

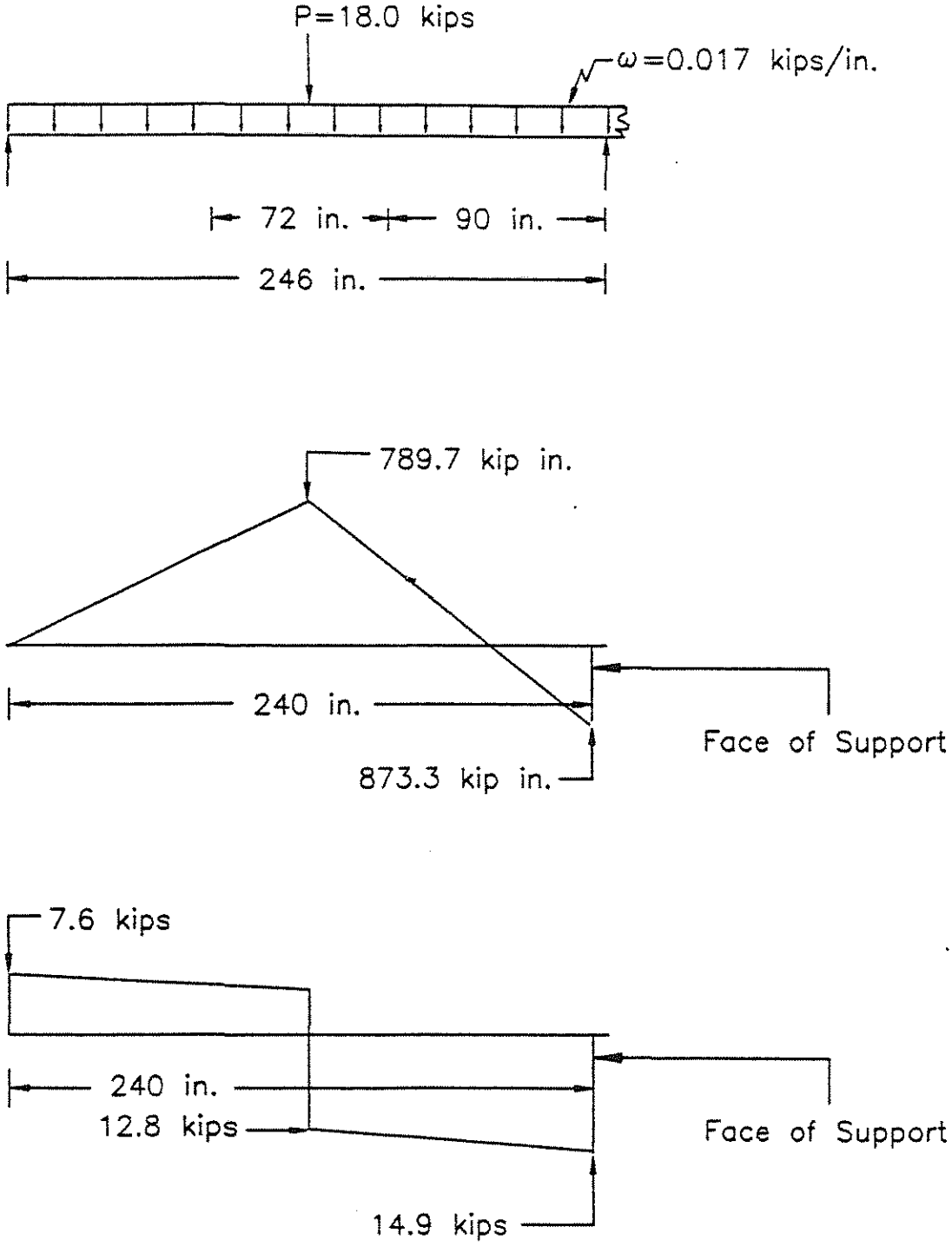

Fig. 2.13 a Bending moment and shear force diagrams at peak load for beam I-1

(negative moment region shear failure in east span)

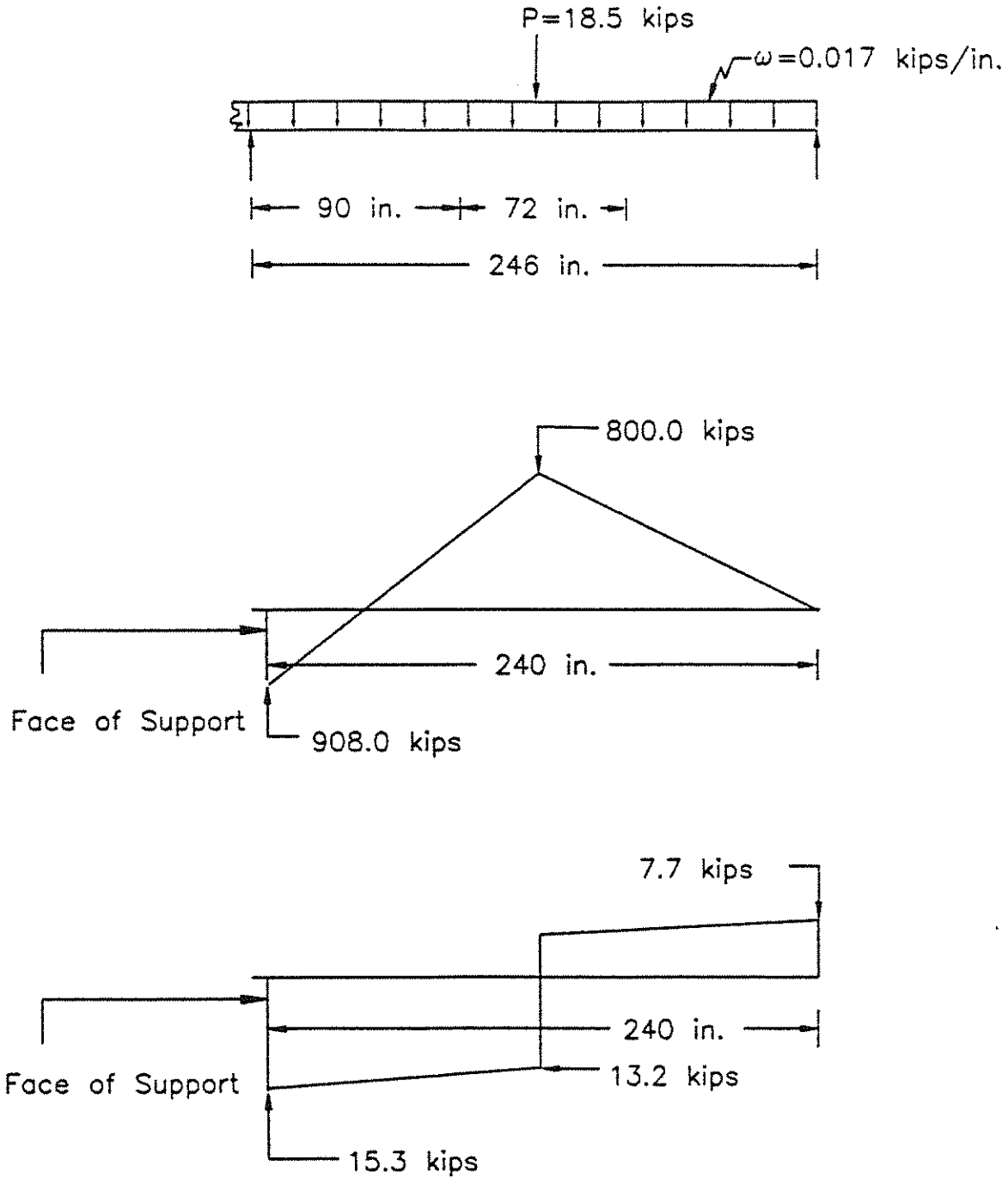

Fig. 2.13 b Bending moment and shear force diagrams at peak load for beam I-1

(negative moment region shear failure in west span)

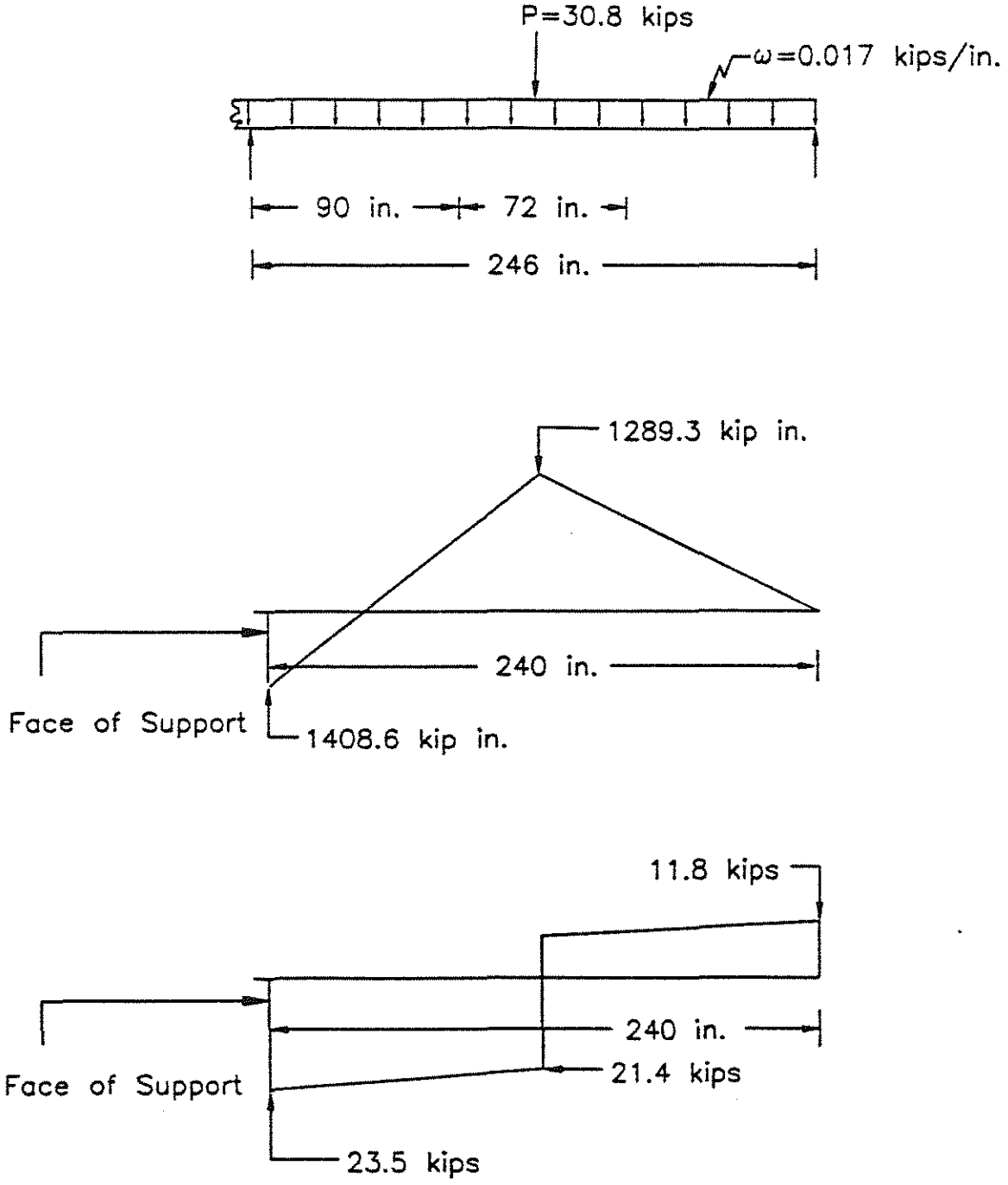

Fig. 2.13 c Bending moment and shear force diagrams at peak load for beam I-2

(negative moment region shear failure in east span)

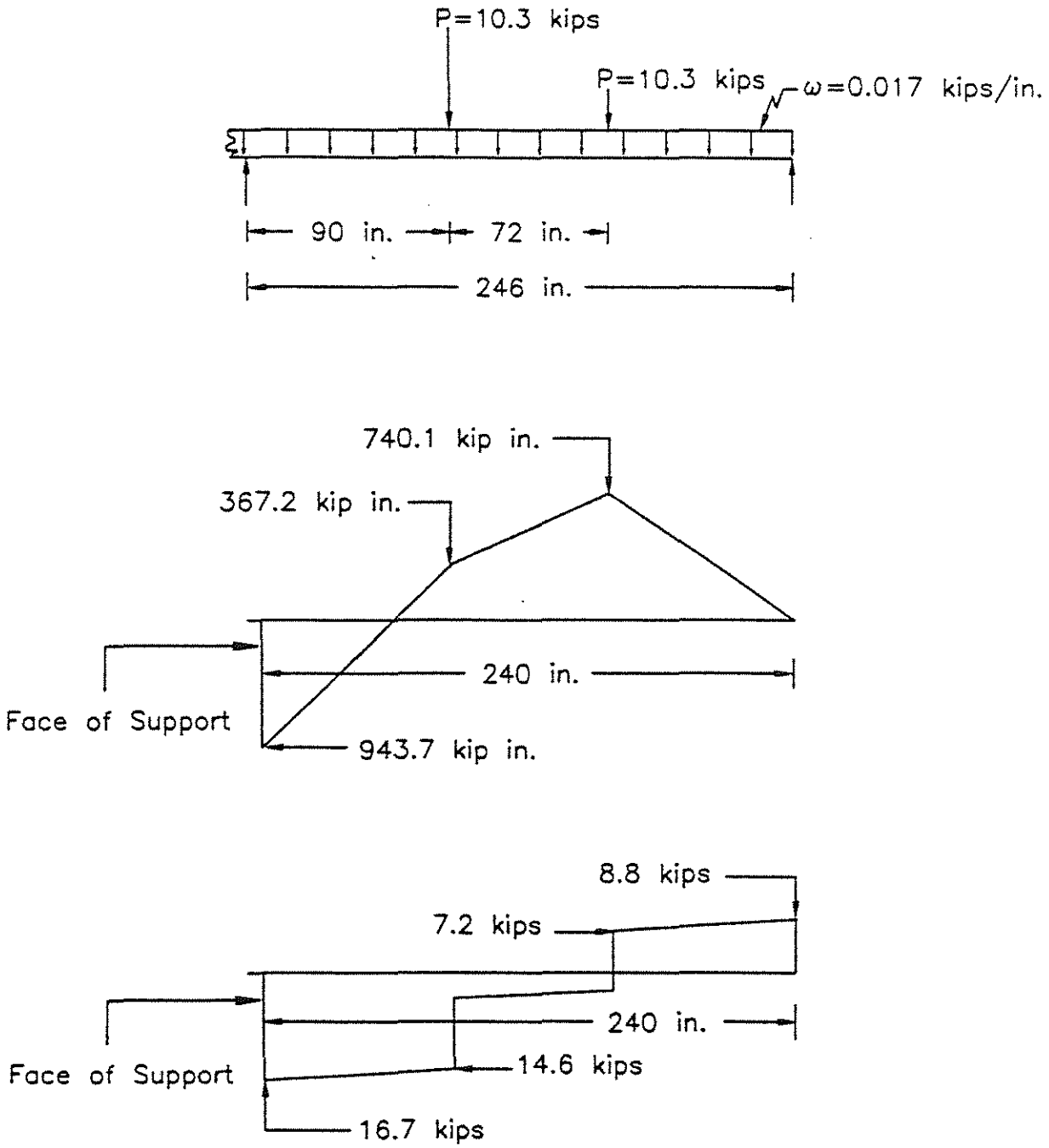

Fig. 2.13 d Bending moment and shear force diagrams at peak load for beam I-3

(negative moment region shear failure in east span)

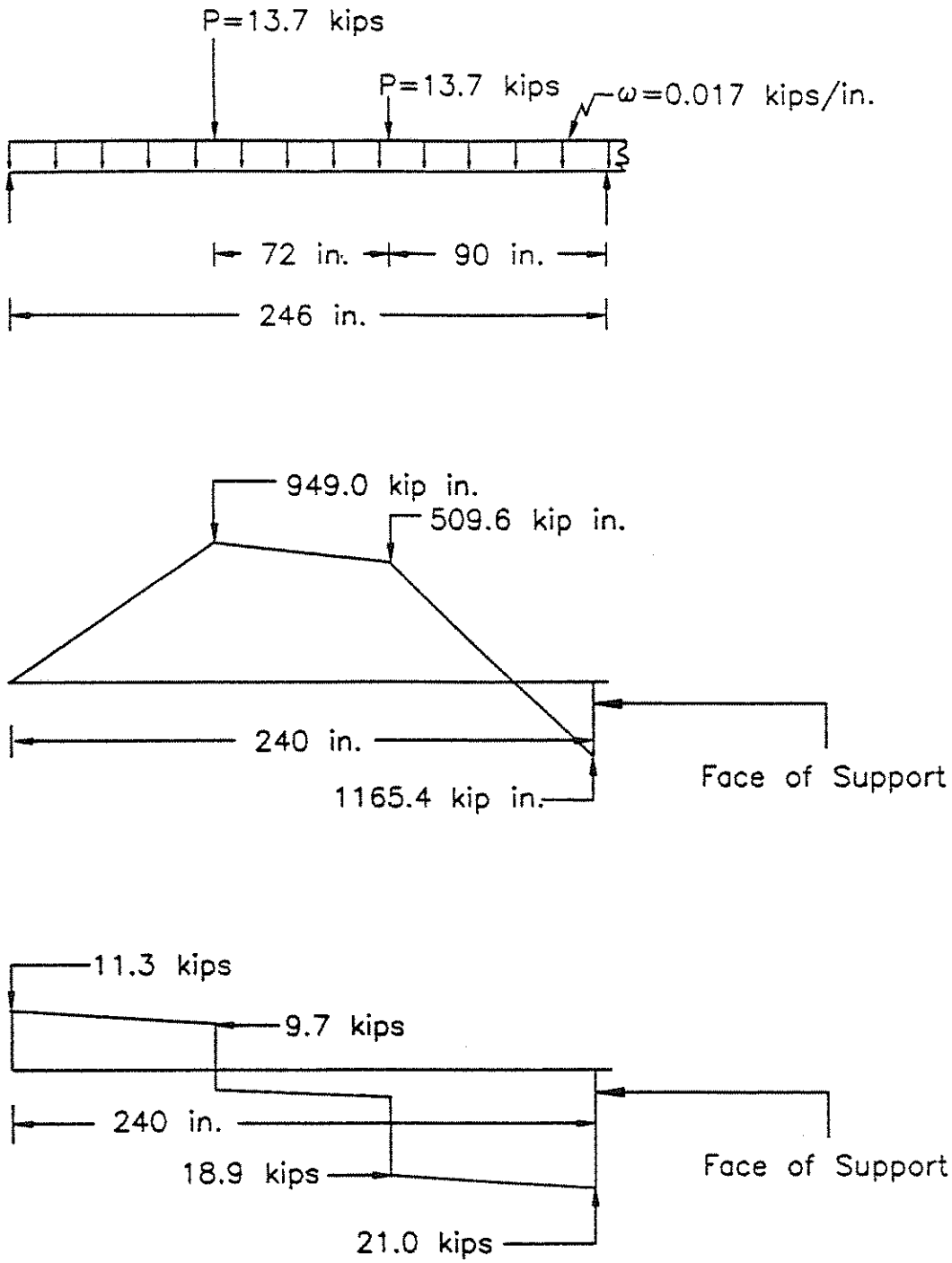

Fig. 2.13 e Bending moment and shear force diagrams at peak load for beam I-3

(negative moment region shear failure in west span)

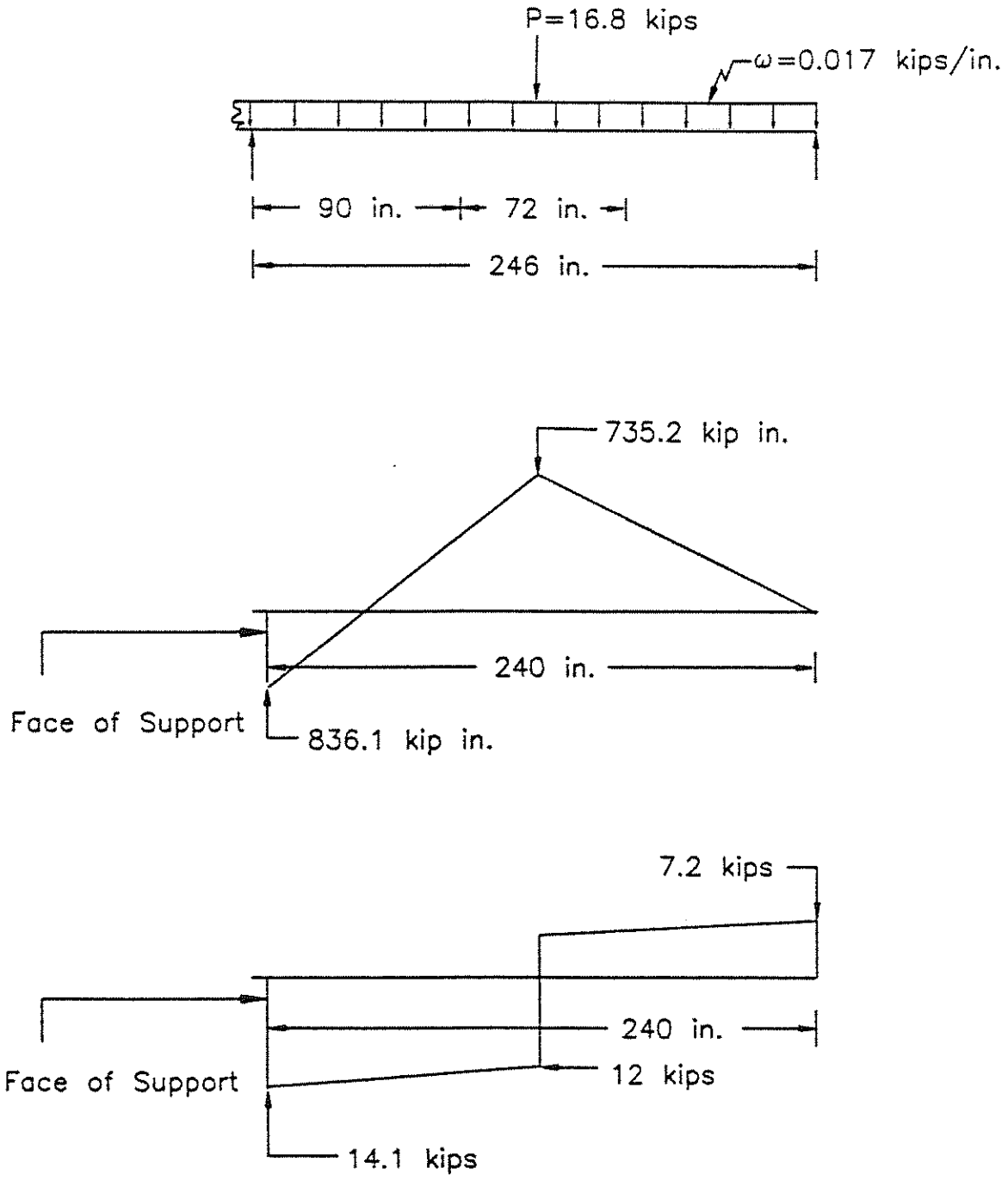

Fig. 2.13 f Bending moment and shear force diagrams at peak load for beam J-1

(positive moment region shear failure in east span)

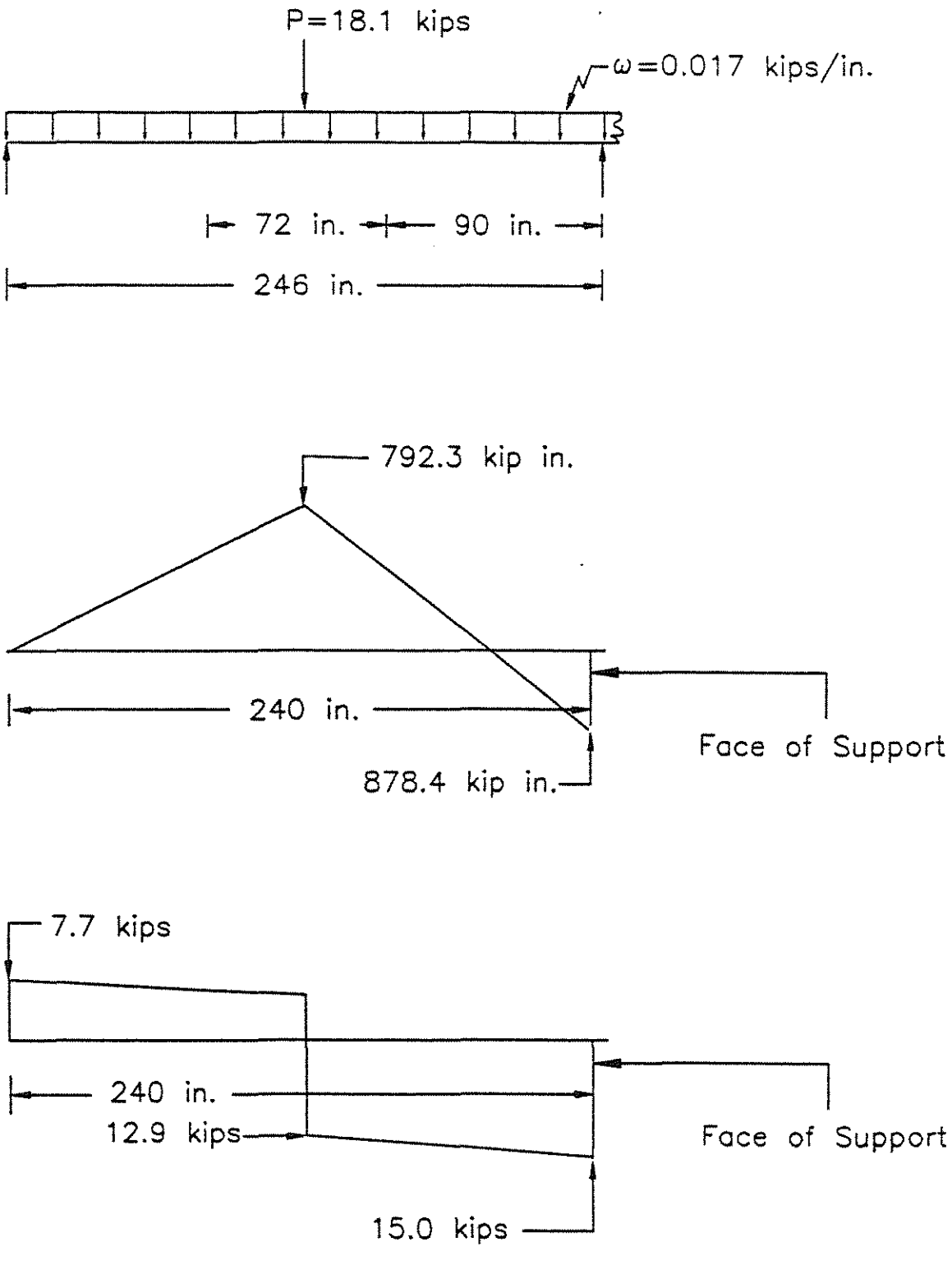

Fig. 2.13 g Bending moment and shear force diagrams at peak load for beam J-1

(negative moment region shear failure in west span)

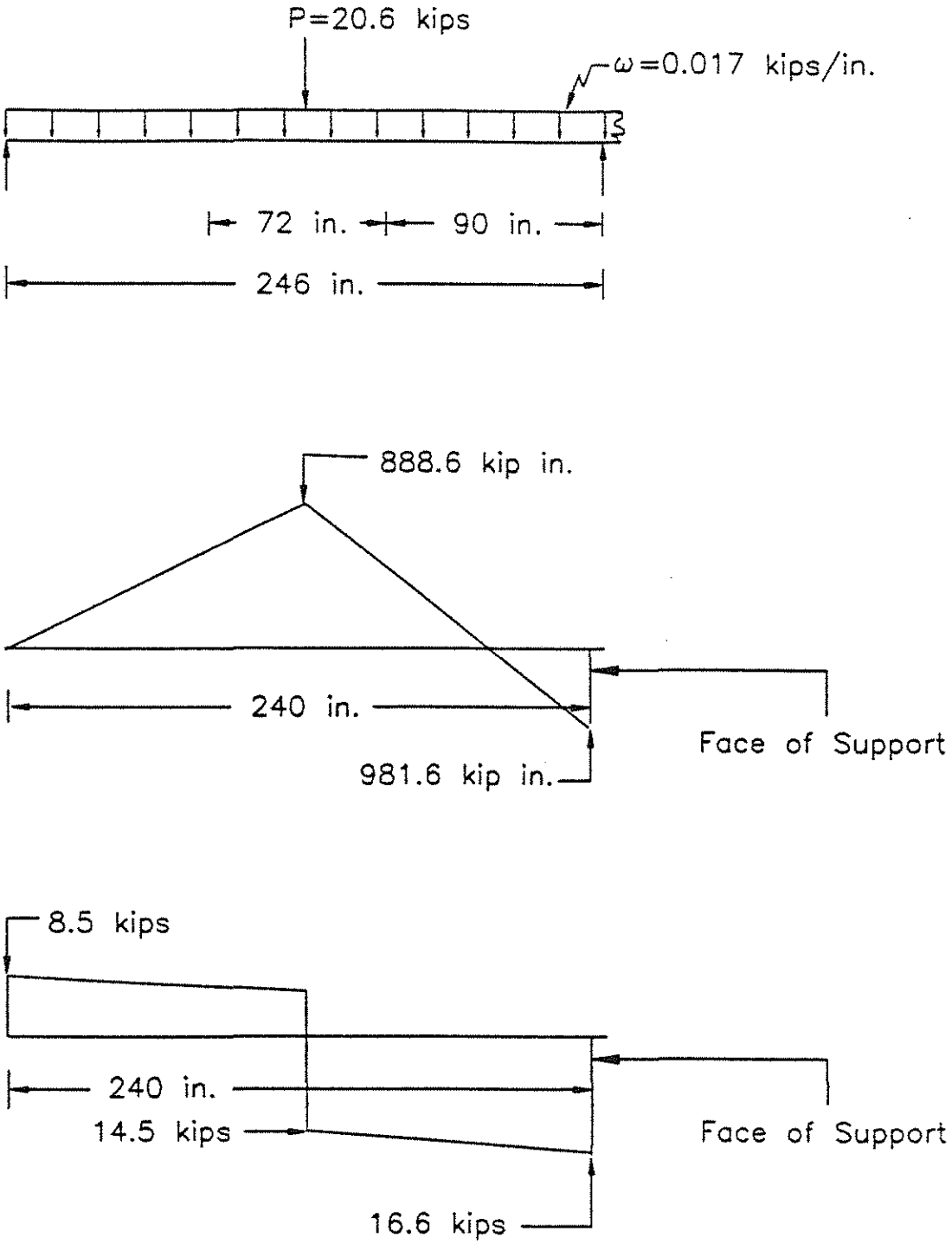

Fig. 2.13 h Bending moment and shear force diagrams at peak load for beam J-1

(positive moment region shear failure in west span)

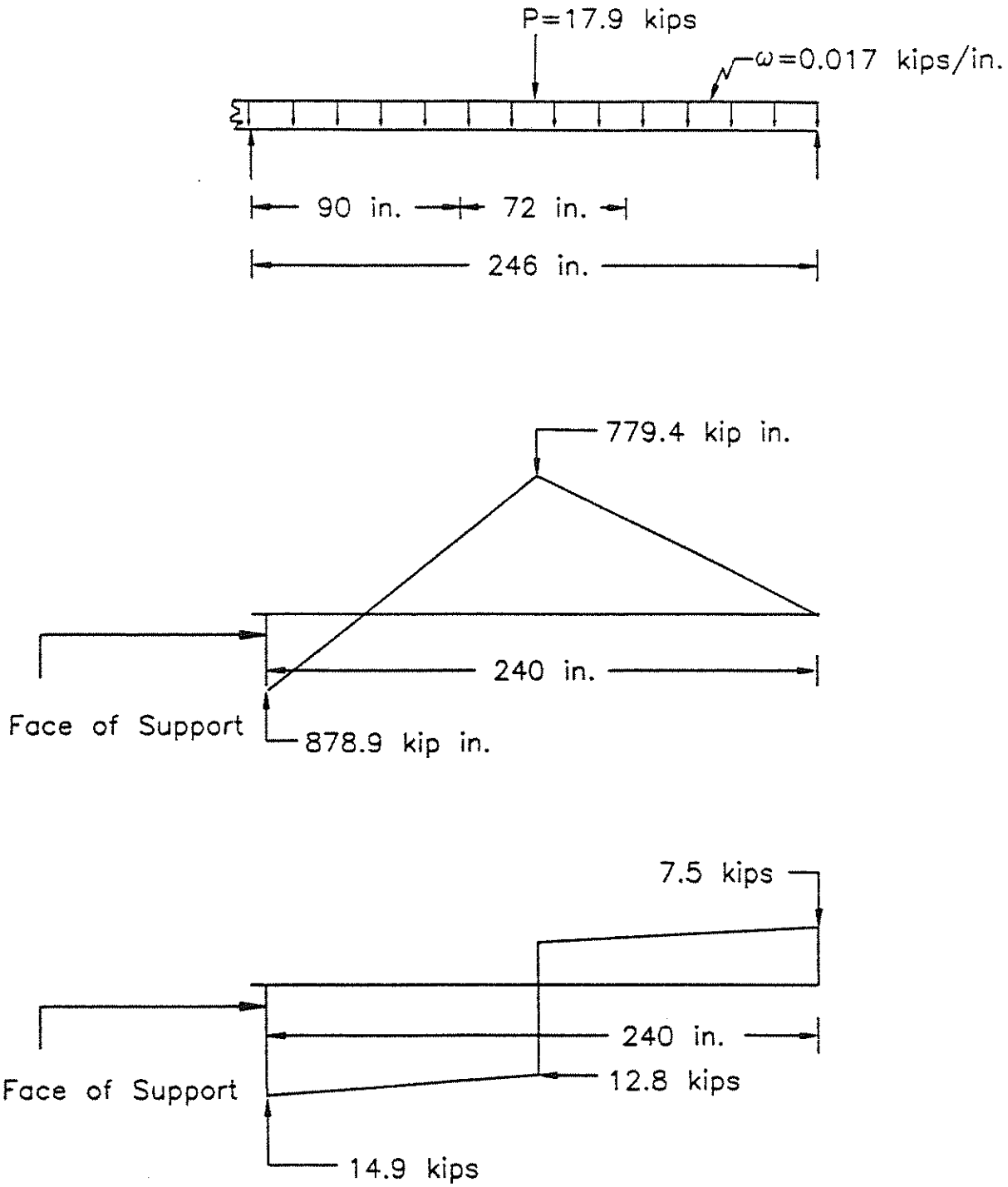

Fig. 2.13 i Bending moment and shear force diagrams at peak load for beam J-1

(negative moment region shear failure in east span)

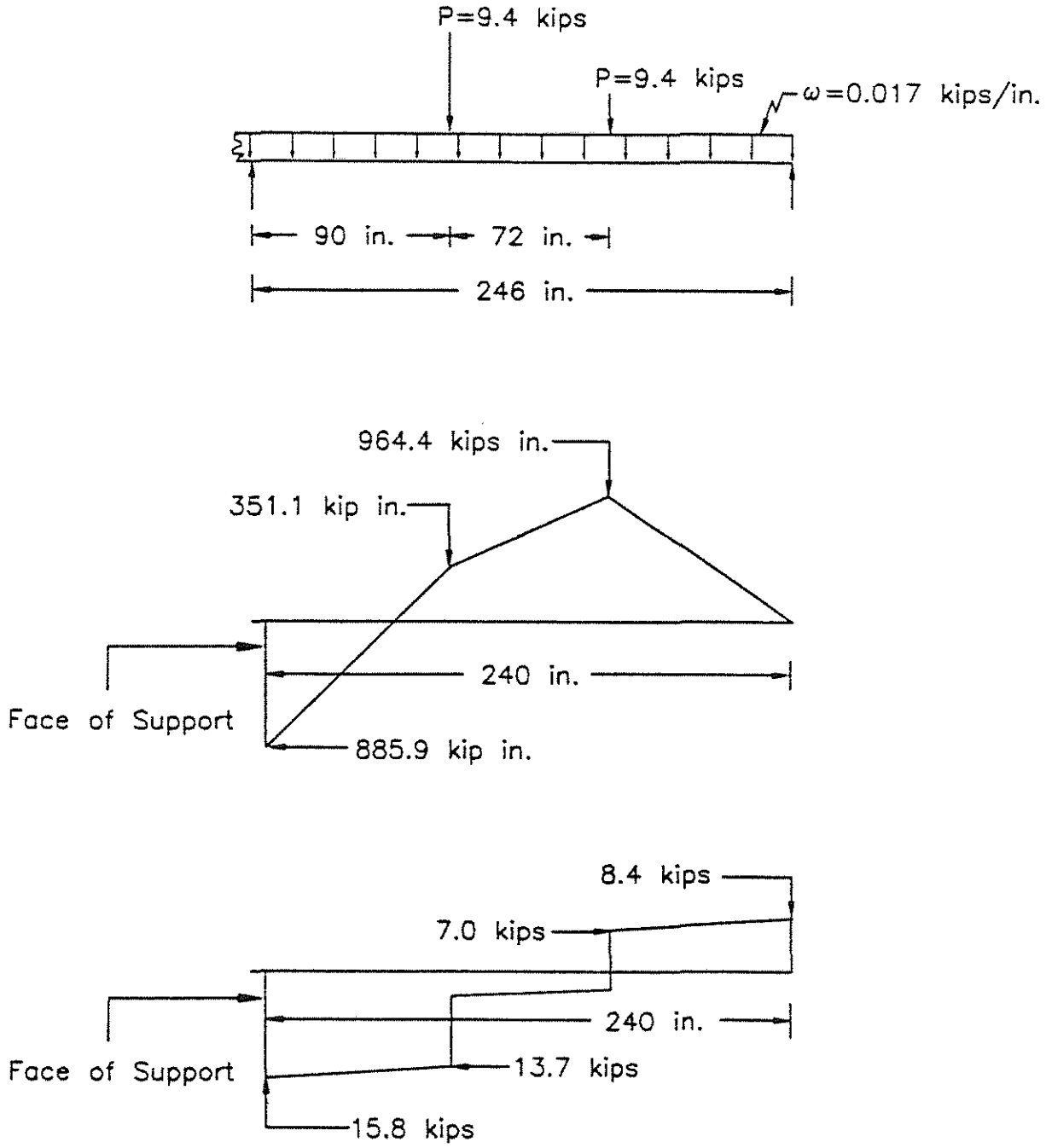

Fig. 2.13 j Bending moment and shear force diagrams at peak load for beam J-2

(negative moment region shear failure in east span)

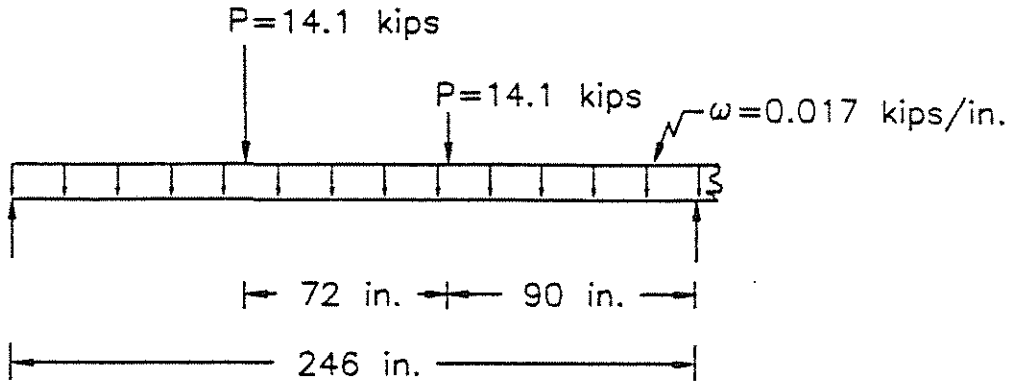

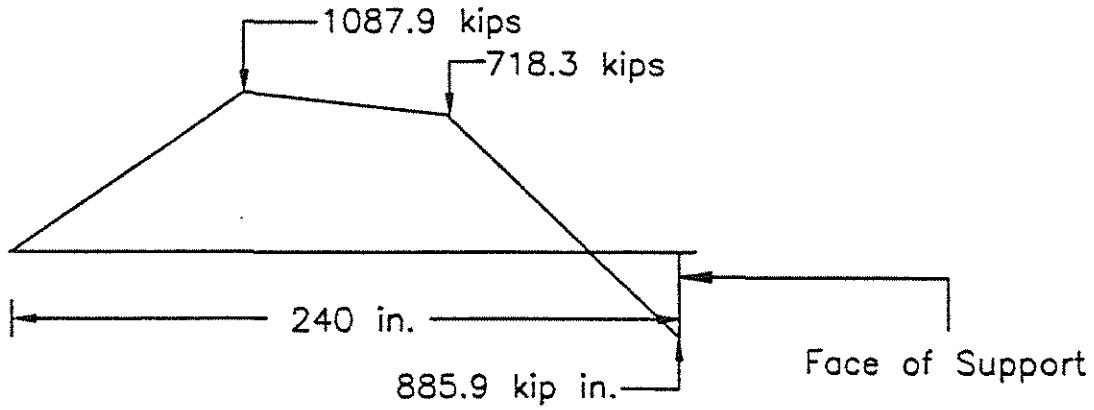

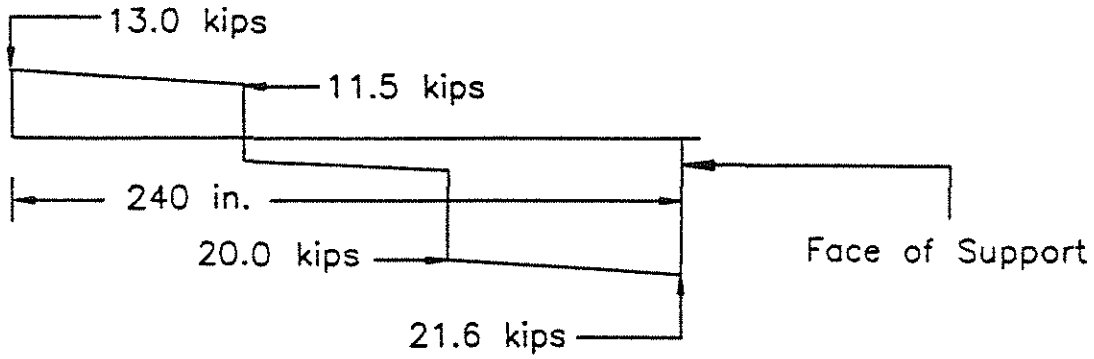

Fig. 2.13 k Bending moment and shear force diagrams at peak load for beam J-2

(negative moment region shear failure in west span)

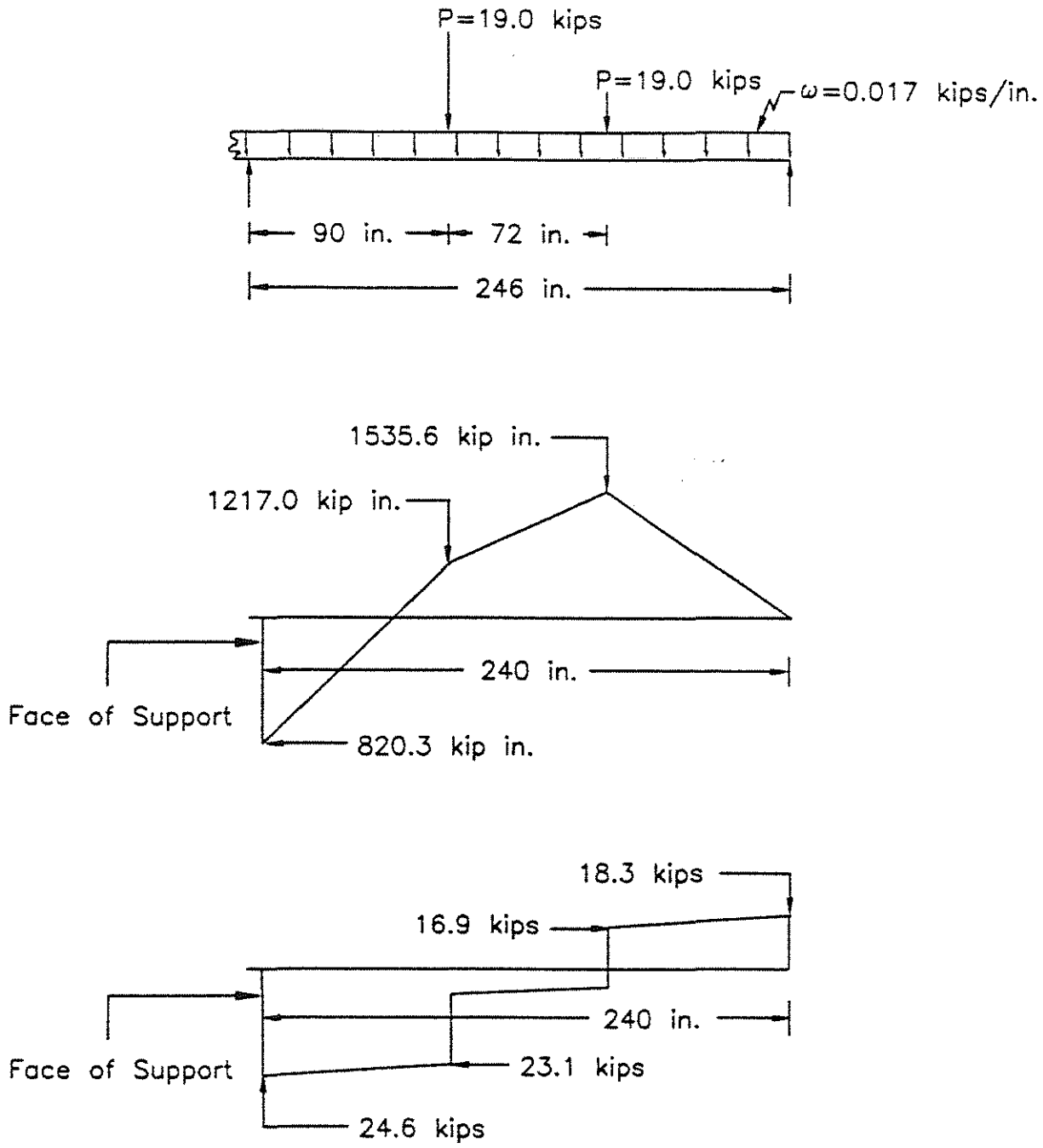

Fig. 2.13 l Bending moment and shear force diagrams at peak load for beam J-3

(negative moment region shear failure in east span)

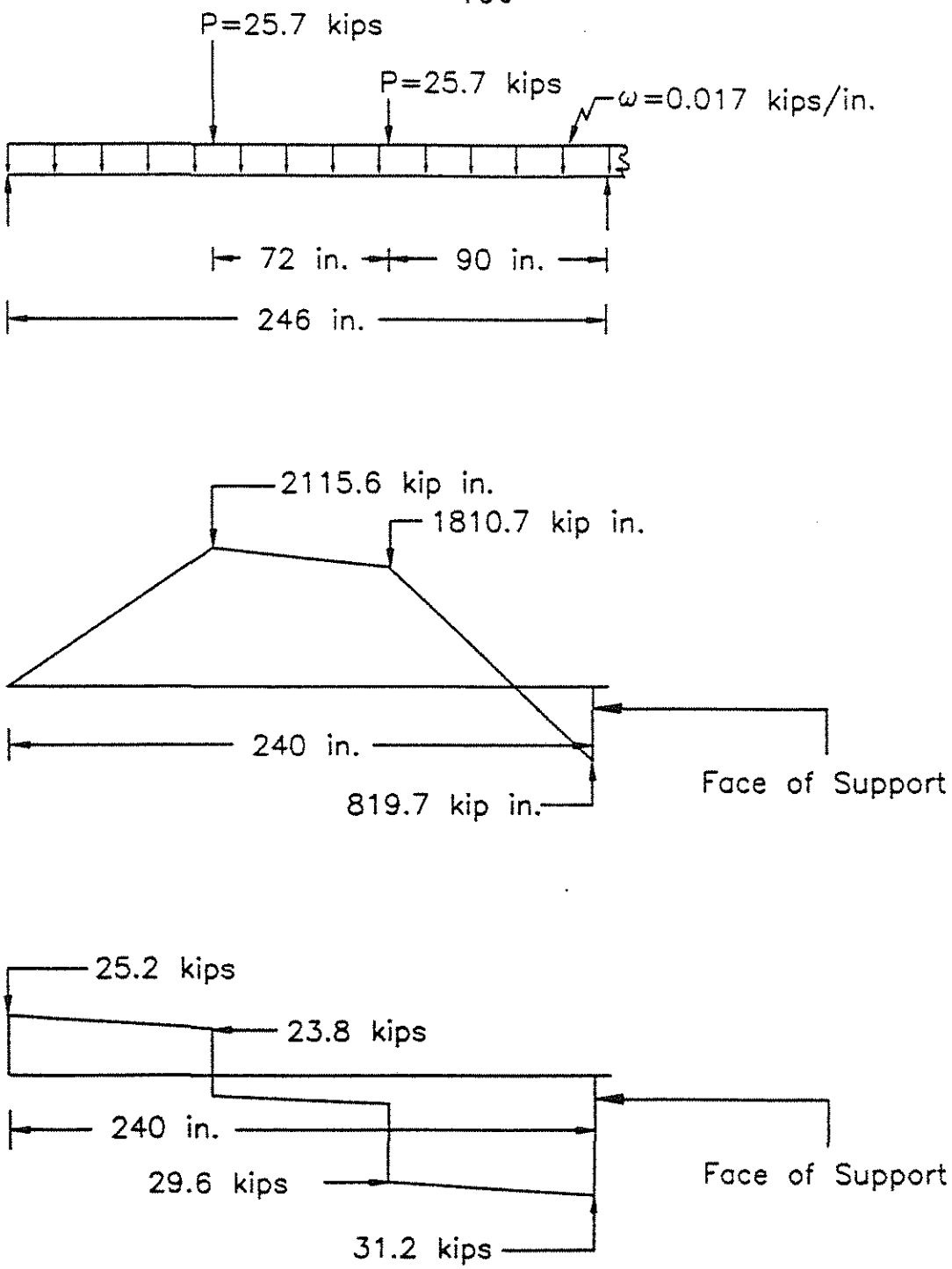

Fig. 2.13 m Bending moment and shear force diagrams at peak load for beam J-3

(negative moment region shear failure in west span)

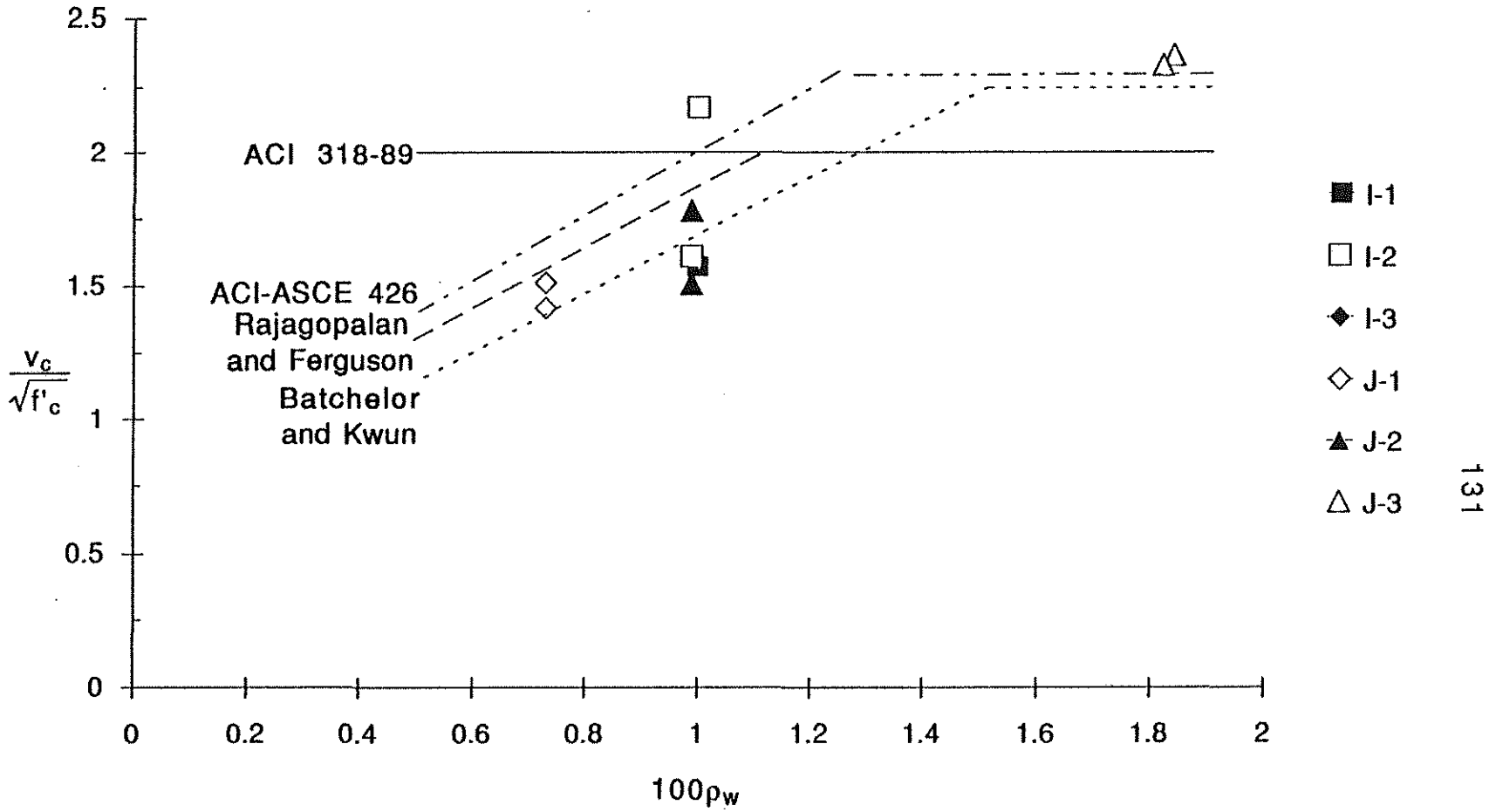

Fig. 3.1 Shear Cracking Stress from Crack Patterns in the Positive Moment Region

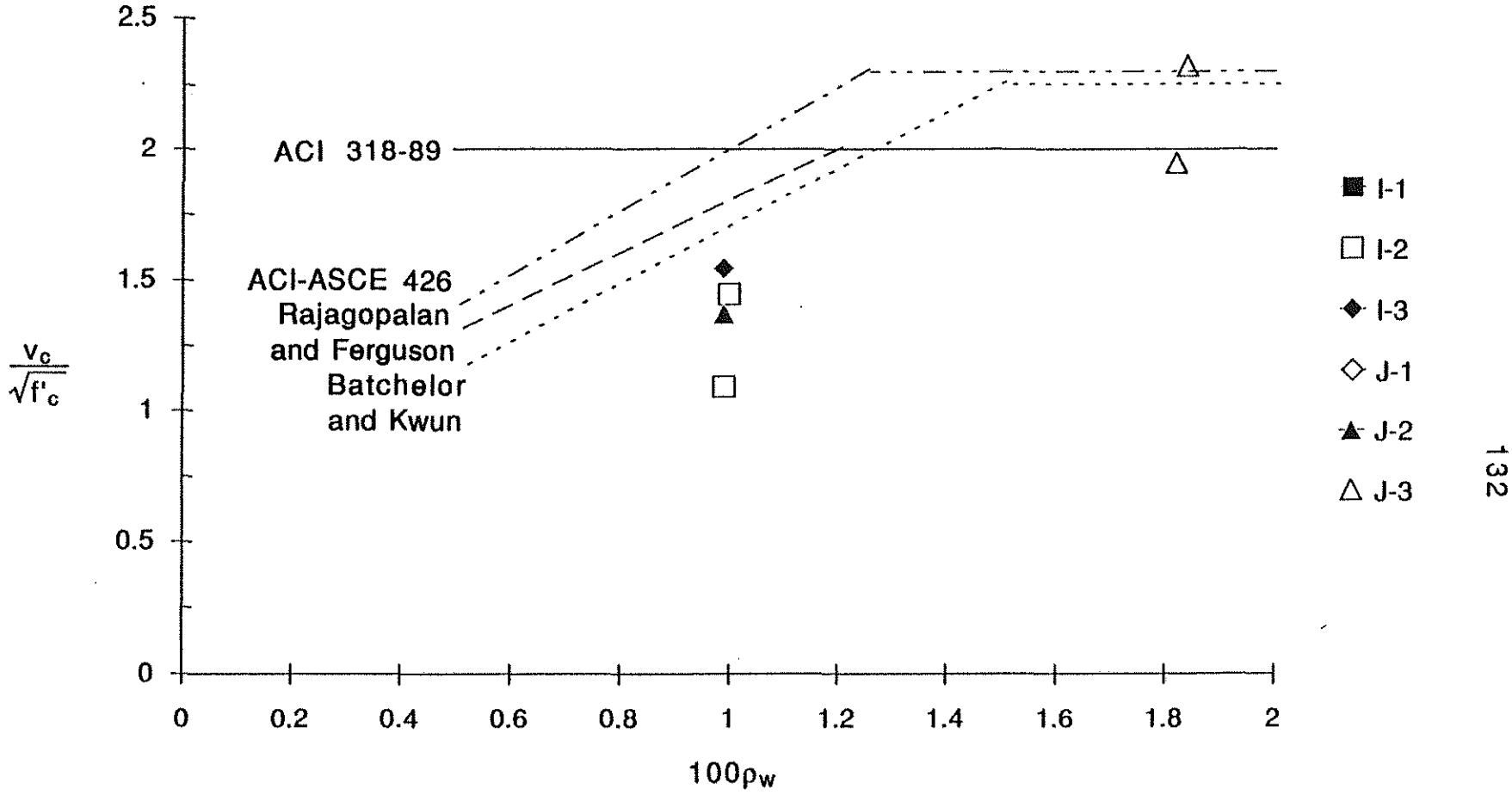

Fig. 3.2 Shear Cracking Stress from Stirrup Strain in the Positive Moment Region

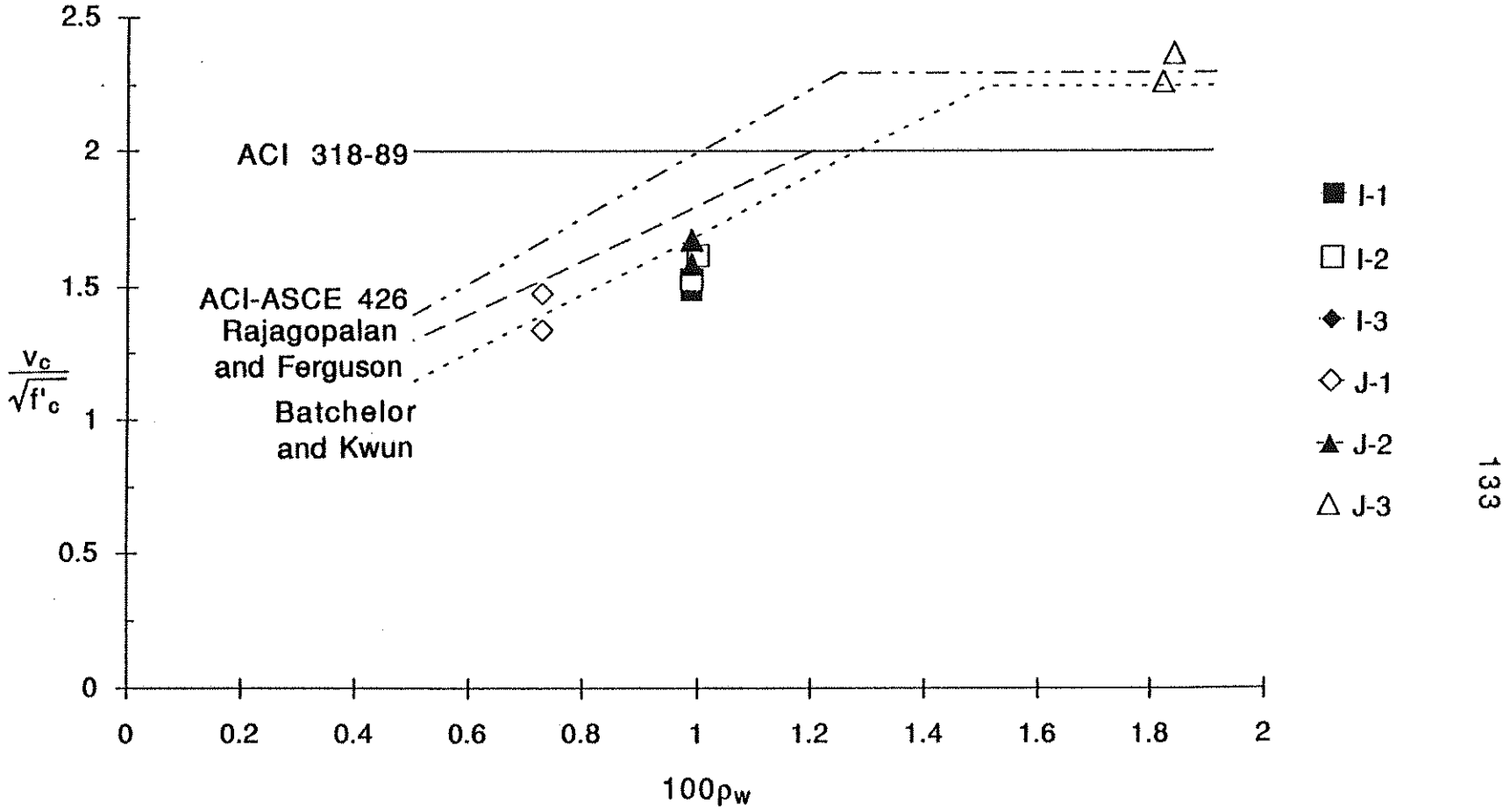

Fig. 3.3 Shear Cracking Stress from Concrete Strain in the Positive Moment Region

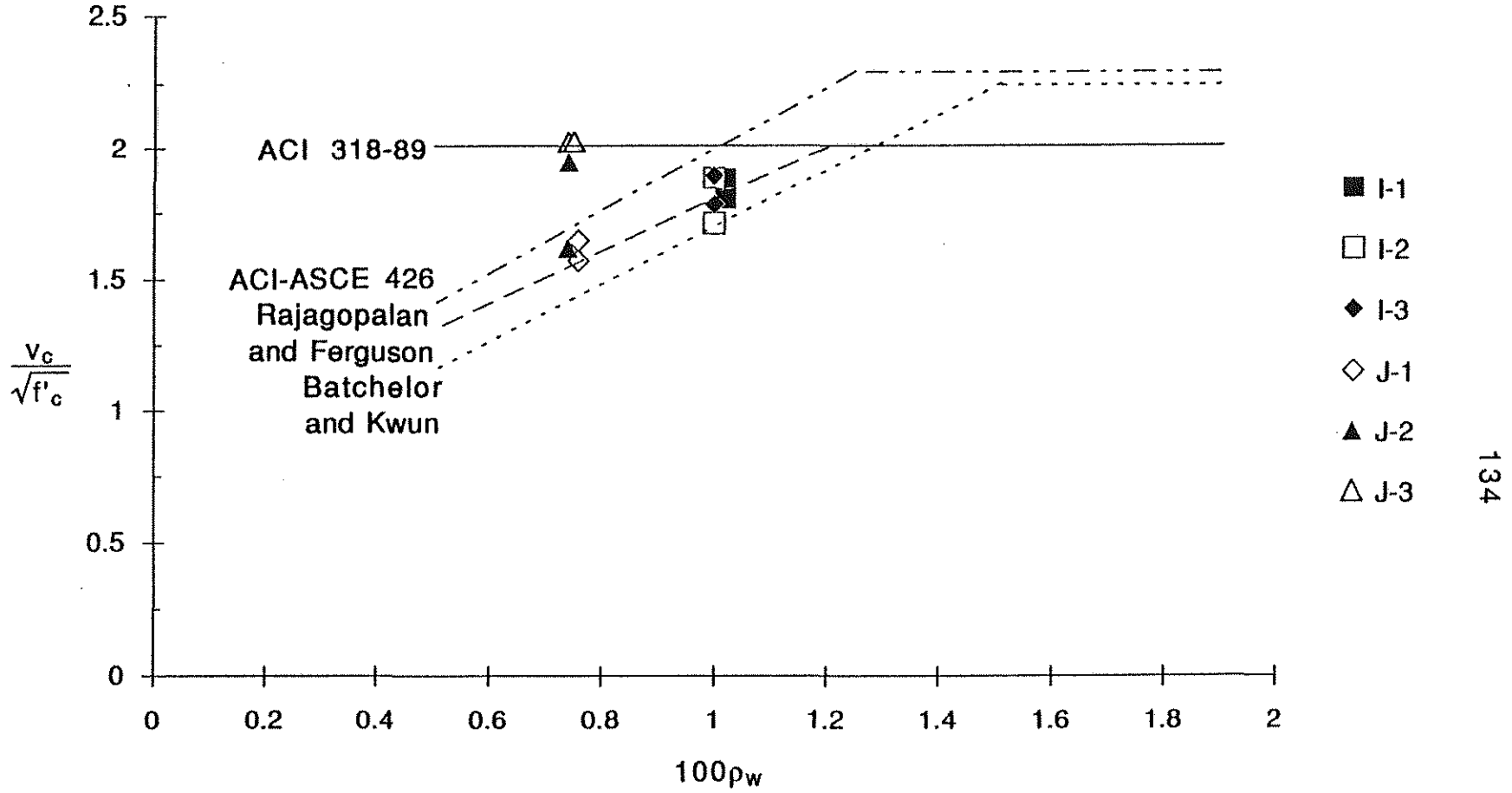

Fig. 3.4 Shear Cracking Stress from Crack Patterns in the Negative Moment Region

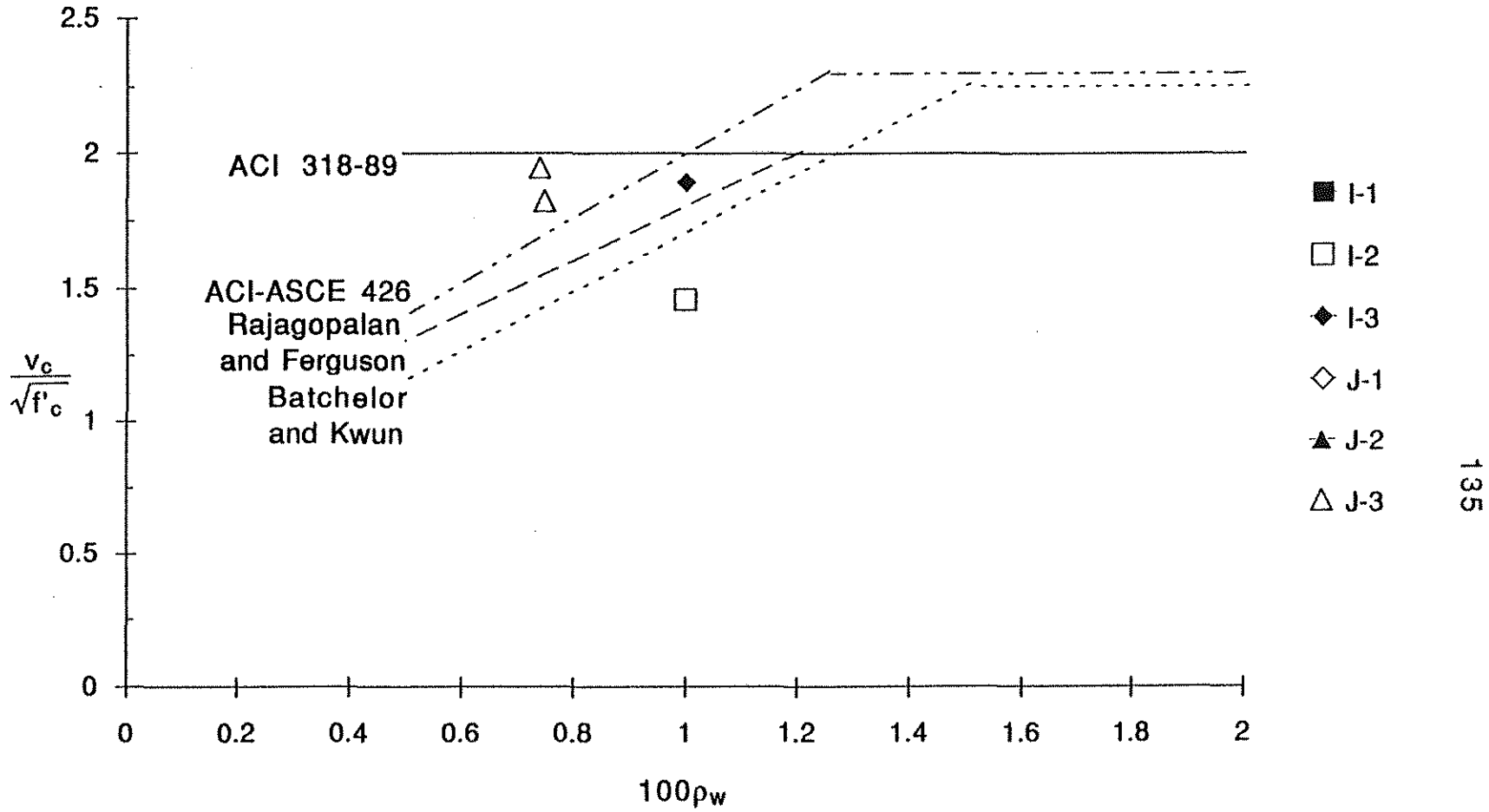

Fig. 3.5 Shear Cracking Stress from Stirrup Strain in the Negative Moment Region

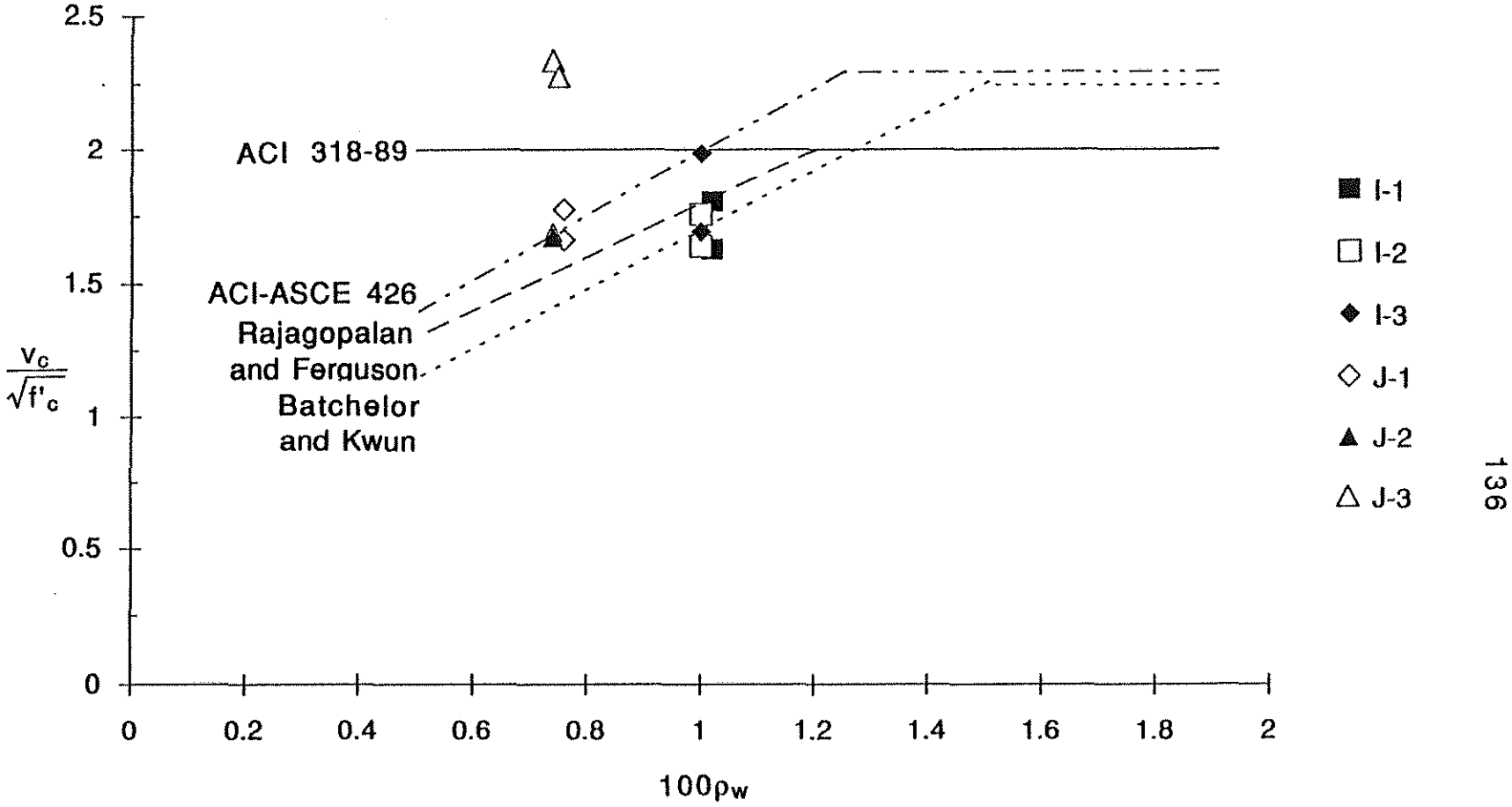

Fig. 3.6 Shear Cracking Stress from Concrete Strain in the Negative Moment Region

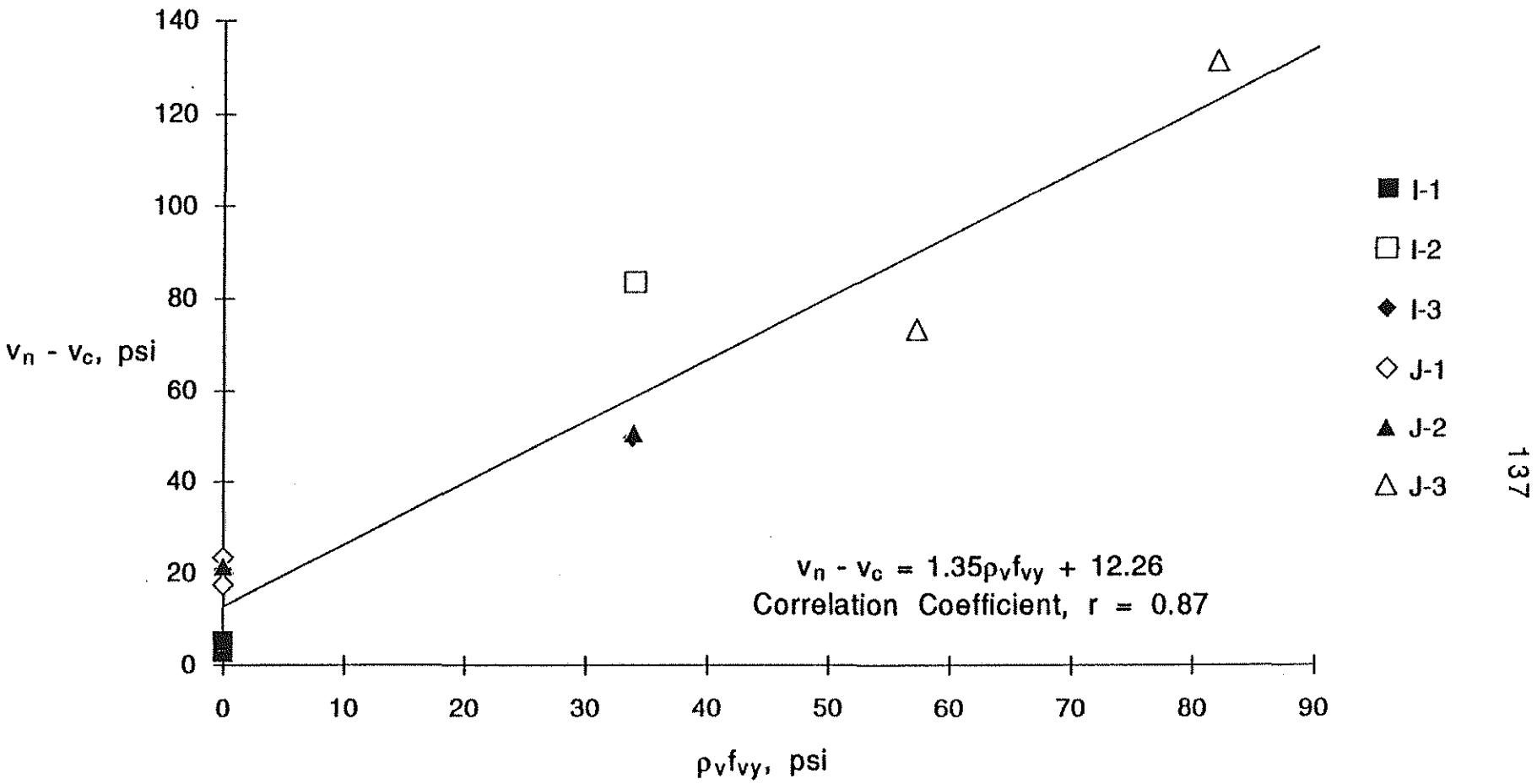

Fig. 3.7 Stirrup Effectiveness in the Negative Moment Region (from current study)

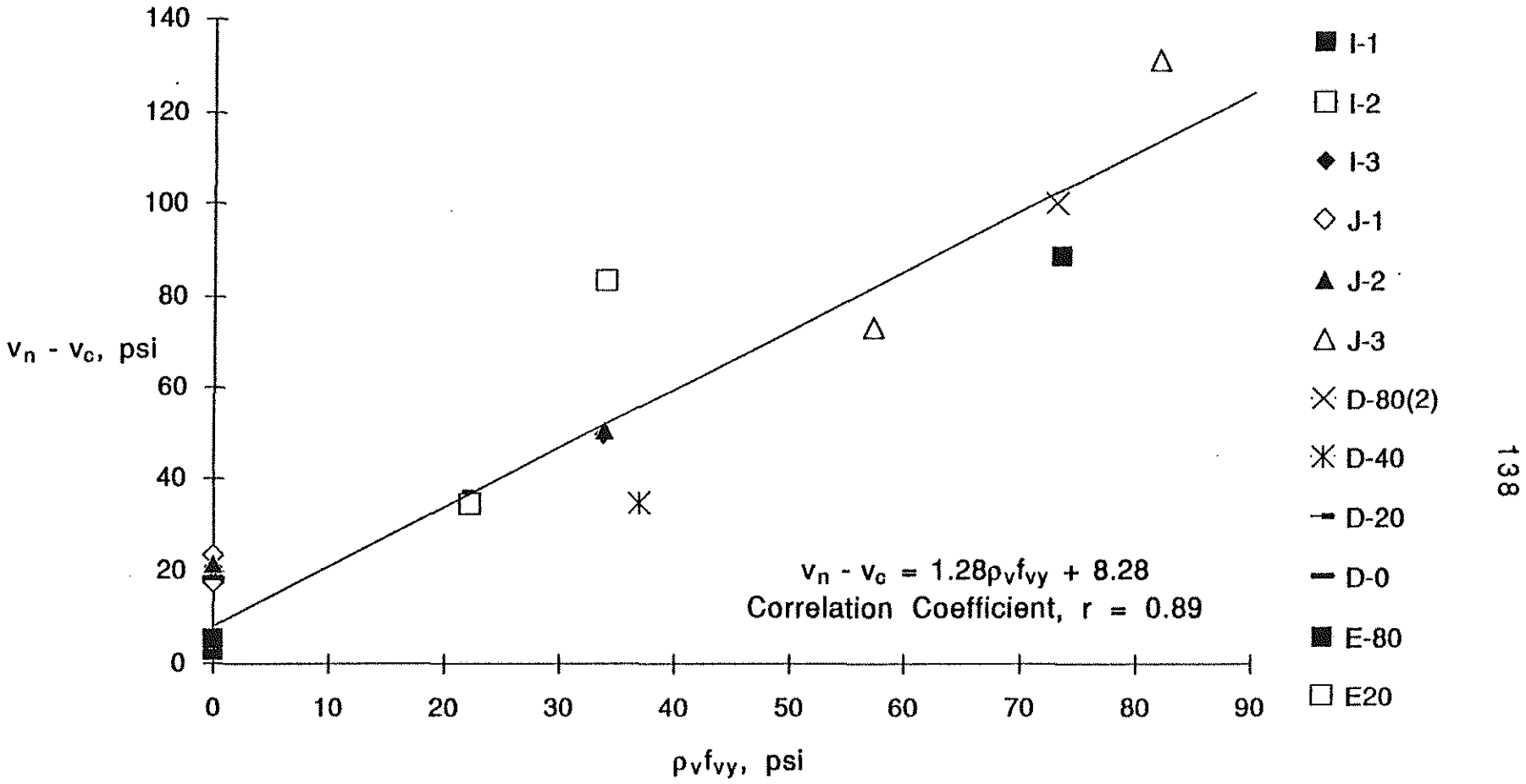

Fig. 3.8 Stirrup Effectiveness in the Negative Moment Region (from current study and results of Rodrigues and Darwin (38,39,40))

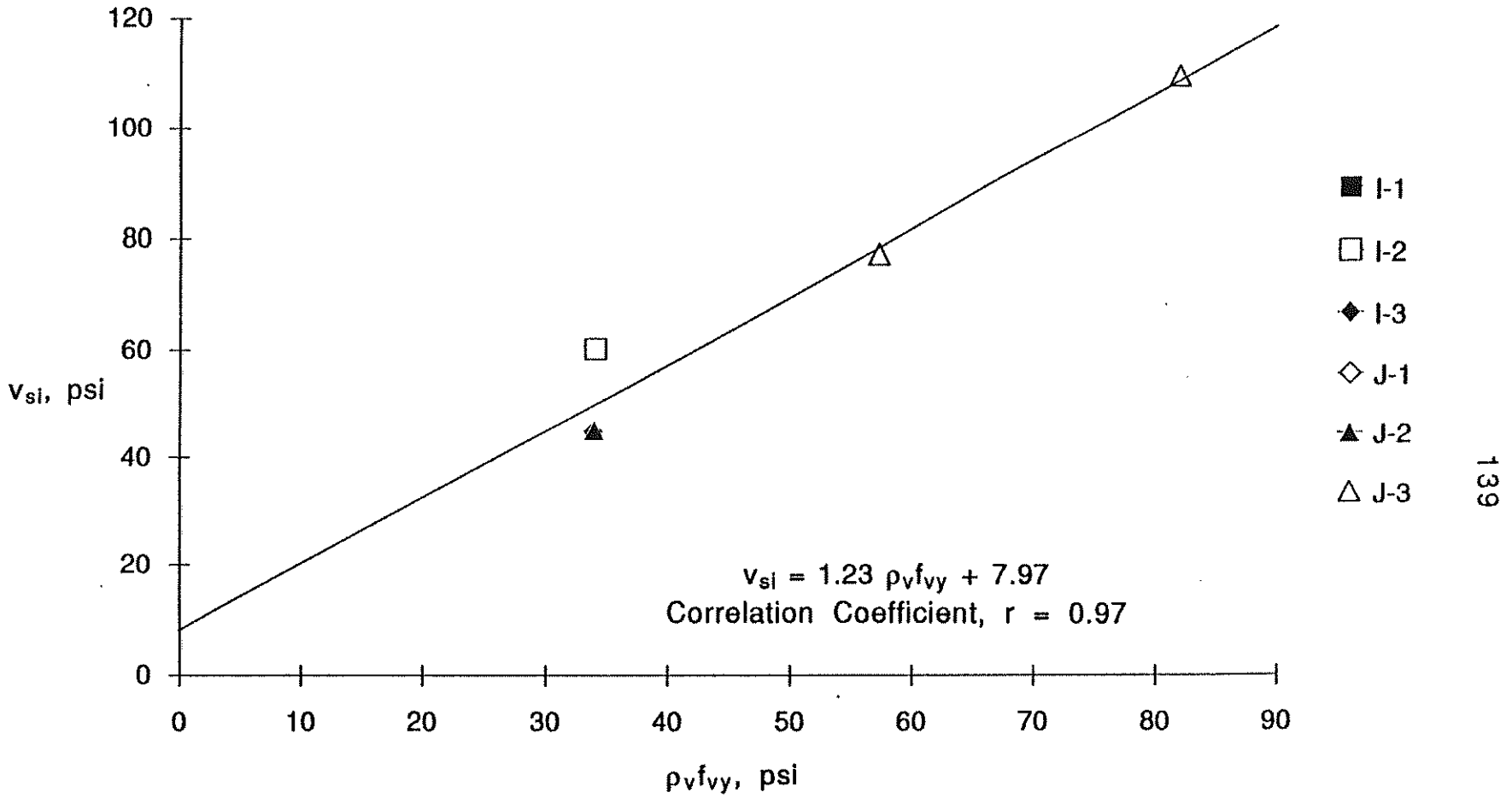

Fig. 3.9 Shear Carried by Stirrups Alone in the Negative Moment Region (from current study)

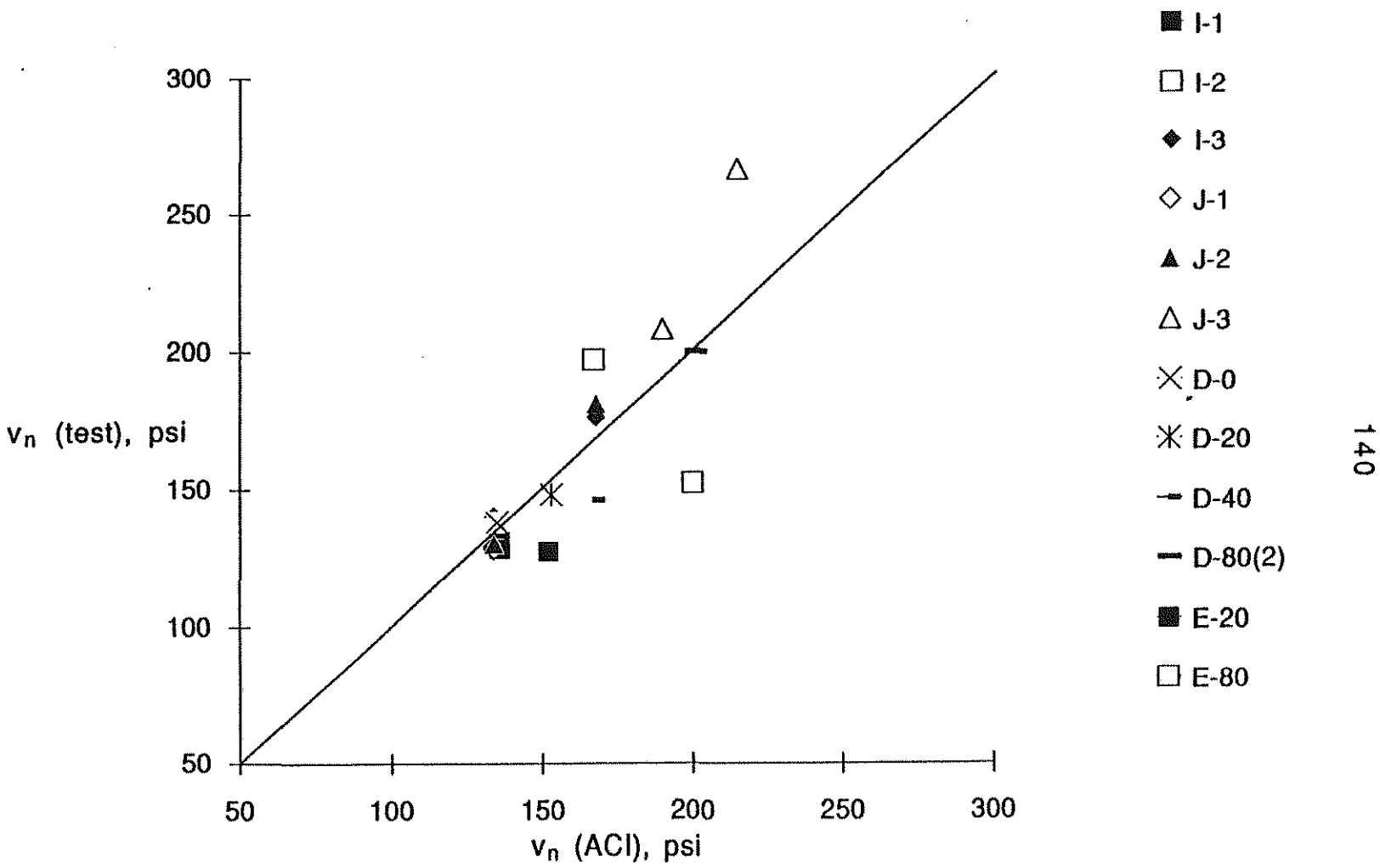

Fig. 3.10 Comparison of Negative Moment Region Nominal Shear Strength, Test vs. ACI (from current study and results of Rodrigues and Darwin (38,39,40))

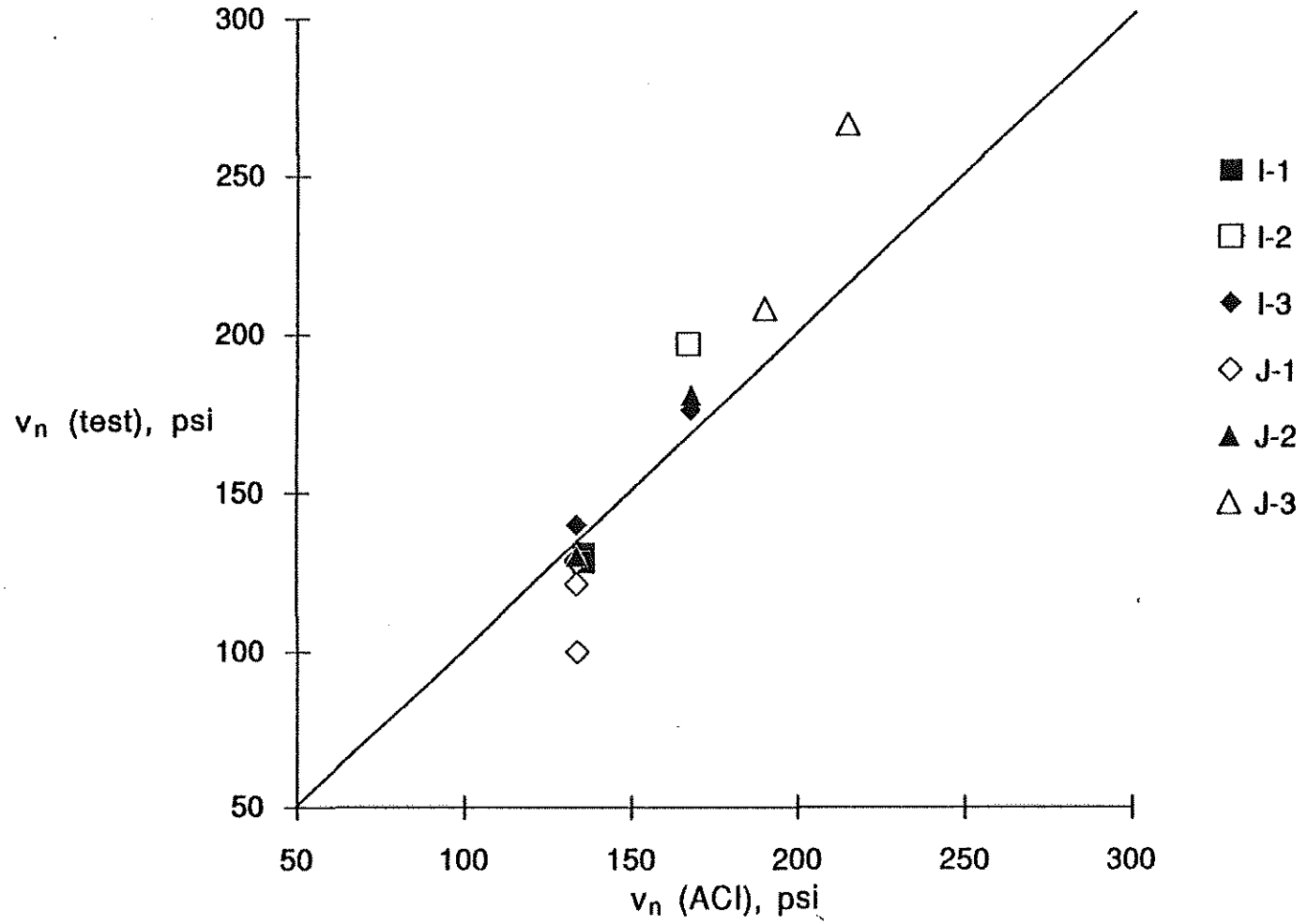

Fig. 3.11 Comparison of Negative Moment Region Nominal Shear Strength, Test vs. ACI (from current study)

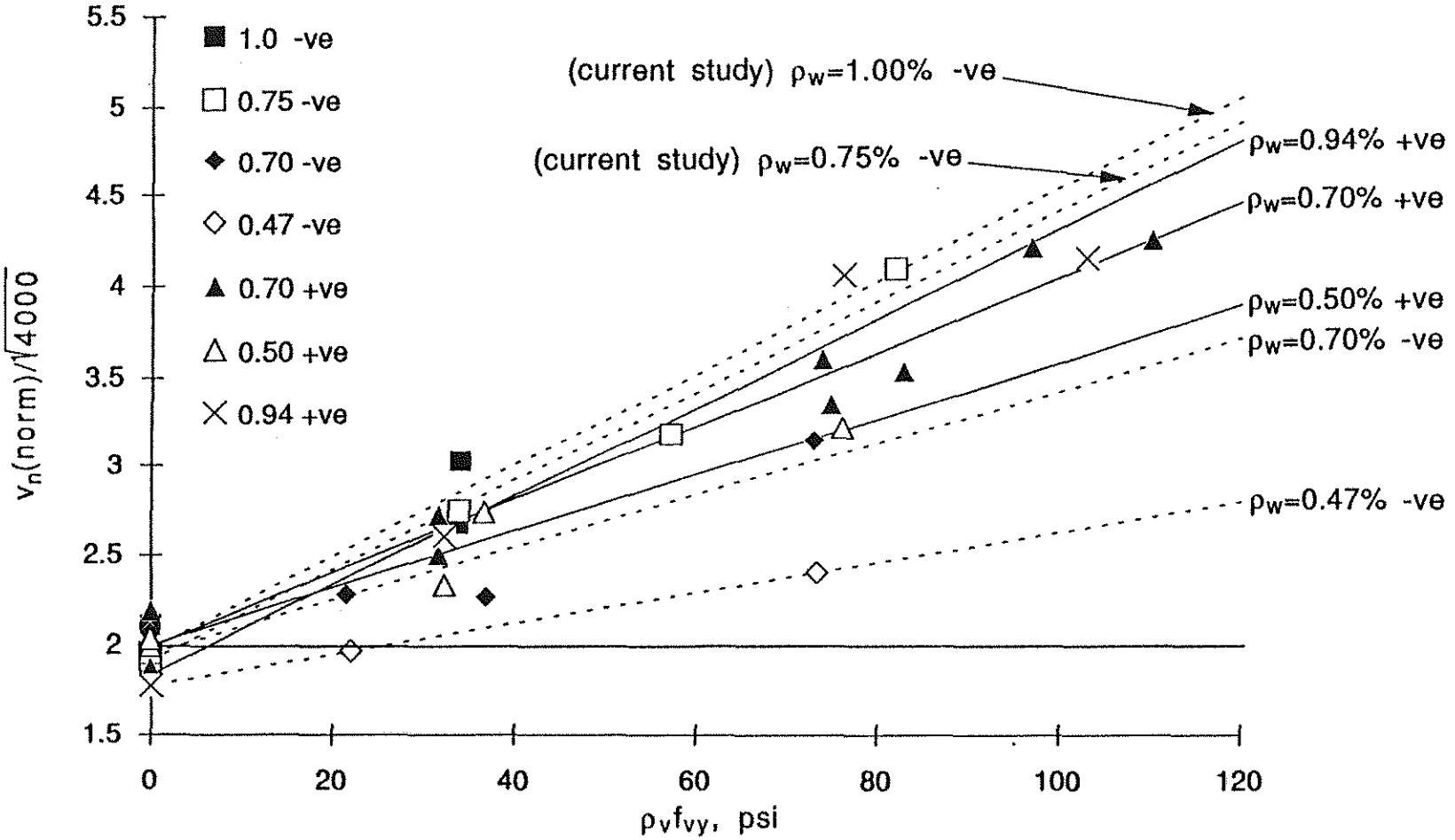

Fig. 3.12 Normalized Nominal Shear Strength versus Nominal Stirrup Strength, Best Fit Lines (from current study and results of Rodrigues and Darwin (38,39,40))

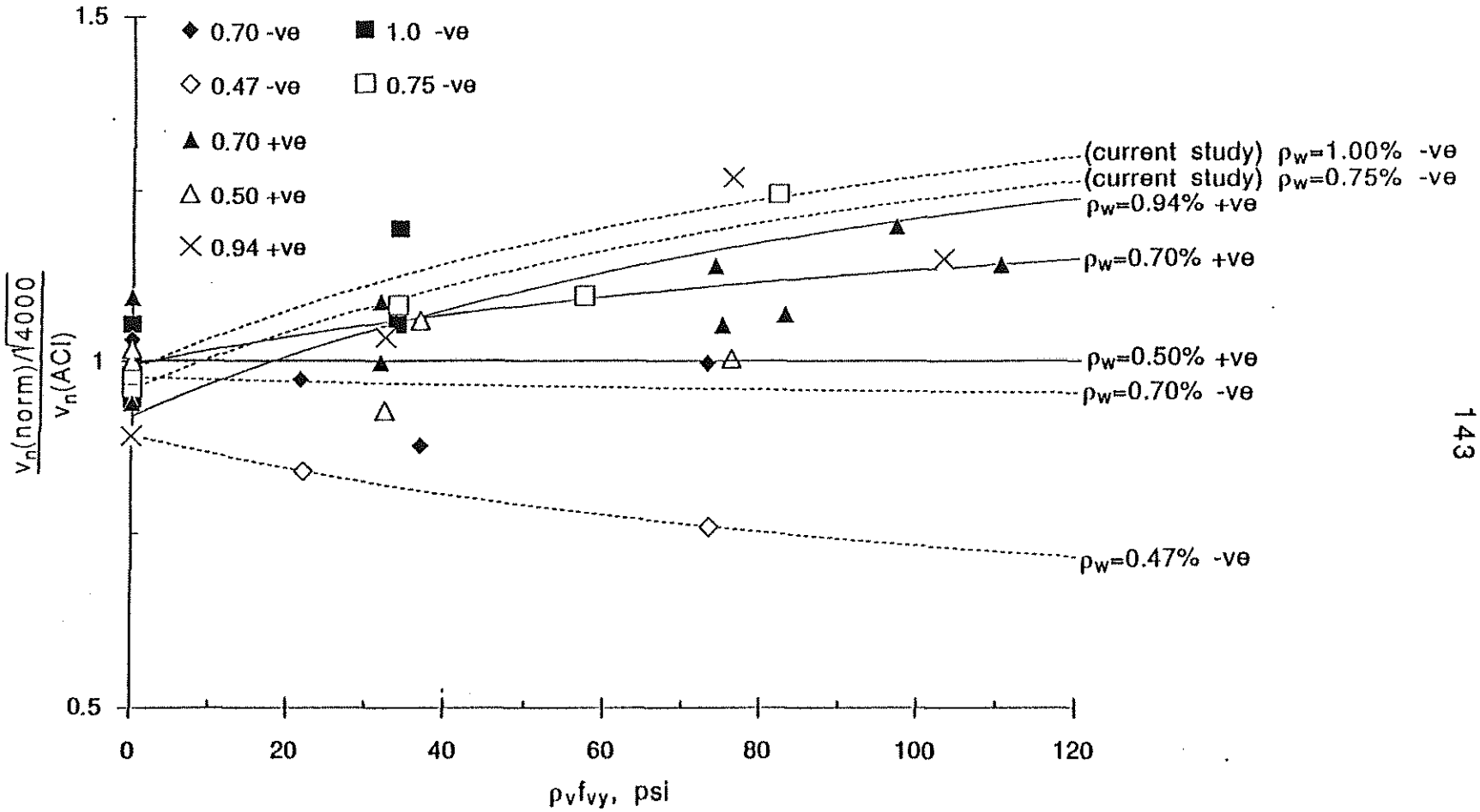

Fig. 3.13 Ratio of Normalized Nominal Shear Strength to Value Predicted by ACI 318-89 (3) versus Nominal Stirrup Strengths

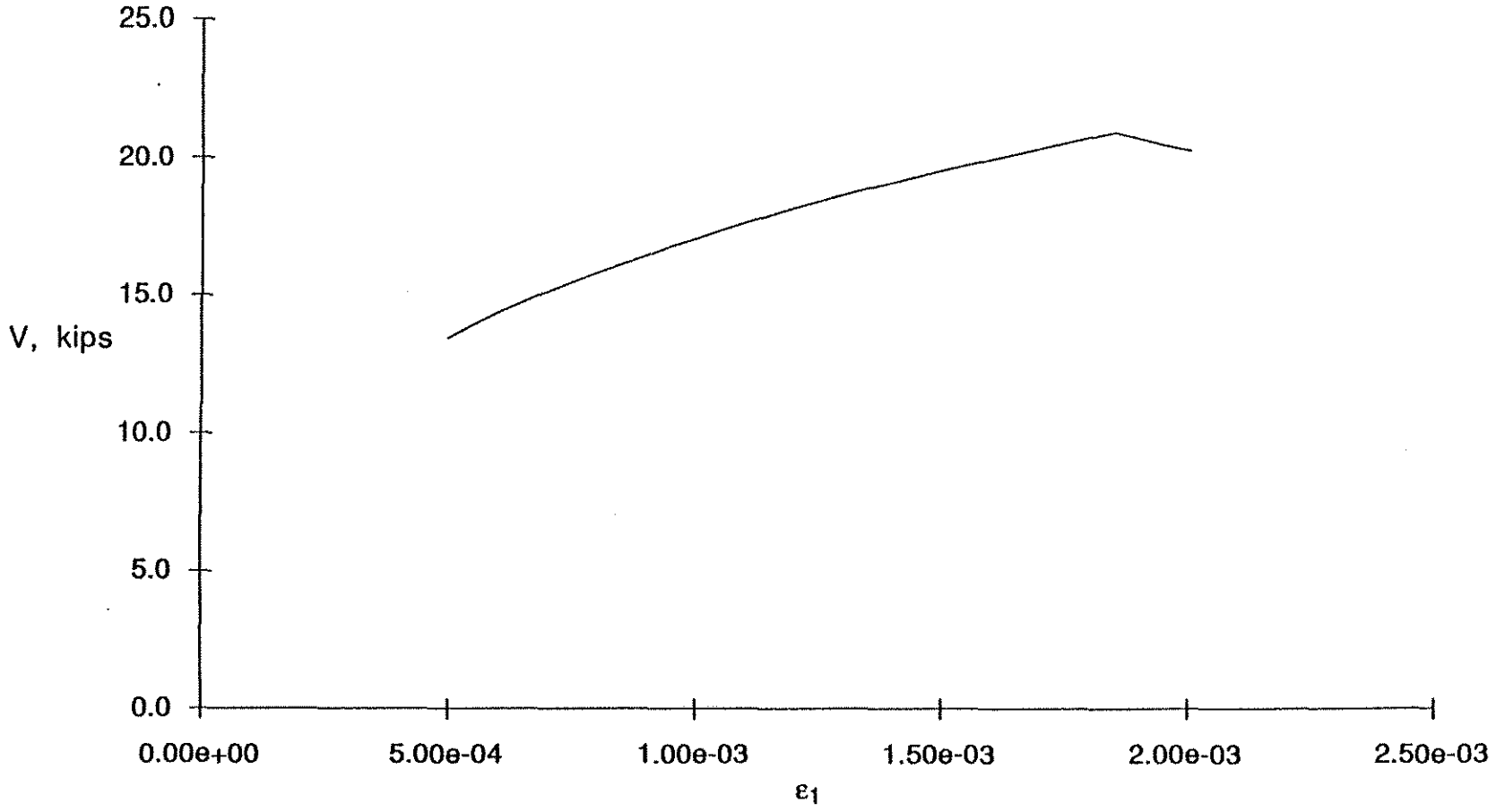

Fig. 3.14 Sample Member Response Using MCFT Response Procedure

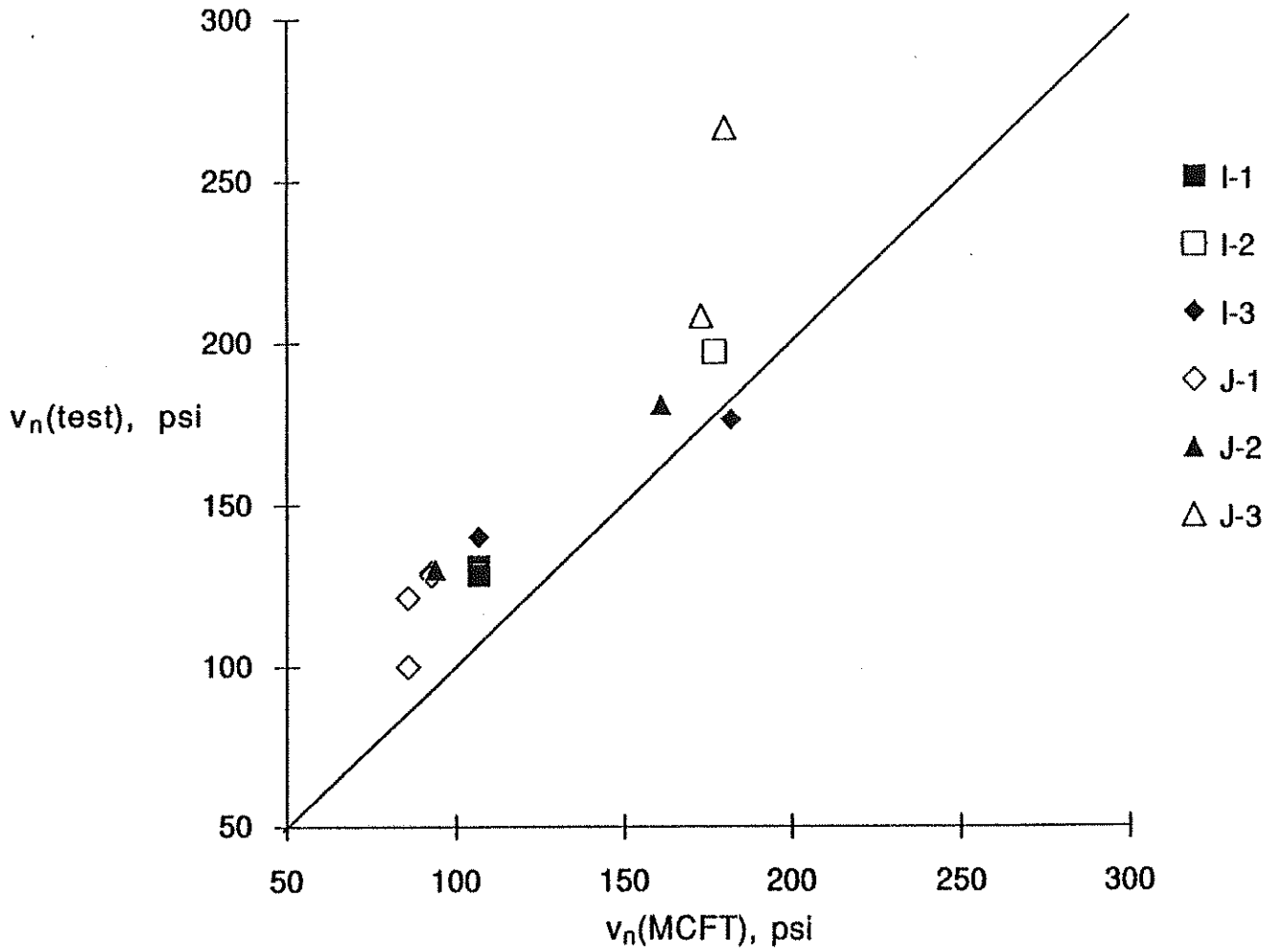

Fig. 3.15 Comparison of Measured Nominal Shear Strength to Nominal Shear Strength from MCFT Response Procedure

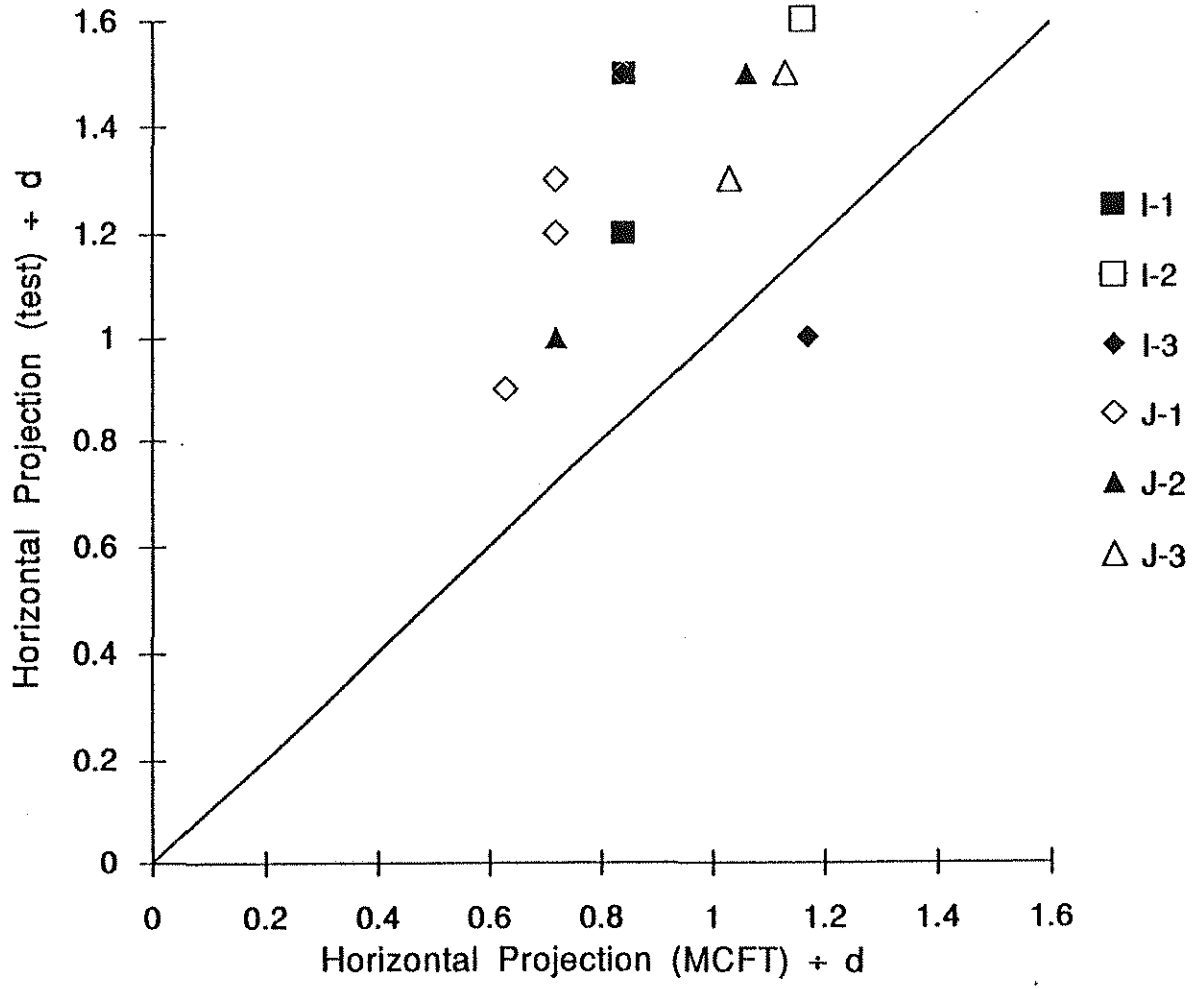

Fig. 3.16 Comparison of Measured Horizontal Crack Projection to Predicted Horizontal Crack Projection from MCFT Response Procedure

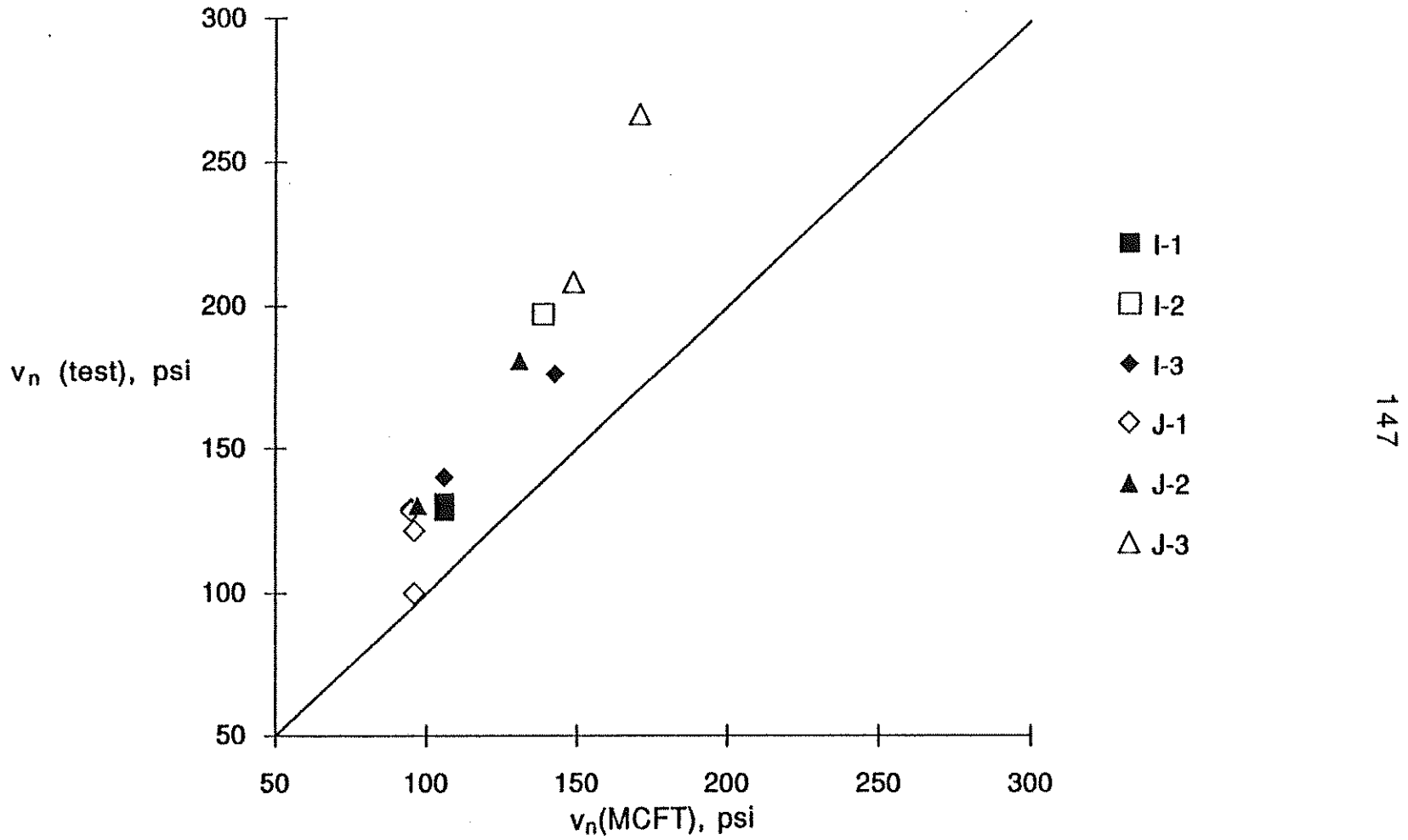

Fig. 3.17 Comparison of Measured Nominal Shear Strength to Nominal Shear Strength from MCFT Design Procedure

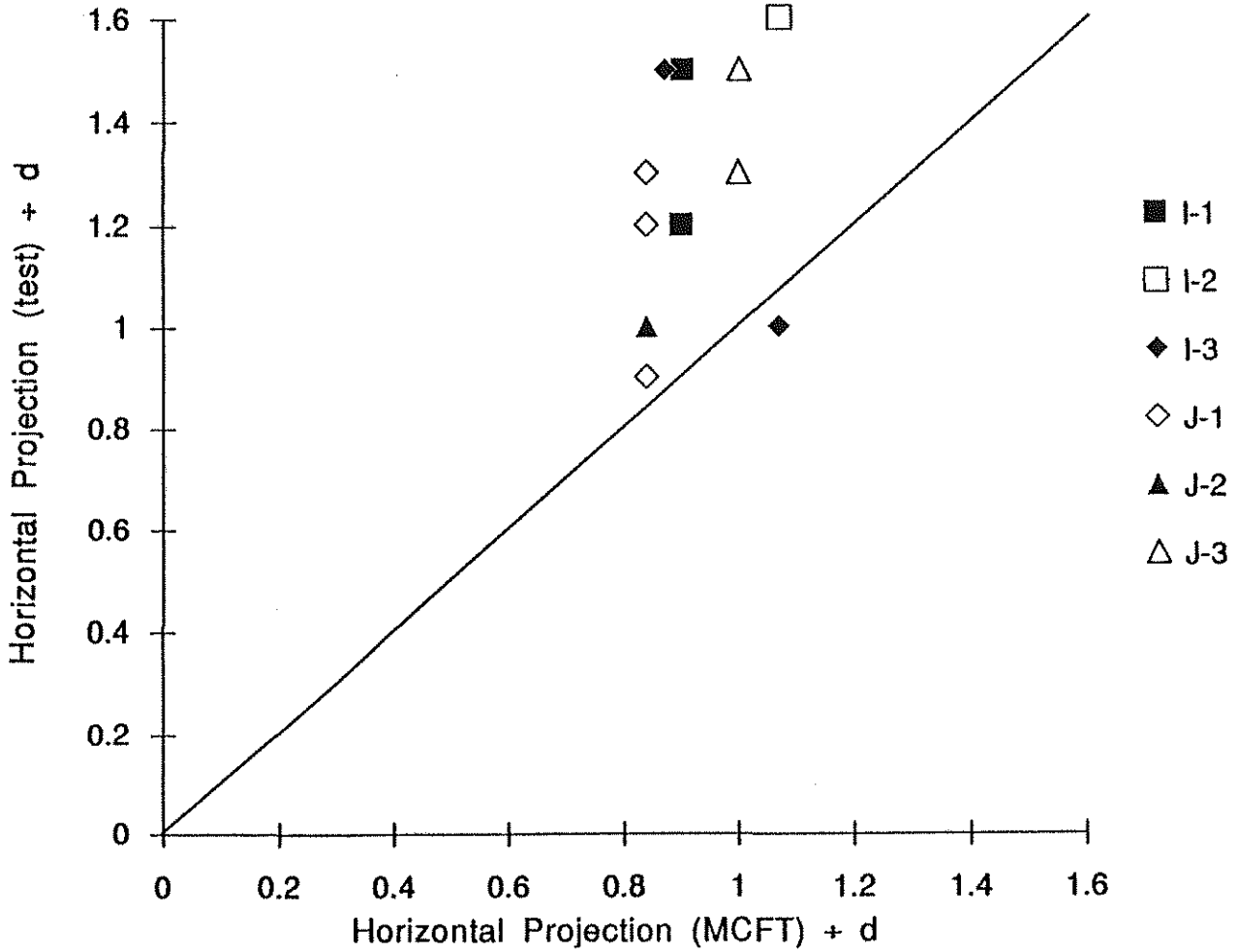

Fig. 3.18 Comparison of Measured Horizontal Crack Projection to Predicted Horizontal Crack Projection from MCFT Design Procedure

APPENDIX A

NOTATION

A_c = area of concrete cross-section

A_s = area of flexural reinforcement

A_v = area of web reinforcement

A_x = area of longitudinal (flexural) reinforcement

a = shear-span, distance from maximum moment section to zero moment section, or height of equivalent compressive stress block on concrete cross-section

b_w = web width of T-beam

C = compression force on concrete cross-section

c = distance from compression face to neutral axis of the cross-section

c_v = horizontal distance from center of the web to inside edge of the stirrup

c_x = vertical distance from neutral axis of the uncracked section to inside edge of the tension steel

d = distance from extreme compression fiber to centroid of flexural reinforcement

d_a = diameter of maximum size aggregate

d_{bv} = diameter of transverse reinforcement (stirrups)

d_{bx} = diameter of longitudinal reinforcing bars

E_c = modulus of elasticity of concrete

E_s = modulus of elasticity of reinforcement

f_1 = average principal tensile stress in concrete

f_2 = principal compressive stress in concrete

f_c = compressive stress in concrete outside of the area $b_w$jd

f_{cr} = cracking strength of concrete

NOTATION (continued)

f'_c = compressive strength of concrete measured on 6 x 12 in. cylinders

f_v = tensile stress in web reinforcement

f_{vy} = yield stress of web reinforcement

f_x = stress applied in x-direction

f_y = stress applied in y-direction, or
yield stress of flexural reinforcement

jd = flexural lever arm

M = applied moment on concrete cross-section

M_u = factored bending moment at section

N = axial tensile force on concrete cross-section

r = coefficient of variation, or
ratio of moment to shear, M/V

s = spacing of transverse reinforcement

s_x = horizontal clear space between longitudinal bars

s_{mv} = average spacing of cracks perpendicular to the transverse reinforcement

s_{mx} = average spacing of cracks perpendicular to the longitudinal reinforcement

$s_{m\theta}$ = average spacing of cracks inclined at θ to the longitudinal reinforcement

T = tensile force on concrete cross-section

V = shear force

V_c = shear strength provided by tensile stresses in concrete

V_n = nominal shear strength (ultimate strength)

v_c = nominal shear stress carried by concrete, $V_c/b_w d$

v_{ci} = shear stress on crack surfaces

NOTATION (continued)

v_n = nominal shear stress, $V_n/b_w d$

v_s = nominal stirrup stress

v_{si} = shear stress carried by stirrup alone

w = crack width

x = distance from point where ε_x is measured to neutral axis

ε_1 = principal tensile strain in concrete

ε_2 = principal compressive strain in concrete

ε_0 = concrete strain at f'_c

ε'_c = concrete strain at f'_c

ε_{cr} = strain in concrete at cracking

ε_{ct} = strain at extreme compression fiber of concrete cross-section

ε_s = strain in flexural reinforcement

ε_t = strain in web reinforcement

ε_x = longitudinal strain

ε_y = transverse strain

γ_{xy} = shear strain relative to x, y axes

θ = angle of inclination of principal compressive stresses in concrete, measured with respect to longitudinal axis

ρ_v = ratio of web reinforcement, $A_v/b_w s$

ρ_x = ratio of reinforcement area to concrete area

ρ_w = ratio of flexural reinforcement, $A_s/b_w d$

ϕ = strength reduction factor